

Doctoral Thesis

Stability and Thermal Conductivity of
Metallic-nanofluids

Song, You Young (송 유 영)

Graduate Institute of Ferrous Technology

Pohang University of Science and Technology

2015

Stability and Thermal Conductivity of Metallic-nanofluids

2015 YY SONG

금속나노유체의
분산안정성 및 열전도도 연구

Stability and Thermal Conductivity of
Metallic-nanofluids

Stability and Thermal Conductivity of Metallic-nanofluids

by

Song, You Young

Graduate Institute of Ferrous Technology

Pohang University of Science and Technology

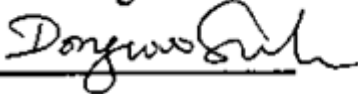
A thesis submitted to the faculty of the Pohang University of Science
and Technology in partial fulfillment of the requirements for
the degree of Doctor of Philosophy in the
Graduate Institute of Ferrous Technology

Pohang, Korea

12. 05. 2014

Approved by

Prof. Dong-Woo Suh



Academic Advisor

Prof. H. K. D. H. Bhadeshia



Co-Advisor

Stability and Thermal Conductivity of Metallic-nanofluids

Song, You Young

The undersigned have examined this dissertation and hereby
certify that it is worthy of acceptance for a doctoral degree
from POSTECH

12/05/2014

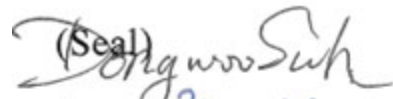
Committee Chair Dong-Woo Suh

Member H. K. D. H. Bhadeshia

Member Jae Sang Lee

Member Youn-Bae Kang

Member Sung Ryong Ryoo

(Seal) 
(Seal) 
(Seal) 
(Seal) 
(Seal) 

Preface

This dissertation is submitted for the degree of Doctor of Philosophy in the Graduate Institute of Ferrous Technology at Pohang University of Science and Technology. The research reported herein was conducted under the supervision of Professor Dong-Woo Suh, Professor of Computational Metallurgy in the Graduate Institute of Ferrous Technology, Pohang University of Science and Technology, and Professor H. K. D. H. Bhadeshia, Professor of Computational Metallurgy in the Graduate Institute of Ferrous Technology, Pohang University of Science and Technology and Tata Steel Professor of Metallurgy, University of Cambridge, between September 2010 and December 2014.

Except where acknowledgement and reference is made to previous work, this work is, to the best of my knowledge, original. Neither this, nor any substantially similar dissertation has been, or is being, submitted for any other degree, diploma or other qualification at any other university.

Some of the work described herein has been or to be published:

Song, Y. Y., Bhadeshia, H. K. D. H., and Suh, D. W.: Stability of stainless-steel nanoparticle and water mixtures, *Powder Technology (in press)*

Song, Y. Y., Bhadeshia, H. K. D. H., and Suh, D. W.: Stainless steel-nanofluids: Stability to Thermal conductivity, *To be submitted*

Song, You Young

December, 2014

DGIFT 송유영 Song, You Young
20100993 Stability and Thermal Conductivity of Metallic-nanofluids
금속나노유체의 분산안정성 및 열전도도 연구
Graduate Institute of Ferrous Technology, 2015,
141p, Advisor : Dong-Woo Suh, Text in English

ABSTRACT

Nanofluid or nanoparticle-fluid is a fluid containing particles that are small enough to remain in suspension over time that sometimes exhibit exceptional properties. While considerable work has been reported on the thermal conductivity of such mixtures based on oxides, inert powders and non-corrosive fluids, there are only few studies on metallic-nanofluids. In addition, there is a need to produce metallic-nanofluids with excellent thermal conductivity with good long term stability, and understand the heat transfer mechanism of these fluids. Therefore, the present work explores both the stability and thermal conductivity of metallic-nanofluids. Fine particles of stainless steel were selected and were dispersed into pure water or ethylene glycol.

As some previous studies have shown the strong relationship between the particle dispersion stability and fluid thermal conductivity, the first step was producing stable nanofluids. Amongst the parameters that are known to influence the dispersion of particles in fluid, it was found that controlling the fluid pH helps to stabilise the mixtures more than the addition of surfactants which is important in obtaining ζ -potentials that are large enough to sustain a significant repulsion between like particles in the fluid. For 0.017 wt% stainless steel-water fluids, pH 11 was the optimal stability condition and the thermal conductivity

enhancement was also highest. This work forms the foundation of future studies on the properties of such mixtures, especially for heavy metallic particles.

The second step was to reveal the relationship between the stability and thermal conductivity at various particle concentrations. Previous studies have shown that the thermal conductivity of fluids containing nanoparticles increased with the particle volume fraction. However, the rate of enhancement and the linearity have been hard to predict. To determine the complete particle dispersion at various concentrations that has not been deeply discussed before, the particle molar absorptivity was used. Under the complete particle dispersion, the thermal conductivity enhancement showed linear relationship with particle volume fraction when stainless steel particles were dispersed into both water and ethylene glycol.

Thermal conductivity enhancement with stainless steel particles in water was 20% and 15% with 0.003 vol.% of particles in water and ethylene glycol, respectively. This is comparable with other metallic-nanofluids which were previously reported, and show that obtaining good particle dispersion is necessary to benefit the particle with high thermal conductivity addition to fluids.

Contents

Contents	iii
1 Introduction	1
1.1 Basic Background	1
1.2 Aim of the Study	7
2 Literature Review	9
2.1 Nanofluids	10
2.2 Dispersion Stability – Theoretical Approach	12
2.2.1 Electrostatic and steric stabilisation	13
2.2.2 Sedimentation	15
2.2.3 Derjaguin, Landau, Verwey and Overbeek theory	19
van der Waals attraction	19
Repulsion	26
Total interparticle potential	28
2.3 Dispersion Stability – Experimental Approach	32
2.3.1 Sedimentation observation	32
2.3.2 Particle morphology	33
2.3.3 Particle size distribution	34

2.3.4	Zeta potential	36
2.3.5	Absorbance	41
2.4	Thermal Conductivity	46
2.4.1	Thermal conductivity of materials	46
	Liquids	50
	Solids	53
2.4.2	Thermal Conductivity of Mixtures	57
2.5	Previous Studies on Thermal Conductivity of Nanofluids	59
2.5.1	Effect Parameters	59
	Particle volume fraction and material	59
	Particle size	60
	Fluid temperature and material	61
	<i>pH</i> of fluid, additives and sonication power and time	63
2.5.2	Mechanisms of Heat Conduction	65
	Liquid-layering	66
	Particle aggregation or Clustering	67
	Brownian motion and Brownian-motion-induced convection	68
3	Experimental	70
3.1	Material	71
3.2	Stability Measurement	73
3.3	Nanoparticle-fluid Production	74
3.4	Transient Hot-wire Method	75
3.4.1	Principle of Measurement	76
3.4.2	Setup	79
3.4.3	Calibration	80

4	Stability of 0.017 wt% Stainless steel–Water Mixture	82
4.1	Introduction	82
4.2	0.017 wt% Production Parameters	84
4.2.1	Light absorption of stainless steel particles	84
4.2.2	Temperature Control	86
4.2.3	Process Scale	88
4.2.4	Sonication Time	91
4.3	<i>pH</i> Effect	93
4.4	Surfactant Effect	97
4.4.1	SDBS Concentration	99
4.5	Optimal Stability Conditions	102
4.5.1	Long term stability	102
4.5.2	Chemical stability	105
4.5.3	Thermal conductivity at optimal conditions	107
4.6	Conclusion	110
5	Stainless steel–Nanofluids: Stability to Thermal conductivity	112
5.1	Introduction	112
5.2	Determining Complete Dispersion	116
5.2.1	Nanofluid production	116
5.2.2	Molar absorptivity of STS particles	117
5.2.3	Complete dispersion condition at various concentrations	120
5.3	Thermal conductivity enhancement	122
5.3.1	Thermal conductivity enhancement under complete dispersion of particles	122
5.3.2	Possibility of overestimate by using transient hot-wire method	123
5.4	Conclusion	127

6 Conclusions

128

References

130

Chapter 1

Introduction

1.1 Basic Background

Suspending solid particles is known to increase the heat conduction of the liquid in which they are dispersed (Maxwell, 1873), because of the greater thermal conductivity of solids than that of liquids (Lide, 2004). Following Maxwell's prediction on the thermal conductivity of heterogeneous mixtures with very dilute suspensions of spherical particles, the interactions among particles can be ignored due to low particle volume fraction, ϕ , as (Maxwell, 1873):

$$\frac{k_{\text{eff}}}{k_f} = 1 + \frac{3\phi\left(\frac{k_p}{k_f} - 1\right)}{\frac{k_p}{k_f} + 2 - \phi\left(\frac{k_p}{k_f} - 1\right)} \quad (1.1)$$

where k_{eff} , k_f and k_p are the thermal conductivities of the mixture, base fluid and particle, respectively, and k_{eff}/k_f is called the thermal conductivity enhancement of the mixture.

Demands for fluids with better heat transfer properties have been growing consistently in the electronics and automotive industries due to miniaturization of devices or

improved energy efficiency. Therefore, many trials had been done to add micrometer or millimeter sized particles into conventional cooling fluids such as water, ethylene glycol and oil. However, because of clogging, erosion and sedimentation of particles in fluid channels, it has been impossible to use these in heat transfer applications (Chitra and Sendhilnathan, 2014; Saidur et al., 2011; Wen et al., 2009; Wong and De Leon, 2010; Yu and Xie, 2012).

A *nanofluid* (or *nanoparticle fluid* suspension), is one with uniformly dispersed and stably suspended nano-sized particles smaller than 100 nm which emerged with the development of modern nanotechnology (Das et al., 2007). After Choi and Eastman (1995) reported the concept of nanofluids that can have significant effective thermal conductivity and Eastman *et al.* showed experimentally that thermal conductivity can be improved almost 60 % when 5 vol.% of CuO is dispersed in distilled water (Eastman et al., 1996), the nanofluid idea has been considered as the future heat-transfer fluids. There has been considerable modern work on nanofluids and the reported properties were promising; enhanced heat transfer properties with only a small addition of particles, even less than 1 vol.%, and benefits of not having the aforementioned problems that fluids with micrometer sized particles had (Chandrasekar and Suresh, 2009; Das et al., 2007; Fan and Wang, 2011; Kleinstreuer and Feng, 2011; Özerinç et al., 2010; Saidur et al., 2011; Saleh et al., 2014; Sundar et al., 2013; Wen et al., 2009; Wong and De Leon, 2010).

However, although considerable theoretical and experimental work has been done since 1995, it seems that the applications of nanofluids are not as widespread as expected (Liu and Li, 2012; Michaelides, 2014). Experimental studies have shown that the effective thermal conductivity of nanofluids is influenced by the volume fraction, size and shape of particles, material properties of the particles and base fluid, acidity and temperature of base fluid, dispersion method and additives such as surfactants

(Das et al., 2007). To explain the underlying basis of enhanced heat conduction in nanofluids, propositions such as liquid-layering, particle aggregation, Brownian motion of particles, *etc.* have been tested and discussed (Kebblinski et al., 2002; Pang et al., 2014; Yu and Choi, 2003). But, none of the constructed models including effect parameters or propositions could reproduce the reported experimental data, and failed to explain the principles. Thus, there is a need of further studies on the heat conduction of nanofluids.

Difficulties of describing the heat transfer mechanism of nanofluids come from the discrepancies in properties between different groups and the thermal conductivity degradation over time. The discrepancies in data is because of different measurement method which is not yet standardised and different stability or dispersion status.

For example, the transient hot-wire method has been used most frequently to measure the thermal conductivity of nanofluids (Paul et al., 2010), but this method was originally constructed for homogeneous gases and liquids, not solid-liquid mixtures. Nanofluids should be categorized as heterogeneous fluids, due to aggregation and sedimentation of particles. Particles are uniformly dispersed in fluids at the initial stage after production, but gradually form flocs or aggregates, become heavier and larger, and finally settle down. With the same combination of nanoparticles and fluids, the measured thermal conductivity can diverge depending on the inhomogeneous distribution of particles which was also pointed out recently by Michaelides (2014). In addition, the time of measurement is also critical in the case of fluids with lower stability; thermal conductivity measured within the short time after production will be higher than that measured after a few days if sedimentation occurs, because the amount of particles that can bring additional heat transfer decreases.

The particles studied range from oxides to intermetallic compounds, metals and carbon nanotubes (Chen et al., 2009; Hwang et al., 2008; Jiang et al., 2003; Li et al.,

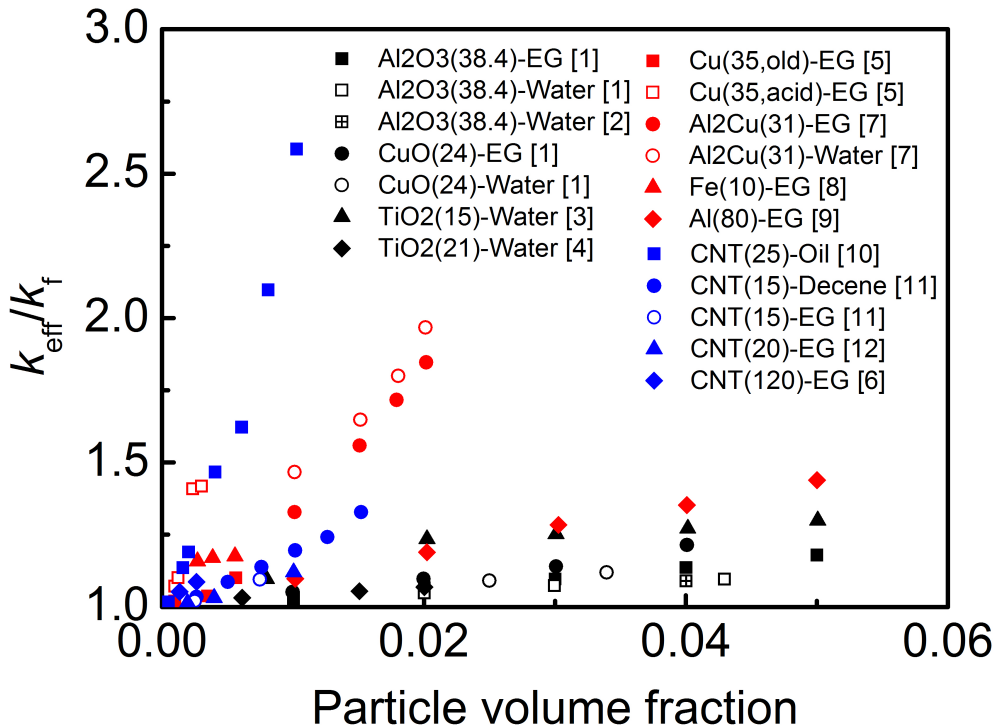


Fig. 1.1 Thermal conductivity enhancement of nanofluids k_{eff}/k_f with respect to particle volume fraction ϕ . Black, red and blue symbols indicate oxides, metals and carbon nanotube particles, respectively. Legend indicates each set of data in nanoparticle(size of particle in nanometre)-base fluid, and EG is ethylene glycol. Original figure from (Fan and Wang, 2011) is reproduced.

[1] Lee et al., 1999; [2] Das et al., 2003; [3] Murshed et al., 2005; [4] Duangthongsuk and Wongwises, 2009; [5] Eastman et al., 2001; [6] Assael et al., 2006; [7] Chopkar et al., 2008; [8] Hong et al., 2005; [9] Murshed et al., 2008a; [10] Choi et al., 2001; [11] Xie et al., 2003; [12] Liu et al., 2005.

2007; Timofeeva et al., 2011; Yang et al., 2012; Yu et al., 2010). As in Fig. 1.1, the thermal conductivity enhancement has been reported to be higher when metallic nanoparticles are dispersed in the fluid than in the case for oxide nanoparticles (Fan and Wang, 2011; Saterlie et al., 2011; Timofeeva et al., 2011), which is explained by the orders of

magnitude greater thermal conductivity of metals than oxides (Lide, 2004). Nonetheless, due to the oxidation, storage and safety problems related to metallic powders (Wiesner et al., 2006) and difficulties in production because of larger particle density or gross chemical reactions between the metallic-particles and fluid, *e.g.* rusting in water, metallic-nanofluids have been studied much less than oxide or nanotube dispersions. Shown in Fig. 1.2, the thermal conductivity degradation of copper-water nanofluids is much faster than oxides, which is slowed down when dispersed into ethylene glycol. This can be explained by the sedimentation rate following Stoke's law (Cosgrove, 2010); viscosity of ethylene glycol is about 100 times than that of water. In addition, the thermal conductivity enhancement of nanofluids has been reported to be higher when the nanofluids were more stable (slower sedimentation) (Li et al., 2008; Wang et al., 2009). Therefore to investigate the heat conduction mechanism of nanofluids and produce nanofluids with good heat transfer properties, stability of nanofluids must be studied and understood first. However, studies on the stability of nanofluids and the relationship with heat transfer properties have not been pursued vigorously.

In conclusion, from thorough reviews of the subject, it can be summarised as:

- a need for study on stability of nanofluids,
- a standard measurement technique applicable to nanofluids,
- thermal conductivity data with consistent parameter control,
- modified or new models to describe/predict the effective thermal conductivity of nanofluids, and
- a study on the mechanism behind the heat transfer in nanofluids.

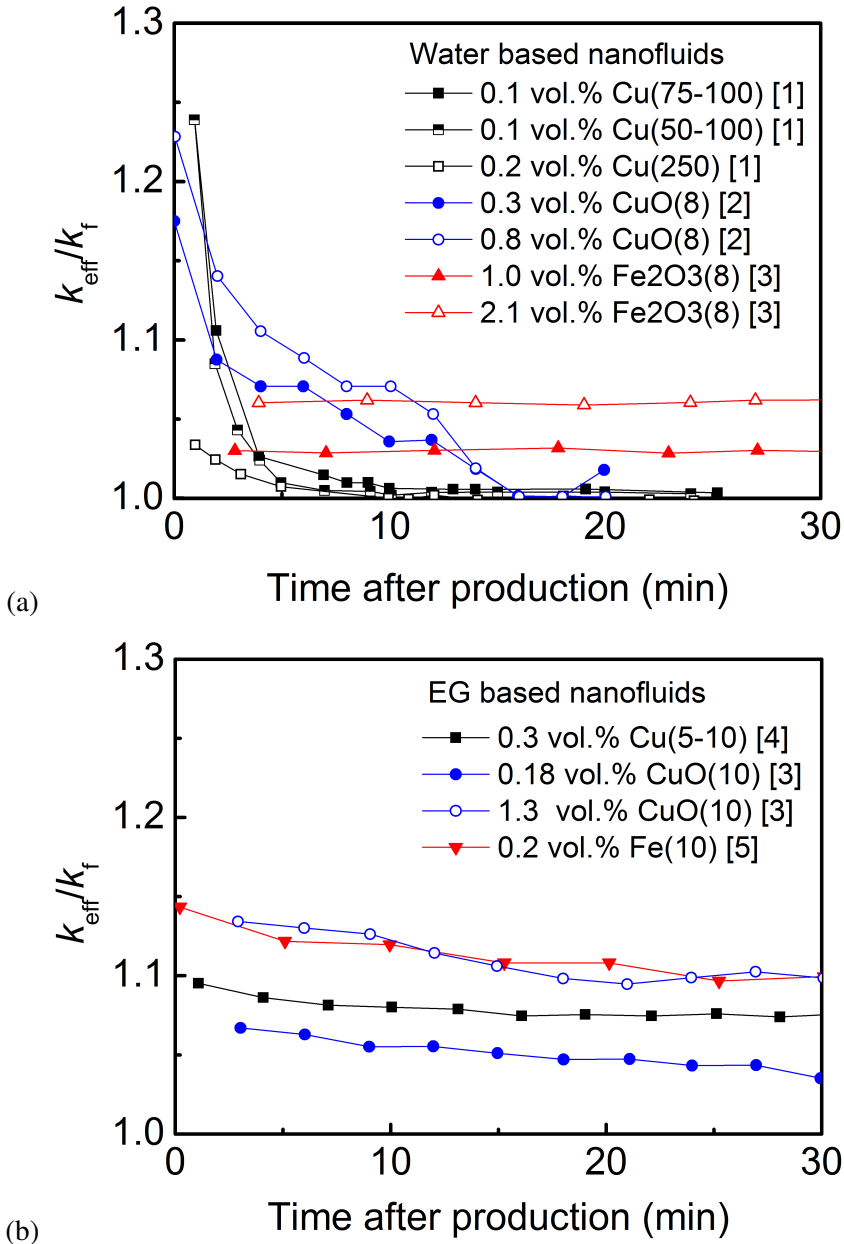


Fig. 1.2 Degradation of thermal conductivity enhancement over time of (a) water based and (b) ethylene glycol (EG) based nanofluids after their production. Particle concentrations and sizes in nanometre are indicated in legends as: volume fraction nanoparticle(size).

[1] Liu et al., 2006; [2] Karthikeyan et al., 2008; [3] Philip and Shima, 2012; [4] Yu et al., 2010; [5] Hong et al., 2006.

1.2 Aim of the Study

Research on nanofluids includes a wide range of knowledge on science and engineering fields. It includes chemistry for best dispersing particles in fluids which includes colloidal dispersion theories, and mechanical engineering for understanding heat transfer theories. It is necessary also to set up apparatus for measuring the properties of nanofluids that definitely needs more discussion and study to find out whether techniques that were used previously to measure fluid properties will all work well in nanofluids. Understanding both stability and heat transfer is important as discussed in previous section. However, it seems that mechanical engineers put responsibility on chemists to solve the stability problem while chemists do not have deep interest in heat transfer applications.

To produce a nanofluid with good thermal conductivity and understand the heat transfer mechanism of it, both the stability and the thermal conductivity were considered in this study. The interest was focused especially on metallic-nanofluids.

First, stable nanofluids are produced at certain concentration on the basis of the colloidal dispersion theories, tested at various concentrations and then a method to determine the sufficient stability of nanofluids are suggested which has not been properly discussed elsewhere. Previous studies found the optimal stability condition for some nanofluids, but were limited to specific concentrations ([Fedele et al., 2011](#); [Hwang et al., 2008](#); [Li et al., 2007](#); [Ojha et al., 2010](#); [Wang et al., 2011](#)).

Second, the thermal conductivity of stable nanofluids produced at various concentrations are measured and the relationship with particle concentration and other parameters are studied experimentally. Transient hot-wire apparatus was constructed, and in addition, the possibility of the overestimate caused by the pulse-like heat transfer reported by Ghosh ([Ghosh, 2010](#); [Ghosh et al., 2013](#)), for example, has been verified.

Last, to understand the mechanism behind the thermal conductivity enhancement

and the additional heat transfer coming from collision of metallic-particles, reported new or modified models and theories were considered and discussed.

Chapter 2

Literature Review

This chapter is the literature review on dispersion stability and thermal conductivity of solid-liquid mixtures. The first section defines what nanofluid is, and the following two sections are about dispersion stability; the latter can be investigated theoretically and experimentally based on colloidal dispersion theories, and both approaches are discussed in detail along with previous studies on each approach. The fourth section begins with the definition of thermal conductivity as the material property of solids and liquids, and then the characteristic of thermal conductivity of heterogeneous solid-liquid mixtures are described. Finally, previous studies on the thermal conductivity of nanofluids are summarised.

2.1 Nanofluids

Before moving on to further discussion, it will be better to define what is a heterogeneous mixture, colloid and nanofluid. When two or more different substances are mixed and not combined chemically, it is a mixture. A mixture is *heterogeneous* if components within the mixture can be distinguished and separated easily, and *homogeneous* if substances are in a single phase (Michaelides, 2014, p. 4). A colloid or *colloidal suspension* is a mixture of insoluble particles smaller than $100\ \mu\text{m}$, (arbitrary) dispersed in another substance which is medium (Israelachvili, 2011, p. xxix).

A nanofluid is when the size of the particles, d_p (diameter for spherical or equivalent diameter for non-spherical shaped particles), is smaller than 100 nm. A colloid or nanofluid are sometimes classified to homogeneous suspensions when the solid particles are distributed uniformly and sedimentation is not observed, showing homogeneous properties behaving as one phase. But generally, nanofluids have heterogeneous characteristics.

The nanoparticles themselves can be ceramics, metals, carbon nanotubes, composites, or alloyed particles as in Fig. 2.1. Oxides such as Al_2O_3 and CuO (Choi and Eastman, 1995; Eastman et al., 2001; Lee et al., 1999) were first and the most used in studies of nanofluids, because they are easy to manufacture and chemically stable in solutions.

Nanoparticles can be produced by physical processes (inert-gas condensation, mechanical milling) or chemical processes (chemical vapor deposition, chemical precipitation, thermal spraying) (Das et al., 2007). Nanofluids can be produced using two methods; particles are simultaneously synthesized and dispersed directly into a base fluid in the one-step method, or particles are first produced and then dispersed into base fluids by mixing or ultrasound agitation in two-step method. The former method is preferable when dealing with metallic particles and can prevent agglomeration which

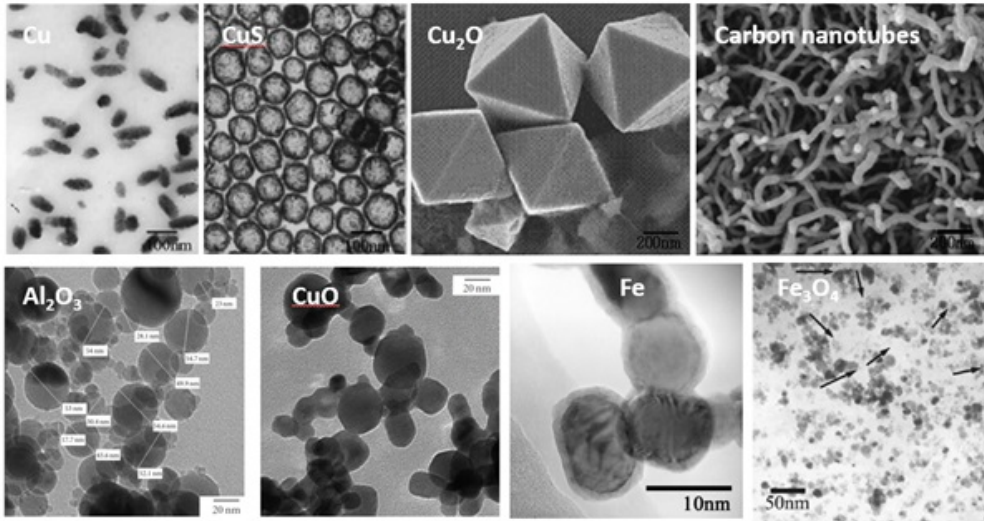


Fig. 2.1 TEM images of dried nanofluids with Cu, CuS, Cu₂O, Carbon nanotubes (Fan and Wang, 2011), Al₂O₃, CuO (Gowda et al., 2010), Fe (Hong et al., 2005) and Fe₃O₄ (Zhu et al., 2006) particles.

is the key issue in using two-step techniques. However, the two-step method is used widely because of it is economical and more suitable for commercial production.

2.2 Dispersion Stability – Theoretical Approach

The stability of a nanofluid follows colloid dispersion theories. Generally, a stable colloidal system becomes unstable by a process of either sedimentation, flocculation and then coagulation, or flocculation, coagulation and then sedimentation (Fig. 2.2). If the particles or the medium with smaller fraction maintains the dispersed initial state from the production for a long time (throughout the time of its usage), then the colloid is called “stable”. Also, if the particles flocculate but do not sediment for a sufficient time, that is also regarded as a stable colloid. Therefore, nanoparticles in the nanofluid should not settle for some time, and the properties should be maintained for that period to be applied in the future.

Fig. 2.3 shows the kinetic behavior and force balance of particles in fluid (Pugh and Bergström, 1994). Nanoparticles in fluid are under these forces and the dispersion state depends on their balance. The balance of gravity, drag and buoyancy can be explained by Stoke’s law and interparticle forces, attraction and repulsion, are explained by Derjaguin, Landau, Verwey and Overbeek (DLVO) theory. Separating shear is the force that particles undergo in mixing processes. Brownian motion and fluid flow will

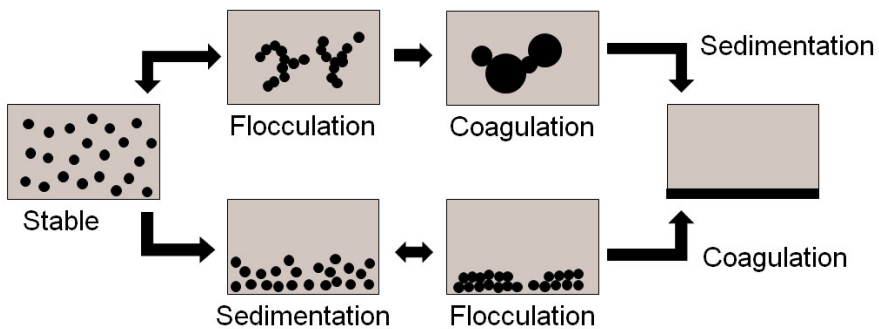


Fig. 2.2 Sedimentation process of a colloidal system. Original figure from Malvern (2011) is reproduced.

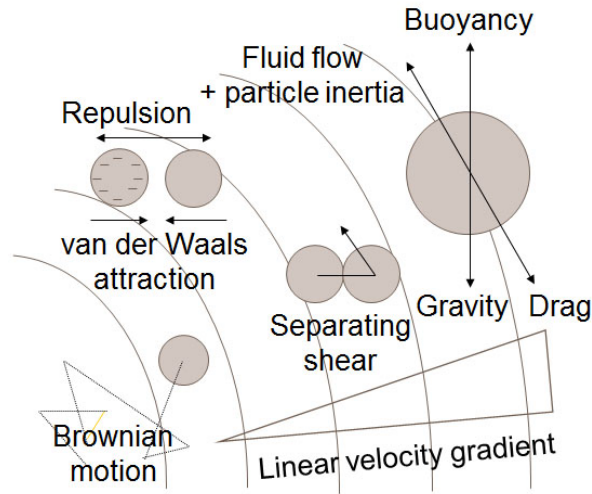


Fig. 2.3 Kinetic behavior and force balance of particles in fluid. Original figure from (Pugh and Bergström, 1994) is reproduced.

be ignored since they are not the main factors to be considered in the production process. In the following subsections, these forces will be discussed in detail.

2.2.1 Electrostatic and steric stabilisation

Particles dispersed in a liquid can be in electrostatic or steric stabilisation state as shown in Fig. 2.4. *Steric* stabilisation is obtained by modifying the particle surface with surfactants or polymers. If surfactants or polymers are well adsorbed on the particle surface, the formed adsorbed layer may prevent coated particles coming into contact. This is an irreversible process, and efficient for non-polar particles that cannot have electrostatic stabilisation.

Surfactants are classified into anionic, cationic, nonionic and amphoteric type. Anionic surfactants have anionic function groups at head, cationic surfactants are positively charged at $pH < 10$, nonionic surfactants have long chained alcohols, and

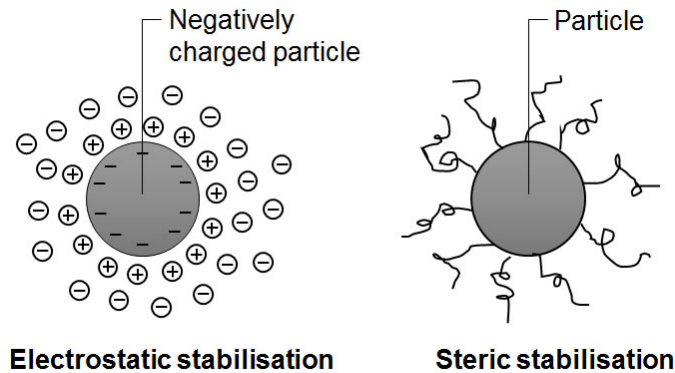


Fig. 2.4 A simple schematic of electrostatic and steric stabilisation of a particle in liquid.

amphoteric surfactants have both cationic and anionic structures (Cosgrove, 2010). Sodium dodecyl sulfate (SDS) and sodium dodecyl benzene sulfonate (SDBS) are anionic, hexadecyltrimethyl-ammonium bromide (CTAB) is cationic and Triton X-100 is nonionic surfactants that were previously used to increase the nanofluid stability (Hwang et al., 2008; Li et al., 2007, 2008; Wang et al., 2011).

Electrostatic stabilisation is obtained when the charged species, e.g. ions, are distributed around particles. Charged particles with identical sign will have repulsive forces between themselves and will not adhere when the repulsion is larger than the attractive force. By adding salts, acids or bases, the *pH* of fluids is controlled and the counter ions or species will surround the charged particles, which will increase the repulsion and stabilise the particles in the fluid.

As in Fig. 2.5, a charged particle in a fluid has a strong inner ion boundary, counter ions distributed close to the surface which is a Stern layer and a diffuse outer layer with less firmly attached ions. The Stern layer and diffuse layer together form the electrical double layer. When the particle diffuses in the fluid, the Stern layer and

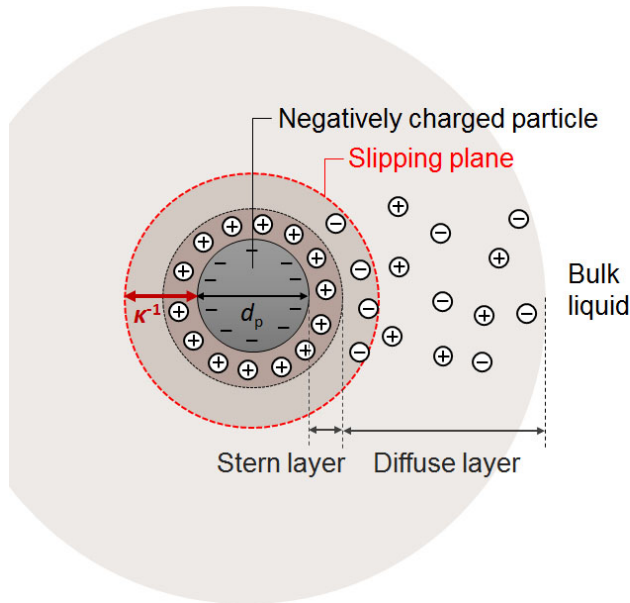


Fig. 2.5 A simple schematic of electric double layer of negatively charged particle.

the inner diffuse layer moves with the particle and the outer diffuse layer moves with the fluid – the plane between the particle movement is called the slipping plane. The *Debye length* κ^{-1} is the distance from the Stern layer to the slipping plane and the *zeta potential* ζ is the surface potential at the slipping plane. Electrostatic stabilisation is a reversible process and the degree of this stabilisation can be measured by the zeta potential (see section 2.3.4 for detail).

2.2.2 Sedimentation

From Stoke's law, the sedimentation velocity v_s of the particle is obtained from the balance of the gravity, drag and buoyancy forces as:

$$v_s = \frac{2 r_p^2 g |\rho_p - \rho_f|}{9 \eta} \quad (2.1)$$

where r_p is the particle radius, g is standard acceleration of gravity 9.806 m s^{-2} , ρ_p and ρ_f are the densities of the particle and fluid, respectively, and η is the fluid viscosity (Cosgrove, 2010). The sedimentation in nanofluids can be prevented or slowed down by reducing the particle size, increasing the fluid viscosity and decreasing the density difference between the particle and the fluid.

For a given particle and fluid, using particles with smaller size will increase the probability to get a stable nanofluid. However, when the particle size becomes smaller its specific surface area increases and the surface energy increases, and because the repulsive potential between particles is also linear to the particle size (Eq. 2.11), the attraction between particles may be larger at a certain critical size. Therefore, only reducing the size of the particles cannot be the solution, and it is important to stabilise the particle surface either by increasing the repulsive forces between particles (electrostatic stabilisation) or modifying the surface of particles using surfactants (steric stabilisation).

Therefore, because density and viscosity of a liquid are strongly dependent on temperature, controlling the temperature during the production is more important. Fig. 2.6 shows that viscosity of water and ethylene glycol decrease rapidly with increase in temperature. As in Fig. 2.7, the sedimentation velocity of particles in the fluid with respect to the temperature increases in order of magnitudes according to Eq. 2.1.

While some studies on the temperature effect to heat transfer properties of nanofluids have been done (Chon et al., 2005; Das et al., 2003; Duangthongsuk and Wongwises, 2009; Mintsa et al., 2009; Murshed et al., 2008b), the temperature effect on stability of nanofluids has not been considered: only a few authors have noted the dispersion temperature (Nasiri et al., 2011). If the sedimentation velocity can be slowed down by controlling temperature, particles can be dispersed more uniformly during

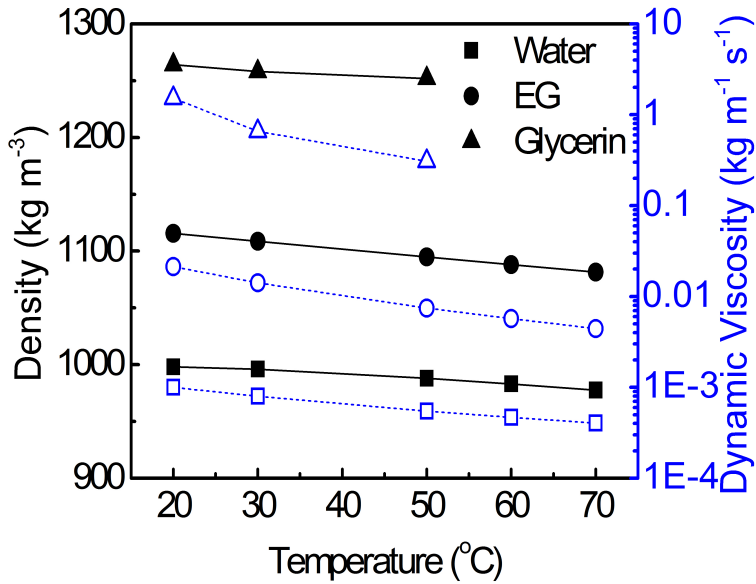


Fig. 2.6 Density and dynamic viscosity at specific temperatures under atmospheric pressure (Bayazitoğlu and Özişik, 1988). Square, circle and triangle are water, ethylene glycol (EG) and glycerin, respectively and black closed symbols with solid lines and blue opened symbols with dot lines are density and dynamic viscosity, respectively.

sonication. The result of the dispersion temperature control is shown in chapter 4.

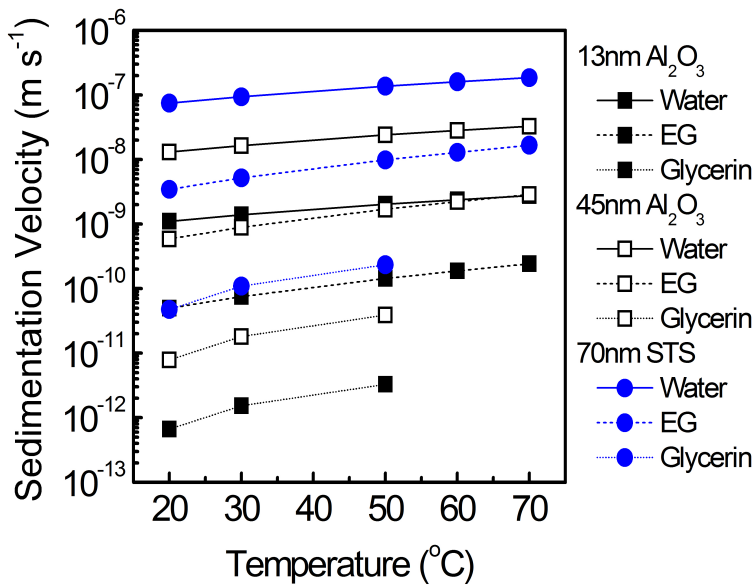


Fig. 2.7 Calculated sedimentation velocity of nanofluids with respect to temperature using Eq. 2.1. Solid, dash and dot lines are water, ethylene glycol (EG) and glycerin based nanofluids, respectively. Black closed square, black opened square and blue circle are when 13 nm sized Al_2O_3 , 45 nm sized Al_2O_3 and 70 nm sized stainless steel (STS) nanoparticles are in fluids. $\rho_{\text{Al}_2\text{O}_3} = 4000 \text{ kg m}^{-3}$, $\rho_{\text{STS}} = 7900 \text{ kg m}^{-3}$, and density and dynamic viscosity from Fig. 2.6 are used in the calculation.

2.2.3 Derjaguin, Landau, Verwey and Overbeek theory

Surface chemistry becomes important for particles smaller than 100nm because the effect of the van der Waals attraction increases relative to the kinetic energy of stirring, so particles can aggregate easily (Pugh and Bergström, 1994). The dispersion of particles can be maintained by adding a surfactant to modify any hydrophobic surfaces of particles, modifying surface charge by pH control, and applying powerful forces by controlling ultrasonic vibration power and time.

The stability of a particle in solution can be calculated by the DLVO (Derjaguin, Landau, Verwey and Overbeek) theory (Derjaguin and Landau, 1941; Verwey and Overbeek, 1948). The total interparticle potential V_T is the summation of van der Waals attraction V_A and electrostatic repulsion between particles V_R with respect to the interparticle surface to surface distance H :

$$V_T(H) = V_A(H) + V_R(H). \quad (2.2)$$

van der Waals attraction

The attraction between particles or a particle and a surface is calculated by the van der Waals attraction (Hamaker, 1937; Russel et al., 1992; Visser, 1972). Attraction force between two particles with identical sphere of radius r_p is:

$$V_A(H) = -\frac{A_{131}}{6} \left[\frac{2r_p^2}{H^2 + 4r_p H} + \frac{2r_p^2}{H^2 + 4r_p H + 4r_p^2} + \ln \left(\frac{H^2 + 4r_p H}{H^2 + 4r_p H + 4r_p^2} \right) \right], \quad (2.3)$$

where A_{131} is the interaction constant of particles (phase 1) in medium (phase 3). This van der Waals attraction between particles of same material still remains even when the particles are embedded in a fluid (Hamaker, 1937), and thus can be applied in colloidal

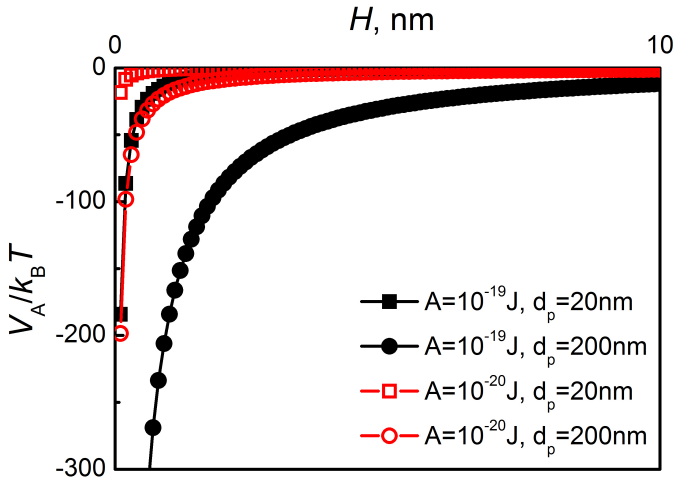


Fig. 2.8 Calculated normalized van der Waals attractive potential using Eq. 2.3 with Hamaker constants and particle sizes of different orders with respect to interparticle surface to surface distance H at $T = 300$ K.

stability.

Fig. 2.8 shows this attraction force between two identical particles with respect to the particle surface to surface distance H is strongly dependent on the particle size for a given constant A_{131} . The attraction between particles will increase continuously while a fluid is used or stored; since particles aggregate gradually, coarsen over time, and then the attractive force may increase depending on the size of particles.

A_{131} is in the order of $10^{-19} - 10^{-20}$ J for most materials, in the range of $2 \times 10^{-19} - 5 \times 10^{-19}$ J for metals (Israelachvili, 2011; Visser, 1972), and considered as very high at 3×10^{-19} J and abnormally low at 0.7×10^{-21} J (Hamaker, 1937). When A_{131} is 10 times higher, the attractive force between particles increases accordingly, so particles with lower A_{131} will have higher probability to be stable in a fluid. This gives explanation of why metallic particles settle down rapidly and hard to be stable in fluid;

metals have higher A_{131} than oxides as listed in Table 2.2.

Hamaker constant The interaction constant A_{131} in Eq. 2.3 can be either the *Hamaker* constant derived from molecular properties or the *Lifshitz–van der Waals* constant from bulk material properties (Visser, 1972).

The Hamaker constant A_{11} of two identical particles at short distance in vacuum is

$$A_{11} = \pi^2 q^2 \lambda, \quad (2.4)$$

where q is the number of atoms per cm^2 and λ is the London–van der Waals constant (Hamaker, 1937; Visser, 1972) and there are several methods to calculate λ (Visser, 1972). For the interaction between two particles of different materials,

$$A_{12} = \pi^2 q_1 q_2 \lambda_{12}, \quad (2.5)$$

where $\lambda_{12} = \lambda_{11} \lambda_{22}$ (Hamaker, 1937; Visser, 1972). Then the interaction constant between two particles 1 in medium 3, A_{131} , can be calculated by assuming the property of A_{11} to be additive:

$$A_{12} = \sqrt{A_{11} A_{22}}, \quad A_{131} = A_{11} + A_{33} - 2A_{13} \simeq (\sqrt{A_{11}} - \sqrt{A_{33}})^2. \quad (2.6)$$

If the properties of materials are provided, the Hamaker constant can be calculated and if not, Hamaker constant can be obtained from experiments (Visser, 1972).

Lifshitz–van der Waals constant The Lifshitz–van der Waals constant can be calculated as:

$$A_{131} = \frac{3}{4\pi} \hbar \int_0^\infty \left(\frac{\epsilon_1(i\xi) - \epsilon_3(i\xi)}{\epsilon_1(i\xi) + \epsilon_3(i\xi)} \right)^2 d(i\xi), \quad (2.7)$$

where $\varepsilon_i(i\xi)$ is the dielectric constant of material i along the imaginary frequency $i\xi$ (Bergström, 1997; Visser, 1972) and \hbar is the Dirac's constant 1.05×10^{-34} J s having $\hbar = \frac{h}{2\pi}$ relation with Planck constant $h = 6.63 \times 10^{-34}$ J s. The dielectric constant is a complex number at real frequency ω :

$$\varepsilon(\omega) = \varepsilon'(\omega) + i\varepsilon''(\omega), \quad (2.8)$$

where the imaginary part $\varepsilon''(\omega)$ is related to the absorption of material and the real part $\varepsilon'(\omega)$ is related to the transmission. The dielectric constant has a relation with the refractive index n in frequency regions as (Bergström, 1997):

$$\varepsilon(\omega) = \varepsilon'(\omega) = n^2(\omega), \text{ if } \varepsilon''(\omega) = 0. \quad (2.9)$$

When a static field with $\omega = 0$ is applied, non-conducting materials have the static dielectric constant $\varepsilon(0) = \varepsilon'(0)$, and Lifshitz–van der Waals constant of two identical particles 1 and medium 3 can be calculated as (Israelachvili, 2011; Murshed et al., 2009; Visser, 1972):

$$A_{131} = \frac{3}{4}k_B T \left(\frac{\varepsilon_p - \varepsilon_m}{\varepsilon_p + \varepsilon_m} \right)^2 + \frac{3\hbar v_e}{16\sqrt{2}} \frac{(n_p^2 - n_m^2)^2}{(n_p^2 + n_m^2)^{3/2}}, \quad (2.10)$$

where ε_p and ε_m are the static dielectric constants of the particle and medium and n_p and n_m are the refractive indices of the particle and the medium. k_B is the Boltzmann constant 1.38×10^{-23} JK⁻¹, T is the absolute temperature of the medium, and v_e is the frequency where the dielectric medium has the strongest absorption peak, 3.0×10^{15} s⁻¹ for water (Israelachvili, 2011; Koo and Kleinstreuer, 2004). Dielectric data can be obtained using various methods and when the static dielectric constant is not given, Lifshitz–van der Waals constant can be calculated using Eq. 2.7.

Table 2.1 The dielectric constants and refractive indices at room temperature of some materials. The refractive indices are given with the corresponding wavelength which was selected near 663 nm (zeta potential measurement wavelength).

[1] [Haynes et al., 2012](#) [2] [Hippel, 1954](#) [3] [Weber, 2010](#) [4] [TFCalc](#) [5] [Filmetrics](#) [6] [El-Kashef, 2000](#) [7] [Birkhoff et al., 1978](#)

Material	Dielectric constant	Refractive index (wavelength, nm)
Al ₂ O ₃	9.34 [1]	1.659 (625) [4]
TiO ₂ (rutile)	86 [2]	2.875 (630) [4]
CuO	18.1 [1]	2.694 (636) [4]
Cu		0.239 (632) [5]
Water	80.1 [3]	1.331 (636) [4]
Ethylene Glycol	41.4 [3]	1.428 (656) [6]
Glycerol	46.5 [3]	1.470 (620) [7]

The comparison of Hamaker and Lifshitz–van der Waals constants is discussed in [Visser \(1972\)](#). It is concluded that these interaction constants are valid at short separations below 20 nm, and if all of the optical data are available, Lifshitz–van der Waals constant can be regarded as the correct one than Hamaker constant. However, optical data are available for a only limited number of materials.

Static dielectric constants and refractive index values from the literature are listed in Table 2.1 and calculated Lifshitz–van der Waals constants using Eq. 2.10 for some materials are listed in Table 2.2 with values from the literature for comparison. Calculated results are close to values from literature, and copper and iron have higher interaction constant than alumina in water.

Table 2.2 Calculated Lifshitz–van der Waals constant A_{131} of particles 1 in fluid 3 using Eq. 2.10 and values in Table 2.1. For values from literature, * and ** indicate Hamaker and Lifshitz–van der Waals constants, respectively. Here, TiO_2 is rutile. [1] Visser, 1972 [2] Krupp et al., 1972

Particle-Fluid	Calculated A_{131} , 10^{-20} J	Literature A_{131} , 10^{-20} J
Al_2O_3 -Water	0.66	0.90*, 1.09** [1], 4.17 [2]
Al_2O_3 -EG	0.35	
Al_2O_3 -Glycerol	0.29	
TiO_2 -Water	6.12	5.9, 10 [1]
TiO_2 -EG	5.45	
TiO_2 -Glycerol	5.13	
CuO-Water	5.24	
CuO-EG	4.48	
CuO-Glycerol	4.21	
Cu-Water		2.73*, 4.58** [1], 17.5 [2]
Fe-Water		29 [1]

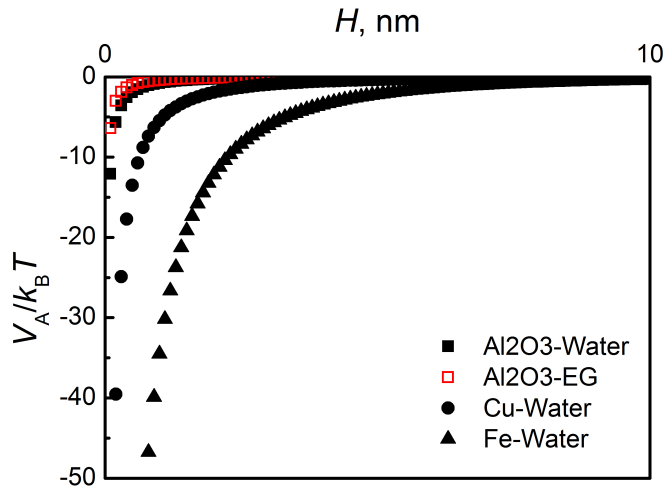


Fig. 2.9 Calculated normalized van der Waals attraction potential using Eq. 2.3 and Table 2.2 for water-based Al₂O₃, Cu and Fe nanofluids with particle size of 20nm with respect to interparticle surface to surface distance H at $T = 300$ K. $A_{131}(\text{Al}_2\text{O}_3 - \text{Water}) = 6.6 \times 10^{-21}$ J, $A_{131}(\text{Al}_2\text{O}_3 - \text{EG}) = 3.5 \times 10^{-21}$ J, $A_{131}(\text{Cu} - \text{Water}) = 4.58 \times 10^{-20}$ J and $A_{131}(\text{Fe} - \text{Water}) = 29 \times 10^{-20}$ J were used in the calculation.

Fig. 2.9 shows the calculated van der Waals attraction between some nanofluids; copper-water and iron-water nanoparticle-fluids have stronger attractive potential than aluminum oxide-fluids due to higher A_{131} . Therefore, particle-base fluid combination having lower Hamaker or Lifshitz–van der Waals constants are more likely to be stable after the nanofluid production, since particle aggregation or flocculation will happen less due to small attraction between particles.

Repulsion

The repulsive potential between two identical particles is calculated as (Murshed et al., 2009; Russel et al., 1992):

$$V_R(H) = 2\pi\epsilon_m\epsilon_0r_p\zeta^2\exp(-\kappa H), \quad (2.11)$$

where ζ is the measured zeta potential (section 2.3.4) and ϵ_0 is the vacuum permittivity $8.85 \times 10^{-12} \text{C}^2 \text{J}^{-1} \text{m}^{-1}$. The Debye length or electrical double layer (EDL) thickness κ^{-1} [nm] of a particle in medium can be calculated as (Li et al., 2007):

$$\kappa^{-1} = \sqrt{\frac{\epsilon_m\epsilon_0k_B T}{2N_A e^2 I}} = 1.9878 \times 10^{-3} \sqrt{\frac{\epsilon_m T}{I}}, \quad (2.12)$$

where N_A is the Avogadro constant $6.022 \times 10^{23} \text{mol}^{-1}$, e is the charge of a proton $1.602 \times 10^{-19} \text{C}$ and I is the ionic strength of the fluid in the unit of $[\text{molL}^{-1}]$ or $[M]$,

$$I = \frac{1}{2} \sum_{i=1}^n c_i z_i^2 \quad (2.13)$$

where c_i is the molar concentration of ion i $[\text{molL}^{-1}]$ and z_i is the charge number of ion i .

In 1:1 electrolyte water, the Debye length of a particle at 300K can be calculated in a simple form of

$$\kappa^{-1} = 0.3083\sqrt{I^{-1}}, \quad (2.14)$$

where the ionic strength in this case is the ionic concentration of H^+ or OH^- ions in water-based nanofluids whose pH value is controlled with hydrochloric acid (HCl) or

Table 2.3 Calculated Debye length κ^{-1} of a particle in HCl- or NaOH- added aqueous fluid at $T = 300\text{K}$. The ionic concentration and Debye length were calculated using Eq. 2.14 and Eq. 2.15, respectively.

pH	Ionic concentration, M	κ^{-1} , nm
1, 13	10^{-1}	0.96
2, 12	10^{-2}	3.04
3, 11	10^{-3}	9.62
4, 10	10^{-4}	30.4
5, 9	10^{-5}	96.2
6, 8	10^{-6}	304
7	10^{-7}	962

sodium hydroxide (NaOH) without any other salt:

$$I = 10^{-\text{pH}} \text{ if } \text{pH} < 7; \quad I = 10^{-14+\text{pH}} \text{ otherwise.} \quad (2.15)$$

Table 2.3 lists calculated Debye length with respect to pH of aqueous solutions. When the fluid is a strong acid or base (pH close to 1 or 13), the Debye length is small because layers formed by the ionic boundary are suppressed by high H^+ or OH^- ion concentrations.

Repulsive forces between particles in medium are influenced by the Debye length, zeta potential and particle size, and the effect of those are shown in Fig. 2.10, Fig. 2.11 and Fig. 2.12, respectively. The zeta potential and particle size determine the repulsive potential at $H = 0$ (particles in contact), at where the repulsion is maximum. Two particles can be in contact state only when they form floc (attached together but can be separated under strong shear force), therefore the meaning of larger $V_R(H \rightarrow 0)$ is the strong repulsion between particles when they are very close to each other. The

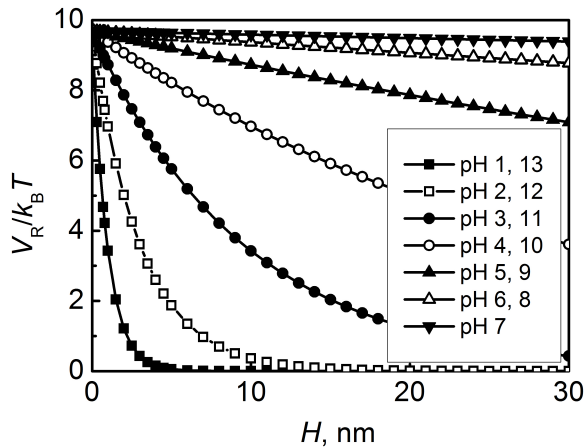


Fig. 2.10 Calculated normalized repulsive potential using Eq. 2.11 and Debye length from Table 2.3 with respect to interparticle surface to surface distance H at $T = 300\text{K}$. Zeta potential of 30mV and particle size of 20nm were assumed.

Debye length decides the degree of decline in repulsive potential according to surface to surface distance. Larger Debye length, thicker ionic boundary around the particle, shows slower decrease in repulsion.

When this repulsion force between two particles is large enough compared with the attractive force for some range of particle surface-to-surface distance, particles floating apart within this range of distance will not adhere together.

Total interparticle potential

Now, by adding the calculated van der Waals attractive potential and repulsive potential using Eq. 2.2, the total interparticle potential can be obtained. Theoretically, increasing the zeta potential, particle size and Debye length increase the repulsion between particles (Eq. 2.11). Since the zeta potential can be increased by controlling fluid pH or by adding surfactants that can modify the surface charge, controlling pH

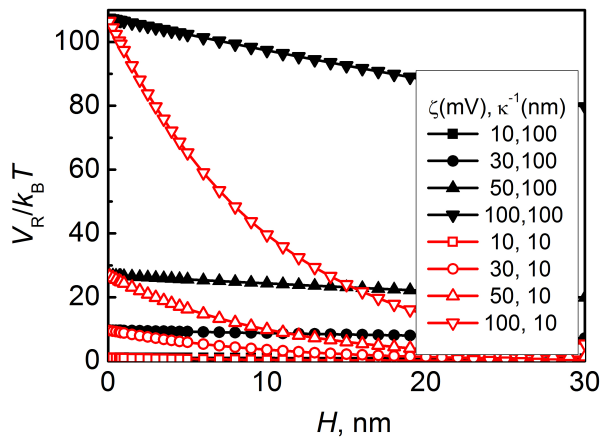


Fig. 2.11 Calculated normalized repulsive potential using Eq. 2.11 with respect to interparticle surface to surface distance H depending on zeta potentials at $T = 300\text{K}$. Debye length of 10 and 100 nm and particle size of 20 nm were assumed.

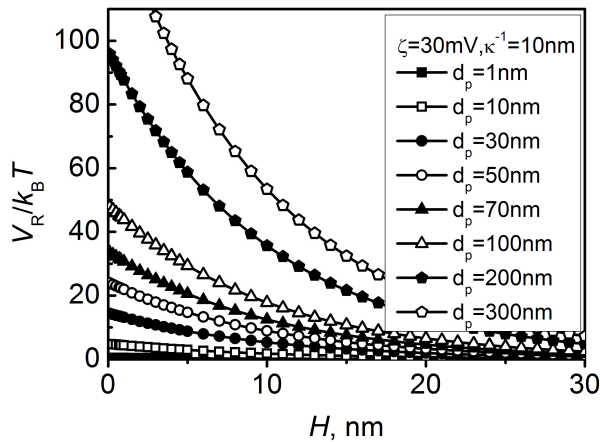


Fig. 2.12 Calculated normalized repulsive potential using Eq. 2.11 with respect to interparticle surface to surface distance H depending on particle size at $T = 300\text{K}$. Zeta potential of 30 mV and Debye length of 10 nm were assumed.

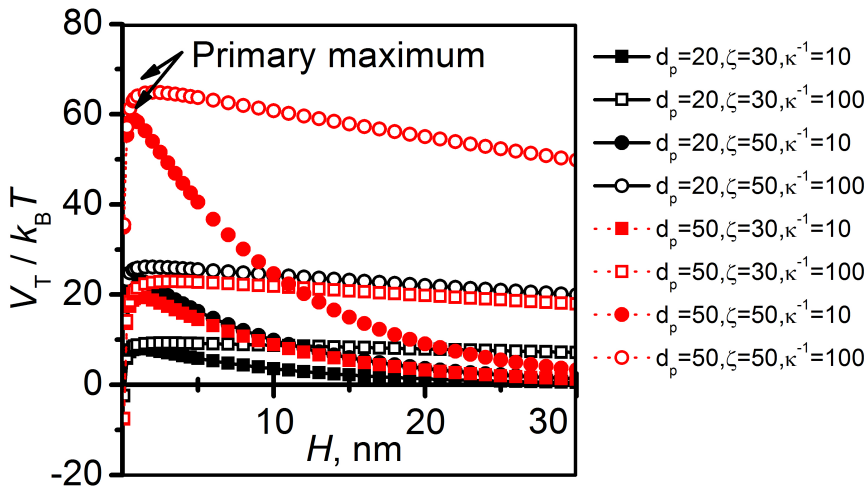


Fig. 2.13 Calculated normalized total interparticle potential of Al_2O_3 -water nanofluid using Eq. 2.11 with respect to interparticle surface to surface distance H at $T = 300$ K. $A_{131}(\text{Al}_2\text{O}_3 - \text{Water}) = 6.6 \times 10^{-21}$ J were used in the calculation. The effect of particle size d_p (nm), zeta potential ζ (mV) and Debye length κ^{-1} (nm) on total potential are verified.

and surfactants are the direct way to increase the repulsive force. However, when pH is controlled to increase the zeta potential, the Debye length decreases (Table 2.3). In addition, while Fig. 2.12 shows that larger particle has stronger repulsion, Fig. 2.8 also shows that a larger particle has a stronger attraction. Therefore, decreasing attractive force and increasing repulsive force for colloidal stability cannot be simply obtained.

Generally, a colloidal suspension is regarded to be stable when the energy barrier, the primary maximum in Fig. 2.13, is over $25 k_B T$ (Schenkel and Kitchener, 1960). Because the maximum energy of Brownian collision is $1.5 k_B T$ (Cosgrove, 2010; Israelachvili, 2011), the primary maximum should be at least $1.5 k_B T$ to avoid the ag-

gregation caused by random movement of particles in fluid even when in stationary. Fig. 2.13 shows the total interparticle potential of Al_2O_3 -water fluid with respect to various zeta potentials, particle sizes and Debye lengths (pH). In the case of Al_2O_3 -nanofluids, the energy barrier of stability is quite high and this is the reason that most of studies of the heat properties of Al_2O_3 -nanofluids did not consider the stability of nanofluids; the sedimentation will occur very slowly, making it impossible to observe the process of instability visually. However, in case of metallic-nanofluids, particles have higher Hamaker constants or larger particle size, and the energy barrier will not reach over $25 k_B T$ easily.

2.3 Dispersion Stability – Experimental Approach

To compare the degree of stability and durability of nanoparticle-fluids, five different methods can be used: sedimentation observation, transmission electron microscope (TEM) observation, particle size distribution measurement, zeta potential measurement and absorbance measurement. In this section, the method of each measurement with brief underlying theory is introduced. The characteristics, how to interpret data and limitations of each method are also discussed.

2.3.1 Sedimentation observation

The sedimentation of a nanofluid can be observed visually over time to examine the durability or long-term stability. If the color of the upper part of the nanofluid in the container becomes close to that of the base fluid and the lower part becomes close to that of the particles, sedimentation is in process. The methods discussed above to produce stable nanofluids, can be compared directly with minimal cost by using this test.

Sedimentation of particles between samples can be compared easily by this test, but by itself it is not sufficient for very dilute or stable samples which have durations over several months that will show no apparent difference in a short time. Also, this observation is more suitable for nanofluids with high particle concentration as this is based on the comparison of the color change of the fluid; the darker, the better because it means less sedimentation. For stable or dilute fluids, sedimentation of particles can be compared by absorbance measurement which will be discussed in section 2.3.5.

For example, the sedimentation test of copper-water nanofluids a week after production in Fig 2.14 shows that the stability of copper-nanofluids can be improved by adding CTAB surfactant or adjusting the *pH* of water.

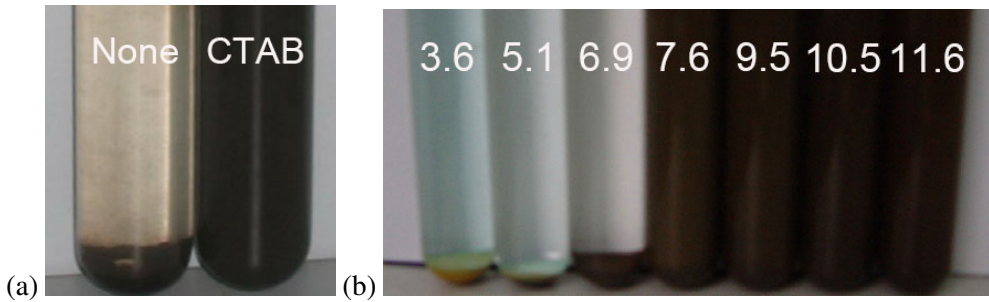


Fig. 2.14 Sedimentation test after a week of its production of 0.1 wt% Cu(25 nm)–water (a) without (left) and with 0.1 wt% CTAB addition (right), and (b) 0.1 wt% CTAB addition and *pH* variation (Li *et al.*, 2007).

2.3.2 Particle morphology

The particle crystalline phase, morphology and size distribution are observed by TEM. When a chemical reduction method is used to produce nanofluid, it is important to verify that the synthesised particles have the targeted composition and crystal structure, and the structure can be analysed by TEM or X-ray diffraction (XRD). Fig. 2.1 shows the particle morphology of various nanoparticles.

Nanofluid stability depends on the production method, and the most-used two-step method requires sufficient and strong dispersion power to break down and disperse particles in the base fluid that were aggregated in the dry powder condition. The breakdown of aggregated nanoparticles over increasing dispersion time or power can be observed by TEM. Hwang *et al.* (2008) produced carbon black–water nanofluids using five different dispersion techniques and showed that the most stable one was prepared by the high-pressure homogenizer. Fig. 2.15 shows the result observed by TEM; particles are separated into smaller aggregates with using more powerful dispersion method, and the authors also verified the result by measuring the particle size distribution of Fig. 2.16.

The TEM sample of nanofluid is made by dropping nanofluid onto a carbon-coated

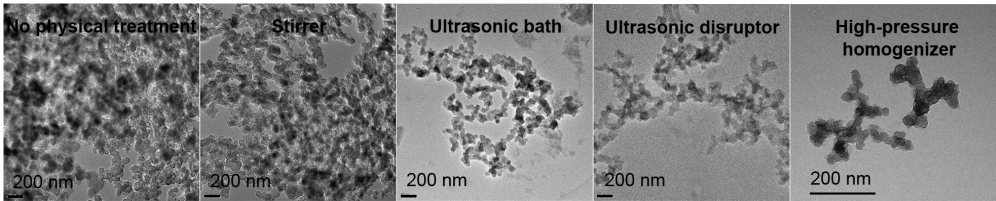


Fig. 2.15 TEM images of carbon black nanoparticles in water-based fluids prepared by two-step methods using various dispersion methods (Hwang et al., 2008).

copper grid and then drying the grid for over 24 hours in an oven or desiccator. However, this method has a limitation since the charge of particle surface can be influenced during the sample preparation process of using pipette, dropping and drying fluid, which is important in dispersion stability. Moreover, particles can be dried in a more aggregated form, overlapped or otherwise. Therefore, particle aggregation over time should also be observed and compared using particle size distribution and absorbance measurements.

2.3.3 Particle size distribution

The size distribution of particles suspended within a liquid can be measured using dynamic light scattering (DLS) theory. According to the Stokes-Einstein equation, the hydrodynamic diameter $d(H)$ (Russel et al., 1992) has a relation with the diffusion coefficient D which depends on the particle size:

$$d(H) = \frac{k_B T}{3\pi\eta D}. \quad (2.16)$$

The measurement is based on the Brownian motion of particles in the fluid – larger particles move slower in the medium, and movement is strongly dependent on the temperature because of temperature and viscosity terms. The diffusion coefficient is

measured by the equipment, and then the hydrodynamic diameter is calculated based on the given information on the particle material and the dispersant.

The hydrodynamic diameter is not the size of the particle itself. As shown in Fig. 2.5, *hydrodynamic diameter* is the sum of particle diameter and Debye length; $d(H) = d_p + \kappa^{-1}$. Therefore, calculated particle size given after the measurement is actually the hydrodynamic diameter of a particle using Eq. 2.16, and is always larger than the real particle size. More detailed explanation on DLS can be found in Milling (1999).

The most generally used base fluids in nanofluid production are water and ethylene glycol, and the viscosity of both decreases rapidly as temperature increases (Fig. 2.6). Thus, it is obvious when temperature increases, viscosity decreases, hydrodynamic diameter increases and the EDL thickness or Debye length increases. This EDL thickness is an important measure in calculating the interparticle potential that increases the repulsion forces between particles (see section 2.2.3).

The measurement of particle size distribution based on DLS has two big limitations: (1) since the diffusion coefficient has to be measured to calculate the particle size, the sample should be dilute for light to be scattered and (2) when the particles are aggregated, the given data from the equipment will be the averaged diameter that is equivalent to one sphere which has the identical diffusion coefficient. Therefore, when several small particles are aggregated stably or when the shape is not spherical, the measured particle size may be far from the real particle or particle aggregate size. However, the aggregation state can be compared between samples or over time because the given data is based on the Brownian motion movement of particles in the fluid, which depends directly on the particle size.

This is supported by the comparison of Fig. 2.15 and Fig. 2.16. Fig. 2.16 shows the average particle size is smallest when using high-pressure homogenizer, the peak

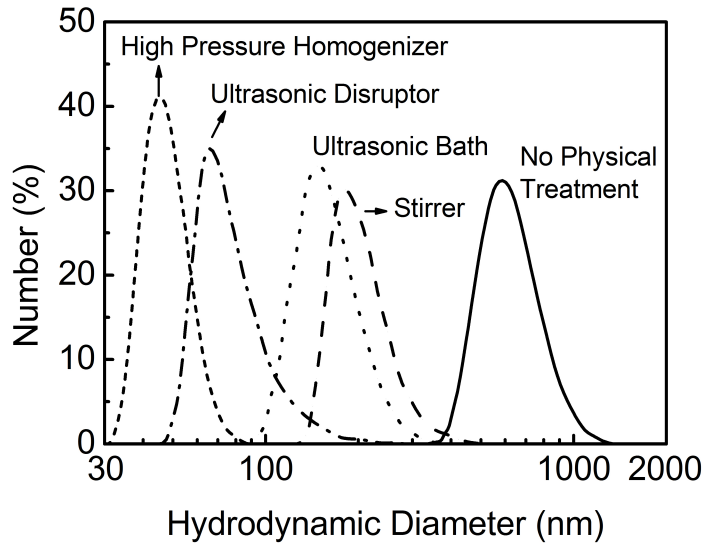


Fig. 2.16 The particle size distribution of 0.5 wt% carbon black (40 nm)–deionized water with 1.0 wt% SDS, produced using various dispersion methods (Hwang et al., 2008).

at 45 nm, and Fig. 2.15 shows the corresponding result. However, particles are aggregated in non-spherical shape, and the the peak at 45 nm is far from the real aggregated particle size as the average particle size of carbon black was indicated to be 40 nm (Hwang et al., 2008).

Hence, DLS can be used to compare the relative, not real, particle or particles size between samples to observe the difference in dispersion or aggregated state right after production or to observe the stability by tracking the increase in particle size over time.

2.3.4 Zeta potential

Previously defined in section 2.2.1, the zeta potential is the surface charge of the slipping plane and can be measured based on the electrophoresis theory. The particle movement in a capillary cell under a given voltage is measured: charged particles

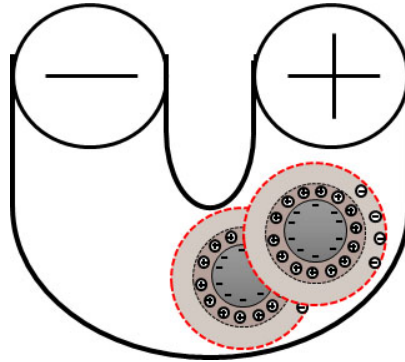


Fig. 2.17 A schematic of charged particles moving to opposite electrode.

move to the electrode with opposite charge and the mobility of the particles are measured as illustrated in Fig. 2.17. Refer to Milling (1999) for detailed explanation.

The electrophoretic mobility U_E , the mobility of the charged particle in the fluid, is a function of zeta potential in Henry's equation (Das et al., 2007):

$$U_E = \frac{2\varepsilon_m \zeta f(\kappa r_p)}{3\eta}, \quad (2.17)$$

where $f(\kappa r_p)$ is the Henry's function depending on the EDL thickness and the particle radius. If the fluid is aqueous media with moderate electrolyte concentration and has a dielectric constant larger than 20 (e.g., 80 for water), $f(\kappa r_p) = 1.5$ by Smoluchowski's approximation. Otherwise, $f(\kappa r_p) = 1.0$ by Hückel approximation. Therefore, the greater the mobility, the higher the zeta potential. The measured zeta potential can be used to calculate the stability of a particle in solution by DLVO theory, which was previously discussed in section 2.2.3.

One important thing to be considered when measuring the zeta potential and particle size distribution is that both measurements assume the colloidal suspension is stable during measurement. Thus, if sedimentation occurs during the measurement,

the data are not reliable; so for example, the quality report given by the equipment should be checked carefully.

A colloidal suspension is considered to be stable when the absolute value of measured zeta potential is over 25 – 30 mV (Das et al., 2007; Schenkel and Kitchener, 1960). Zeta potential is strongly dependent on the pH value of the fluid; $|\zeta|$ is higher when charged particles are surrounded by more counter ions, and a fluid at pH close to 1 or 13 has higher H^+ or OH^- ion concentration, so H^+ or OH^- ions can sufficiently form stern and diffuse layers to the slipping plane.

The *isoelectric point* (IEP) is a pH when the electrophoretic mobility is zero and the *point of zero charge* (PZC) is a pH when the net charge of the surface of the particle is zero (Parks, 1965). Generally, IEP and PZC can be used interchangeably, but IEP can be compensated by surroundings while PZC is the bulk phenomena; when surfactant is used, IEP changes.

Fig. 2.18 shows the typical zeta potential in relation to pH of the fluid. The sign of zeta potential of a colloidal system is decided as following:

$$\left\{ \begin{array}{l} \zeta > 0 \quad \text{if } pH < \text{IEP} \\ \zeta = 0 \quad \text{if } pH = \text{IEP} \\ \zeta < 0 \quad \text{if } pH > \text{IEP}. \end{array} \right. \quad (2.18)$$

In HCl or NaOH added aqueous fluid without salts, H^+ ions prevail at $pH < 7$ and OH^- ions prevail at $pH > 7$. When the net charge of the surface reaches zero, it means the equilibrium of cations and anions; pH at PZC or IEP. Either the concentration of cations or anions on the surface will be larger when $pH \neq \text{IEP}$.

The isoelectric points for some solids are listed in Table 2.4. Knowing the isoelectric point helps finding optimal pH that increase the dispersion stability of nanofluids; pH of fluid can be controlled to be far from IEP or surfactants can be used to stabilise

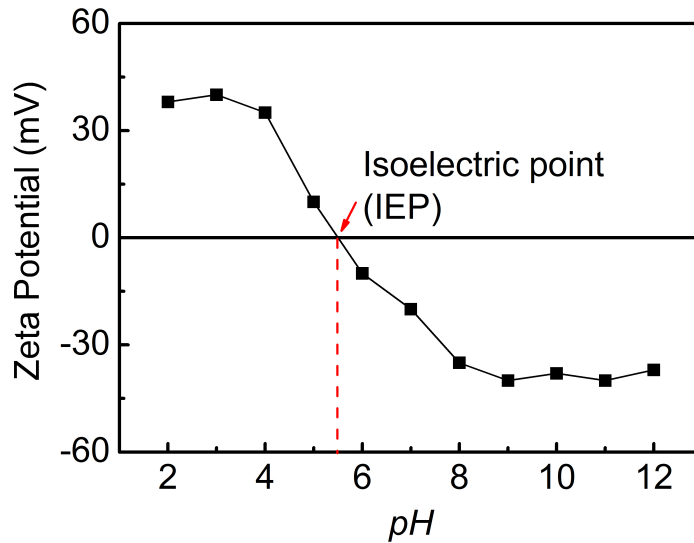


Fig. 2.18 Typical example of change in zeta potential with respect to pH of the fluid.

Table 2.4 Isoelectric point (IEP) of some solids (Parks, 1965; Parks and Bruyn, 1962).

Material	Isoelectric points (pH)
Al_2O_3	5, 6.6, 6.94, 9.2
TiO_2 (rutile)	4.7, 6.2, 6.7
CuO	9.5 ± 0.4
Cu	9.4 – 10.1
Fe	11.3 – 12.4
Cr	8.2 – 9.3
Ni	7.9 – 10.3

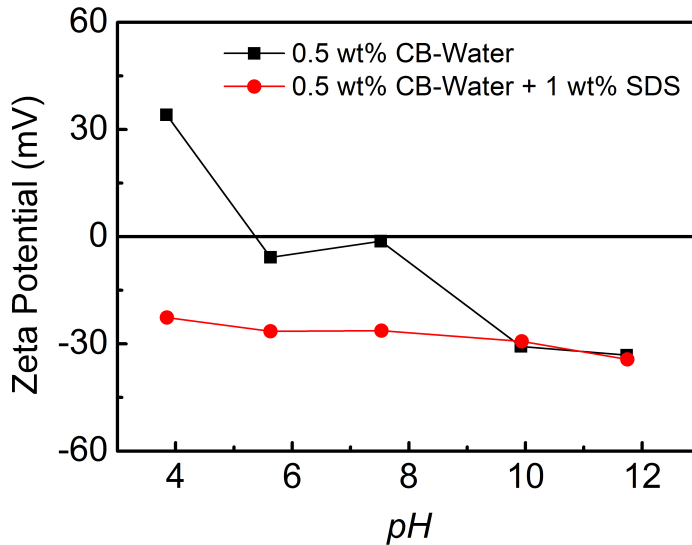


Fig. 2.19 The zeta potential change by SDS surfactant addition to carbon black (CB)-water nanofluids with respect to pH (Hwang et al., 2008).

the particle surface at pH near IEP. In most cases, IEP of oxides are $pH < 7$ and metals are $pH > 7$, so those oxide particles will be stabilised in acidic solution more easily.

Fig. 2.19 shows the effect of pH control and surfactant addition in carbon black-water nanofluids (Hwang et al., 2008). The zeta potential is in the stable range when the pH of fluid is controlled to below 4 or over 10 without surfactant addition. After SDS addition, the absolute zeta potential increased in big degree at $pH 6 - 8$, at where particles could not be stabilised electrostatically. When surfactants are added, they will be adsorbed on the particle surface and influence the electrophoretic mobility.

However, it is difficult to measure the zeta potential of nanofluids at high particle concentrations, with dark particle color or non-aqueous base fluids. Although, the particle size distribution or zeta potential can be measured by the equipment, the reliability of the data (*e.g.* correlation coefficient given by the equipment) can be low. Therefore, the stability of nanofluids should be investigated by using various methods,

not using one method solely.

2.3.5 Absorbance

The absorbance of a colloid is a measure of how much the particles in the fluid absorb light. Absorption is a feature of colloids since the particles dispersed in the fluid will absorb energy and light will scatter when exposed to a beam of light if they do not dissolve and stay in well-dispersed state.

An instrument directs light of a specific wavelength upon the sample at a certain position as in Fig. 2.20. By Beer-Lambert law, the absorbance A is a function of the transmittance T , the fraction of transmitted light through a given thickness of the absorbing medium contained in a transparent cell (Swinehart, 1962; Tam and Zardecki, 1982).

$$T = \frac{I}{I_0}, \quad (2.19)$$

where I_0 and I are the intensities of the incident light and transmitted light, respectively. The percent transmittance $\%T = 100T$ is also frequently used. Then, absorbance is,

$$A = \log \frac{1}{T} = \log \frac{100}{\%T} = 2 - \log \%T. \quad (2.20)$$

If all of the light passes through the medium (no absorption), $\%T = 100$ and $A = 0$.

If the absorbance is measured repeatedly over time under identical conditions and without moving the sample, the measured absorbance will change. Particles in the fluid will gradually settle down, and the fluid where the light passes will have a lower concentration and be closer to water as in Fig. 2.21. The absorbance of a fluid and its particle concentration has a linear relationship, which is also described by Beer-Lambert law (Swinehart, 1962; Tam and Zardecki, 1982). The amount of absorbed

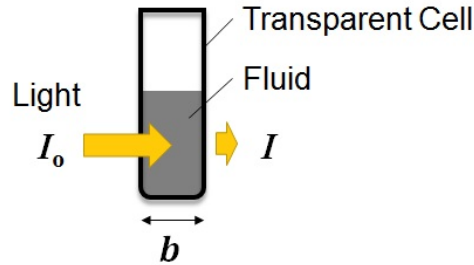


Fig. 2.20 A schematic of absorbance measurement using a UV-vis-Spectrophotometer, for example.

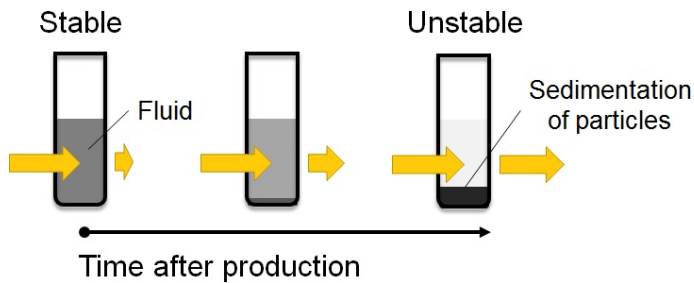


Fig. 2.21 A schematic of absorbance measurement over time. The intensity of absorbed light decreases and transmitted light increases.

light depends on the concentration of particles in the fluid c :

$$A = \epsilon bc \quad (2.21)$$

where ϵ is the molar absorptivity of the particle and b is the path length of the sample in Fig. 2.20.

The molar absorptivity or molar extinction coefficient ϵ is a measure of how strongly a material absorbs light at a particular wavelength and the unit is $[\text{m}^2 \text{mol}^{-1}]$ or $[\text{L mol}^{-1} \text{cm}^{-1}]$. This coefficient can be obtained experimentally by measuring the

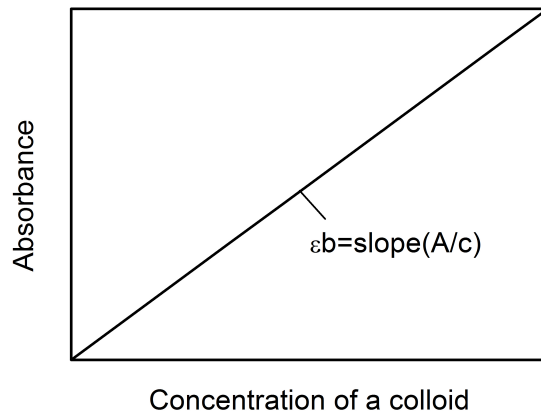


Fig. 2.22 Absorbance as a function of a colloid concentration (both in linear scale).

absorbance at several concentrations. Because the molar absorptivity is a material property and the path length is fixed during measurements, the slope of absorbance versus colloid concentration in Fig. 2.22 is the product of the molar absorptivity ϵ and the path length b . Thus, the concentration decrease over time due to sedimentation of particles can be calculated by the measured absorbance over time.

Fig. 2.23 shows the absorbance and zeta potential change of 0.05 wt% Al_2O_3 -water by pH variation and surfactant concentration studied by Wang *et al.* (2011). After 24 hours of the production, at pH around 6, the absorbance is highest and the magnitude of zeta potential is also largest. When SDS is added at the optimal pH 6 fluid, zeta potential did not change much but the absorbance increased from 0.8 to 1.2 with 0.10 wt% SDS addition implying sedimentation of particles become quite slower. This figure shows a close relationship between zeta potential and absorbance; when sedimentation is slower (absorbance decrease is slower), $|\zeta|$ are higher in most cases.

This method does not have the limitations that previously mentioned measure-

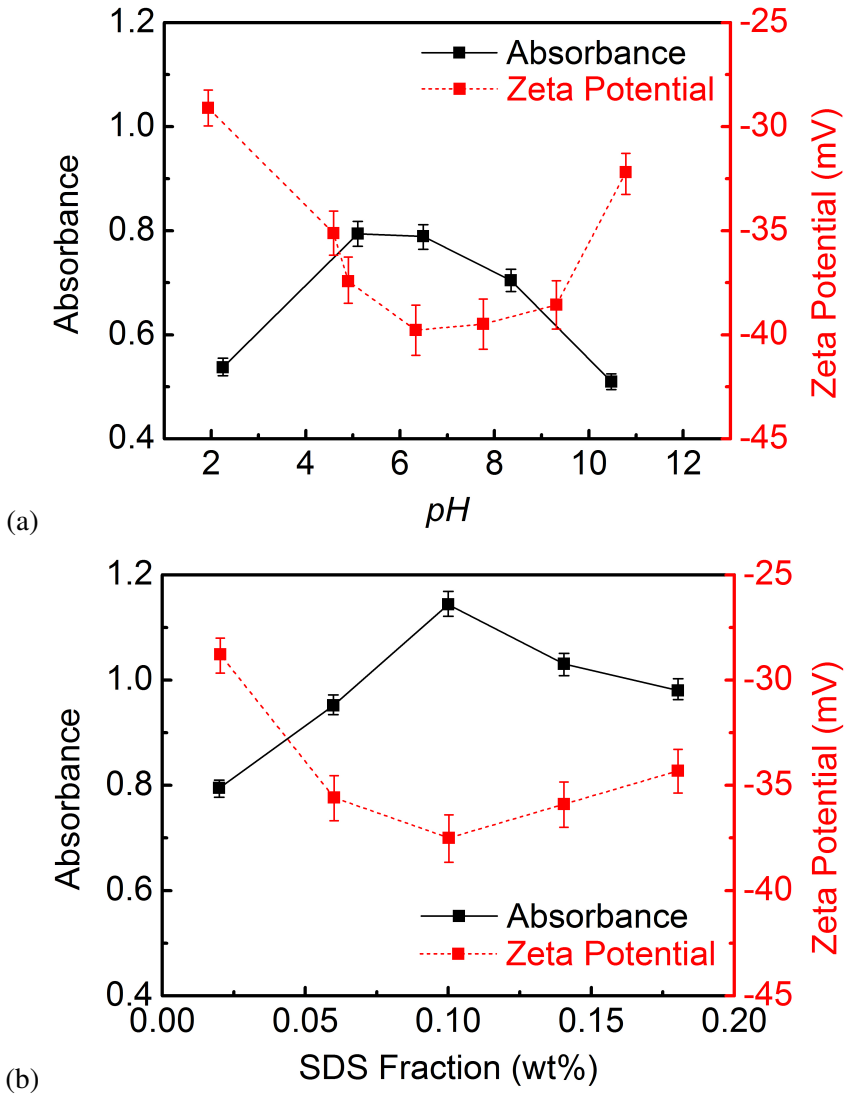


Fig. 2.23 Zeta potential and absorbance of 0.05 wt% Al₂O₃-Water nanofluid after 24 hours. (a) With *pH* variation without any additives and (b) added SDS fraction effect at optimal *pH* around 6. Original figure from (Wang et al., 2011) is reproduced.

ments have: it is applicable for low to high concentration, measurement is available during sedimentation, and it is possible to compare sedimentation rate. Although the force balance of particles and fluid molecules cannot be explained in detail with absorbance measurements, it is the easiest method to observe the overall stability for various nanofluids. If the absorbance of the nanofluid does not change for a certain period, it can be considered as a “stable nanofluid.”

2.4 Thermal Conductivity

As shortly discussed in section 1.1, the significantly enhanced heat conduction property of nanofluids cannot be explained up to date. To describe the mechanism, there is a need to understand what is heat conduction and thermal conductivity and their characteristics thoroughly. In this section, the fundamentals needed to understand the heat conduction of nanofluids will be reviewed; from single phase liquids and solids to their heterogenous mixtures. Since the base fluids studied are water and ethylene glycol and particles are aluminum oxide and stainless steel in this work, the review will be focused especially on those.

2.4.1 Thermal conductivity of materials

Heat transfer is defined as the thermal energy transfer due to a temperature difference (Incropera, 2011). There are three modes of heat transfer as in Fig. 2.24; conduction, convection and radiation. Conduction is heat transfer caused by molecular vibration, so it happens at even in stationary medium which may be a solid or a fluid. Heat can be transferred between a surface and a moving fluid which is convection. Radiation is heat transfer between surfaces without intervening medium. Heat is not transferred by a single mode in nature, but one mode may be dominant enough that the others can be neglected.

Heat transfer processes can be quantified in terms of appropriate rate equations, used to compute the amount of energy being transferred per unit time (Incropera, 2011). Fourier's law is the rate equation for heat conduction (Fourier, 1822):

$$q'' = -k\nabla T, \quad (2.22)$$

describing q'' is heat flux [W m^{-2}] in the direction of the heat flow which is propor-

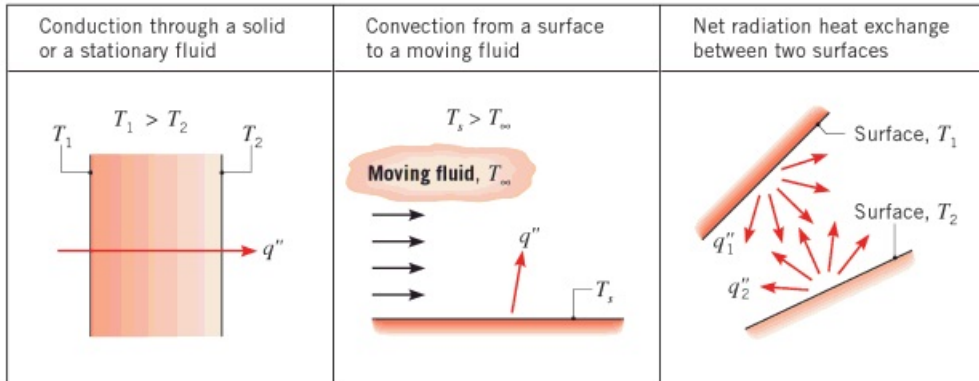


Fig. 2.24 Conduction, convection and radiation heat transfer modes from (Incropera, 2011).

tional to the temperature gradient ∇T in that direction with a constant k which is the thermal conductivity.

Thermal conductivity k with the unit of $[\text{W m}^{-1} \text{K}^{-1}]$, is a measure of the capability of a medium to conduct heat and a property depending on the material and the temperature. Fig. 2.25 shows the thermal conductivity of various materials and Fig. 2.26 shows the effect of temperature. Solids than liquids or gases, and metals than others have higher thermal conductivity. Thermal conductivity of common base fluids such as water is less dependent on temperature of $20 - 100^\circ\text{C}$ than copper, aluminum oxide, *etc* (Das et al., 2007). This is due to their different atomic structures and heat carriers. Carrier of heat depends on the media types; free electrons for metallic solids and liquids, electrons and phonons for nonmetallic solids and liquids, and atoms and molecules for gases. Dominant heat carrier is phonon in nonmetallic and free electron in metals. Detailed explanation on heat carriers with underlying theories are well discussed in (Kaviany, 2008, p. 1-9).

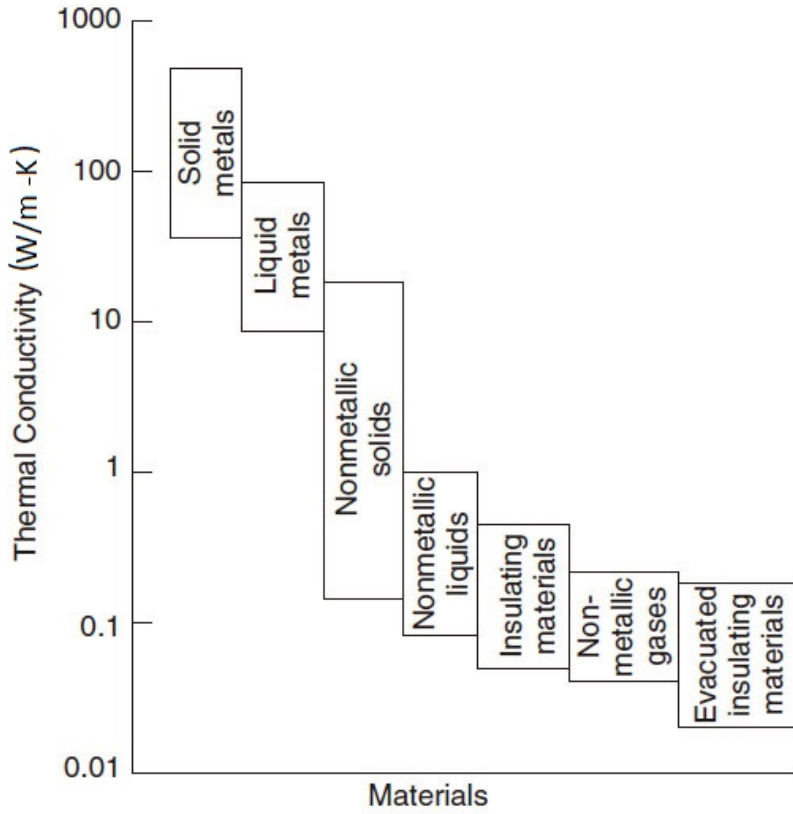


Fig. 2.25 Ranges of values of thermal conductivity of various materials from (Das et al., 2007).

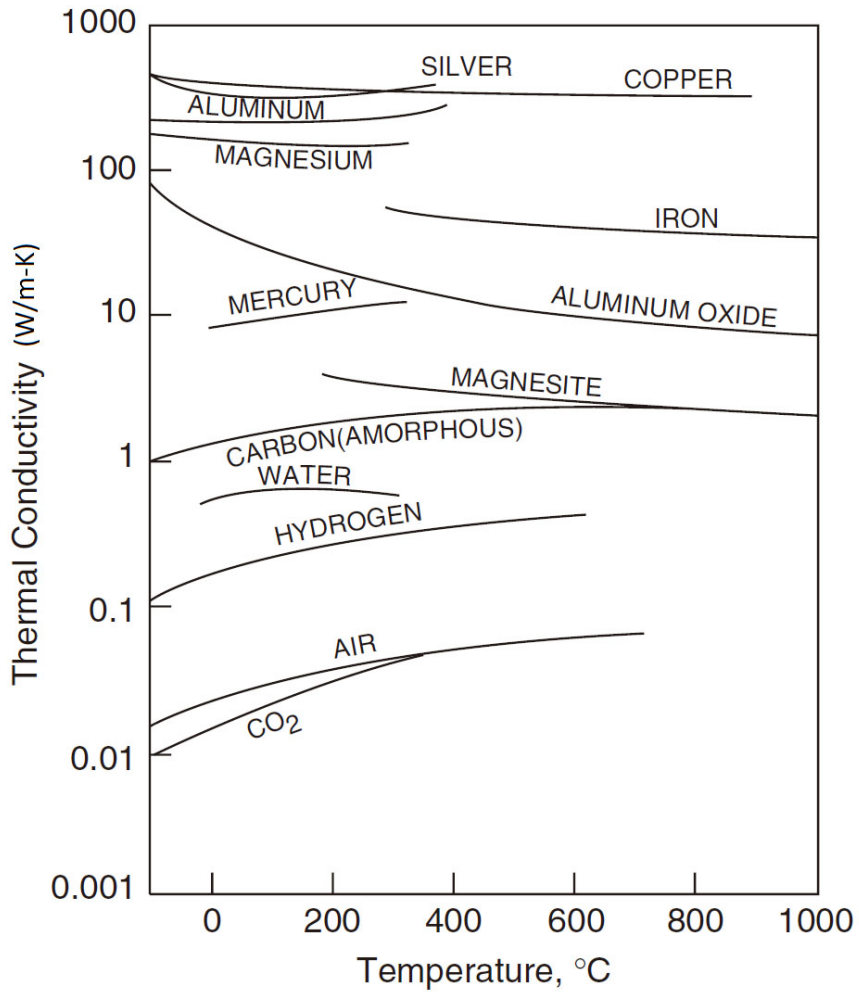


Fig. 2.26 Effect of temperature on thermal conductivity from (Das et al., 2007).

Liquids

Based on molecular properties, thermal conductivity of dense liquid k_f can be calculated as (Michaelides, 2014; Powell et al., 1941):

$$k_f = 2.793 \left(\frac{c_V}{c_p} \right)^{1/2} k_B \left(\frac{N_A}{V_m} \right)^{2/3} u \quad (2.23)$$

where V_m is the molar volume with the unit of $[\text{m}^3 \text{mol}^{-1}]$, c_V and c_p are specific heat at constant volume and constant pressure $[\text{J g}^{-1} \text{K}^{-1}]$, respectively, and u is the velocity of sound in the liquid. It is shown in (Powell et al., 1941) that calculated thermal conductivity using Eq. 2.23 agrees with experimentally observed data within the deviation of $\pm 20\%$.

Horrocks and McLaughlin (1963) derived the temperature dependence of liquids to thermal conductivity by the vibrational theory as:

$$\frac{1}{k_f} \frac{dk_f}{dT} = -\alpha \left\{ \frac{1}{3} - \left(\frac{\delta \ln v}{\delta \ln V_m} \right)_p \right\} \quad (2.24)$$

where α is the thermal expansion coefficient and $\gamma = \left(\frac{\delta \ln v}{\delta \ln V_m} \right)_p$ is the Grüneisen constant which is dimensionless.

Then, Viswanath and Rao (1970) used the equation of state for the liquid and the assumption that satisfies for temperature in the range of $0 - 150^\circ \text{C}$ to derive the following relationship:

$$\left(\frac{k_f(T)}{k_f(T_0)} \right) = \left(\frac{T}{T_0} \right)^{-n}, \quad (2.25)$$

where $k_f(T)$ is the thermal conductivity at temperature T . They showed a good agreement with the experimental results of paraffins and alcohols, and stated that finding accurate $k_f(T_0)$ and n is desirable.

Table 2.5 Molar mass M , specific heat capacity at constant pressure c_p , density ρ , speed of sound in given liquids u , isothermal compressibility κ and cubic thermal expansion coefficient α of water and ethylene glycol (EG) at room temperature of 20 – 25 °C. All data are from (Lide, 2004).

	M [g mol ⁻¹]	c_p [J g ⁻¹ K ⁻¹]	ρ [g cm ⁻³]	u [m s ⁻¹]	α [10 ⁻⁶ K ⁻¹]	κ [10 ⁻¹⁰ Pa ⁻¹]
Water	18.015	4.18	0.99821	1497	206	4.591
EG	62.07	2.41	1.108	1658	626	3.64

To verify the applicability of Eq. 2.23, Eq. 2.24 and Eq. 2.25 to water and ethylene glycol, calculated results are compared with experimental data from literature. Physical and thermal properties needed for calculations at room temperature except c_V and γ are listed in Table 2.5. Specific heat at constant volume can be derived from the specific heat at constant pressure as:

$$c_p - c_V = \frac{\alpha^2 T}{\rho \kappa}, \quad (2.26)$$

and the molar volume is $V_m = M/\rho$. Then, the thermal conductivity at room temperature can be calculated using Eq. 2.23, and Table 2.6 shows the results are within $\pm 4\%$ of experimental data from literature.

The Grüneisen constant γ can be calculated either using c_p or c_V as:

$$\gamma = \left(\frac{\delta \ln v}{\delta \ln V_m} \right)_p = \frac{u^2 \alpha}{c_p}, \quad (2.27a)$$

$$\gamma = \left(\frac{\delta \ln v}{\delta \ln V_m} \right)_p = \frac{\alpha}{\kappa c_V \rho}. \quad (2.27b)$$

Calculated Gruneisen constant of water using Eq. 2.27a and Eq. 2.27b are 0.110 and

Table 2.6 Calculated specific heat at constant volume c_V using Eq. 2.26 and the thermal conductivity k using Eq. 2.23 of water and ethylene glycol (EG) at room temperature of 20 – 25 °C compared with data from literature, [*] Kuroki et al. (2001) and [**] Lide (2004). Calc. and Ref. indicate calculated and literature values, respectively.

Material	c_V [J g ⁻¹ K ⁻¹]		k [W m ⁻¹ K ⁻¹]		% Error $\frac{ k_{\text{calc}} - k_{\text{ref}} }{k_{\text{ref}}} \times 100$
	Calc.	Ref. [*]	Calc. k_{calc}	Ref. k_{ref} [**]	
Water	4.15	4.08 (43 °C)	0.5961	0.5984 (20 °C)	0.39 %
EG	2.12		0.2922	0.256 (25 °C)	3.62 %

Table 2.7 The Grüneisen constant γ with constant specific volume of 1.00 cm³ g⁻¹ (Knopff and Shapiro, 1970) and thermal conductivity k [W m⁻¹ K⁻¹] (Lide, 2004) of water at temperature range of 0 – 100 °C.

T	0	10	20	30	40	50	60	70	80	90	100
γ		0.025	0.103	0.173	0.230	0.279	0.324	0.363	0.402		
k	0.561	0.580	0.598	0.615	0.631	0.644	0.654	0.663	0.670	0.675	0.679

0.108, respectively, which is close to the calculated result from (Knopff and Shapiro, 1970) listed in Table 2.7. Using Eq. 2.27 and integrating Eq. 2.24 with respect to T , thermal conductivity of a liquid can be expressed as a function of temperature.

However, whilst γ is independent of temperature at most crystalline solids (Lide, 2004), it strongly depends on the temperature of liquid. For example as in Table 2.7, γ is 0.02 at 10 °C and increases up to 0.4 at 80 °C (Knopff and Shapiro, 1970). Thus, Eq. 2.24 cannot be integrated simply with respect to T . There can be several ways to express $\frac{1}{k_f} \frac{dk_f}{dT}$ of Eq. 2.24 as a function of temperature, but not explicit nor simple general equation for liquids exist.

In addition, the value of n of Eq. 2.25 increases from -0.83 at 30 °C to -0.52 at 100 °C for $T_0 = 293.15$ K, so both Eq. 2.24 and Eq. 2.25 cannot describe the tempera-

ture dependent water thermal conductivity exactly. Therefore, it is better to use fitting function instead for each base fluids, as the measured thermal conductivity of water and ethylene glycol at 0 – 100°C are easy to find in literature.

Solids

Thermal conductivity data of solids at various temperature can be found from literature listed in Table 2.8. As shown in Fig. 2.27, metallic elements generally have higher thermal conductivity than others.

Heat in solids exist and transport by vibrations and waves of phonons and translations of free electrons. Dominant heat carrier is phonons in dielectric materials and free electrons in metals (Michaelides, 2014). The (total) thermal conductivity of metals k_{metal} is (Ho et al., 1972; Kaviany, 2008; Michaelides, 2014):

$$k_{\text{metal}} = k_e + k_{\text{ph}} \approx k_e \quad (2.28)$$

because the contribution by electron is orders of magnitude higher than phonons in metals, where k_e and k_{ph} are thermal conductivities due to electrons and phonons, respectively.

Table 2.8 Previous studies on thermal conductivity of various elements, metals, and alloys at low to high temperatures.

Reference	Studied solids	Temperature range
Powell and Blanpied (1954)	Metallic elements and alloys	0 – 300 K
Rosenberg (1955)	High purity 32 metals	10 – 40 K
Ho et al. (1972)	Elements	1 – 10 ³ K

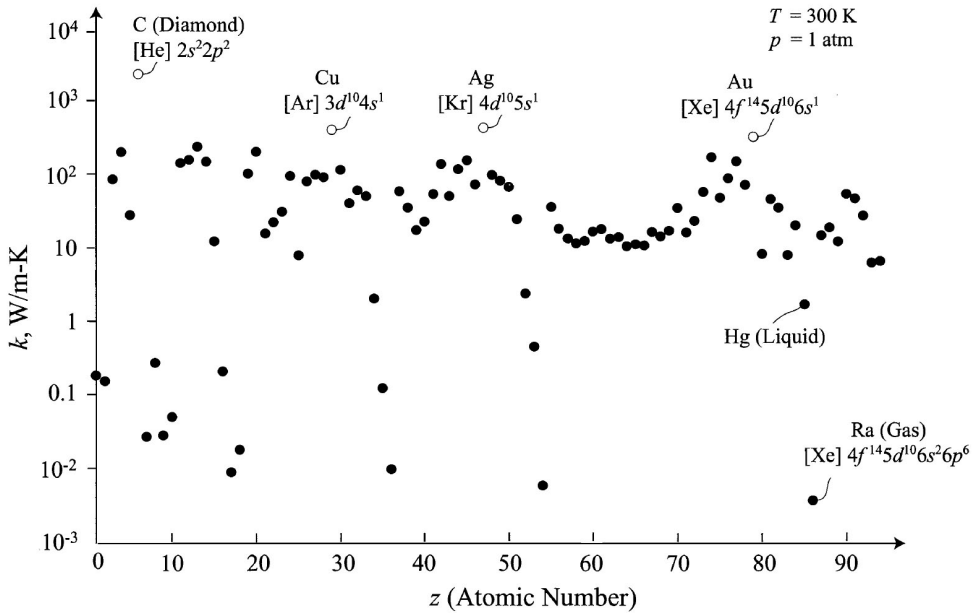


Fig. 2.27 Thermal conductivity of elements at 300 K from (Kaviany, 2008).

The electronic thermal conductivity of metals has a linear relationship with electrical conductivity by the Wiedemann-Franz-Lorenz law (Kaviany, 2008; Kumar et al., 1993; Tritt, 2004):

$$\frac{k_s}{\sigma_e T} = \frac{\pi^2}{3} \left(\frac{k_B}{e} \right)^2 = 2.44 \times 10^{-8} \text{ W}\Omega\text{K}^{-2} = N_L, \quad (2.29)$$

where σ_e is the electrical conductivity of metal [$\Omega^{-1}\text{m}^{-1}$] and N_L is the Lorentz number. Table 2.9 shows experimentally observed Lorentz number depends on temperature but all are very close to $2.44 \times 10^{-8} \text{ W}\Omega\text{K}^{-2}$. At high temperatures, all metals generally follows this law, but not at low temperatures as shown in Fig. 2.28.

Fig. 2.29 shows the experimental total thermal conductivity of gold, copper and iron in the temperature range of 1 – 1000 K is similar to the electrical thermal conduc-

Table 2.9 Mean Debye temperature T_D [K] (Kaviany, 2008, p. 582-583) and Lorenz number N_L [$\text{W } \Omega \text{K}^{-2}$] at specific temperature of gold, copper (Kaviany, 2008, p. 169) and iron (Kumar et al., 1993).

	Au	Cu	Fe
T_D	170	315	400
N_L at 273 K	2.35×10^{-8}	2.23×10^{-8}	
N_L at 373 K	2.40×10^{-8}	2.33×10^{-8}	
N_L at 2 – 100 K			2.5×10^{-8}

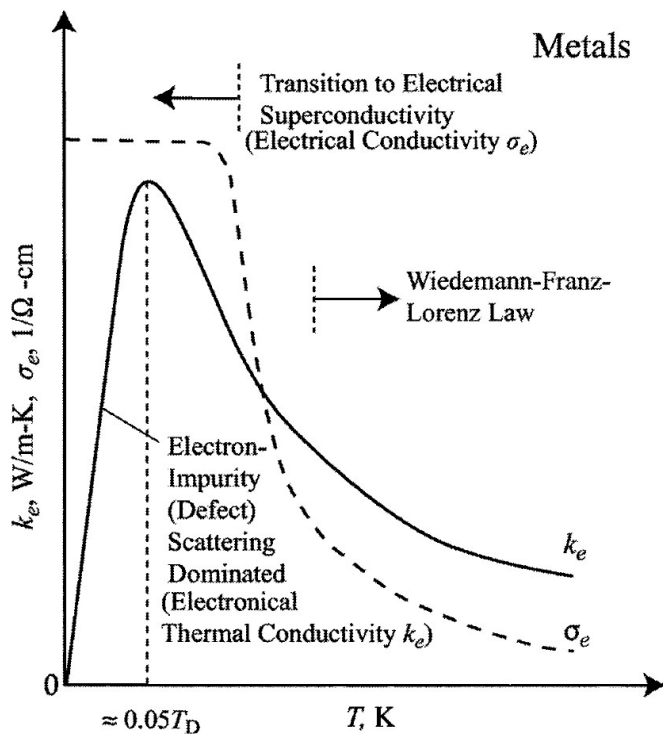


Fig. 2.28 The electrical conductivity and electronic thermal conductivity of metals with respect to temperature from (Kaviany, 2008).

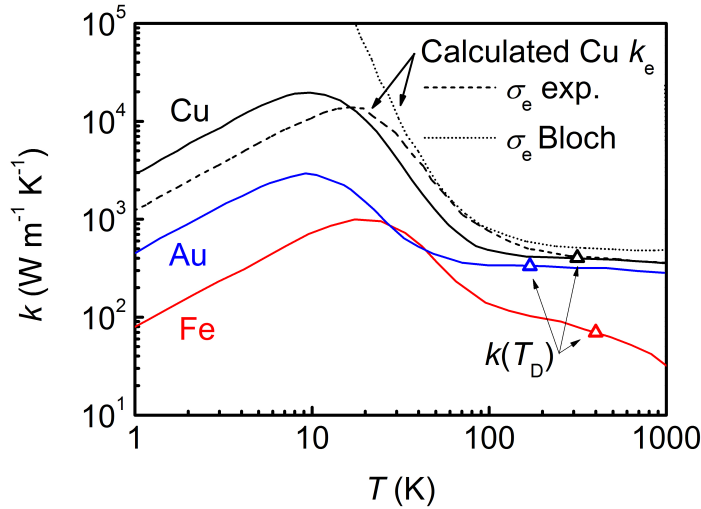


Fig. 2.29 Measured total thermal conductivity of gold, copper and iron with respect to temperature and calculated electronic thermal conductivity of copper using Eq. 2.29 with electrical conductivity from experiment and Bloch model of Eq. 2.30. Thermal conductivities at Debye temperature $k(T_D)$ are indicated with a triangular symbol. Original figure from (Kaviany, 2008) is reproduced.

tivity graph in Fig. 2.28. The calculated electrical thermal conductivity of copper using Eq. 2.29 well matches to experimental thermal conductivity at temperature above 0°C when experimental electrical conductivity data at various temperatures exist.

When the electrical conductivity data of a metal at various temperature is not known, it can be calculated approximately using Bloch model as (Kaviany, 2008):

$$\frac{\sigma_e(T_D)}{\sigma_e(T)} = 3.7 \left(\frac{T}{T_D} \right)^5 \int_0^{T_D/T} \frac{x^5 e^x}{(e^x - 1)^2} dx \quad (2.30)$$

when the electrical conductivity at Debye temperature T_D is known; T_D of gold, copper and iron is listed in Table 2.9. Fig. 2.29 shows that prediction of copper k_e using calculated σ_e from Eq. 2.30 is also quite close to the experimental values at temperature above 100 K. Thus, at room temperature and above, it can be concluded that heat in

copper is mostly carried by free electrons.

Because only the heat conduction at temperature between 0 to 100 °C will be considered in this work, the Wiedemann-Franz-Lorenz law with the Bloch model is applicable to describe the thermal conductivity of metallic particles. The electrical resistivity and thermal conductivity for iron and some chromium and nickel added iron-based alloys at 90 – 400 K can be found in (Williams et al., 1981).

2.4.2 Thermal Conductivity of Mixtures

Thermal conductivity of solid-liquid heterogeneous mixtures can be described by the Maxwell's model of Eq. 1.1 which consider the thermal conductivities of solid particle and base liquid and particle volume fraction with the assumption of particles are spherical and mixture is very dilute (Maxwell, 1873).

After Maxwell, there were several attempts to extend the model considering other effects such as the shape of non-spherical particles (Hamilton and Crosser, 1962), wide ranges of particle volume fractions (Bruggeman, 1935), particle interactions (Cheng and Vachon, 1969; Davis, 1986; Jeffrey, 1973; Lu and Lin, 1996), *etc.*

Hamilton and Crosser (1962) considered the shape of non-spherical particles adding the particle shape factor n as:

$$\frac{k_{\text{eff}}}{k_f} = \frac{\alpha + (n-1) - (n-1)(1-\alpha)\phi}{\alpha + (n-1) + (1-\alpha)\phi}, \quad (2.31)$$

where $\alpha = \frac{k_p}{k_f}$ is thermal conductivity ratio of particle and fluid. $n = 3$ for spherical particles and the model becomes identical to Maxwell's, and $n = 6$ for cylindrical particles. This model is valid when the particle volume fraction is very small, $\phi \ll 1$, like Maxwell's model.

Particle interactions are considered by Jeffrey (1973) and Davis (1986). Jeffrey's

model is:

$$\frac{k_{\text{eff}}}{k_f} = 1 + 3\beta\phi + (3\beta^2 + \frac{3\beta^3}{4} + \frac{9\beta^3}{4^2} \frac{\alpha+2}{2\alpha+3} + \frac{3\beta^4}{4^3} + \dots)\phi^2, \quad (2.32)$$

where $\beta = \frac{\alpha-1}{\alpha+2}$, and Davis' model is:

$$\frac{k_{\text{eff}}}{k_f} = 1 + \frac{3(\alpha-1)}{(\alpha+2) - (\alpha-1)\phi} [\phi + f(\alpha)\phi^2 + O(\phi^3)]. \quad (2.33)$$

where $f(\alpha) = 2.5$ for $\alpha = 10$, $f(\alpha) = 0.5$ for $\alpha = \infty$. In both models, high-order terms represent considered the pair interactions of randomly dispersed spheres.

Lu and Lin (1996) considered near- and far-field pair interactions and also spherical and non-spherical particles:

$$\frac{k_{\text{eff}}}{k_f} = 1 + a\phi + b\phi^2, \quad (2.34)$$

where $a = 2.25$, $b = 2.27$ for $\alpha = 10$ and $a = 3.00$, $b = 4.51$ for $\alpha = \infty$ are for spherical particles (Choi et al., 2001).

Theoretical models introduced in this section are called “conventional models”. It will be shown in section 2.5.2 that the thermal conductivity enhancement of nanofluids to the base fluids cannot be explained fully by conventional models.

2.5 Previous Studies on Thermal Conductivity of Nanofluids

Increase in the effective thermal conductivity of fluids is important in improving the heat transfer behavior of fluids and its value is also important in other heat transfer modes such as convection. Therefore, being able to predict the effective thermal conductivity of nanofluids and understanding the underlying mechanisms are important to apply nanofluids in heat transfer applications.

2.5.1 Effect Parameters

At first, experiments have been focused on to the parameters that enhance the thermal conductivity of nanofluids. The volume fraction, material, size and shape of nanoparticles, the material and acidity of the base fluid, temperature of nanofluids, sonication power and time, and additives are reported to influence the thermal conductivity of nanofluids (Chandrasekar and Suresh, 2009; Das et al., 2007; Fan and Wang, 2011; Kleinstreuer and Feng, 2011; Özerinç et al., 2010).

Particle volume fraction and material

Particle volume fraction and type of the material effects are well shown in Fig. 1.1. Thermal conductivity increases as more particles are added to the base fluid. Although there needs more investigation to set a model to predict the thermal conductivity of nanofluids including other effect parameters, both experimental results and theoretical models in section 2.4.2 and section 2.5.2 show near-linear relationship between enhancement and particle fraction. The enhancement also varies in terms of the type of nanoparticles; generally enhancement is larger in the order of nanotubes, metallic particles, and ceramics as in Fig. 1.1.

Particle size

It was thought that a decrease in the size of the dispersed particles results in an increase in the thermal conductivity of nanofluids (Jang and Choi, 2007), but there are also contrary experimental observations that Beck et al. (2009) reported. These contrary size effects are compared in Fig. 2.30 with 3 vol.% Al₂O₃-water nanofluids. Jang and Choi (2007) proposed the model considering the particle size and fluid temperature as parameters (black dash) which well matched to the measured enhancement of Masuda et al. (1993) and Lee et al. (1999) (black symbols).

Beck et al. (2009) used Al₂O₃ particles with various sizes and observed the enhancement decreasing when particles becoming smaller and explained this is because of phonon scattering at the solid-liquid interface. The particle size effect was observed at 2, 3 and 4 vol.%, and then the conductivity enhancement was fitted including particle volume fraction and size as parameters. The red dash line is the fitted model of

$$\frac{k_{\text{eff}}}{k_f} = 1 + \xi_{\text{gm}} \phi (1 - \exp^{-0.025d_p}), \quad (2.35)$$

at 3 vol.% Al₂O₃-water; $\xi_{\text{gm}} = 4.4134$ for water, $\phi = 0.03$ and d_p in nanometre unit. The experimental results from (Das et al., 2003; Oh et al., 2008; Xie et al., 2002) represented in blue symbols in Fig. 2.30 seems to be close to the fitted formula of Eq. 2.35. However, this model is empirical using fitting constants, and describes only some of the data available, not all, and has no physical meaning in using constants such as 4.4134 and -0.025 . Therefore the model may not properly predict the enhancement when volume fraction or particle type is changed.

The effect of particle(s) size to thermal conductivity enhancement needs more study to verify its role. While the initial particle size (size of a particle) effect was discussed as aforementioned, some researchers focused on to the aggregate size. Par-

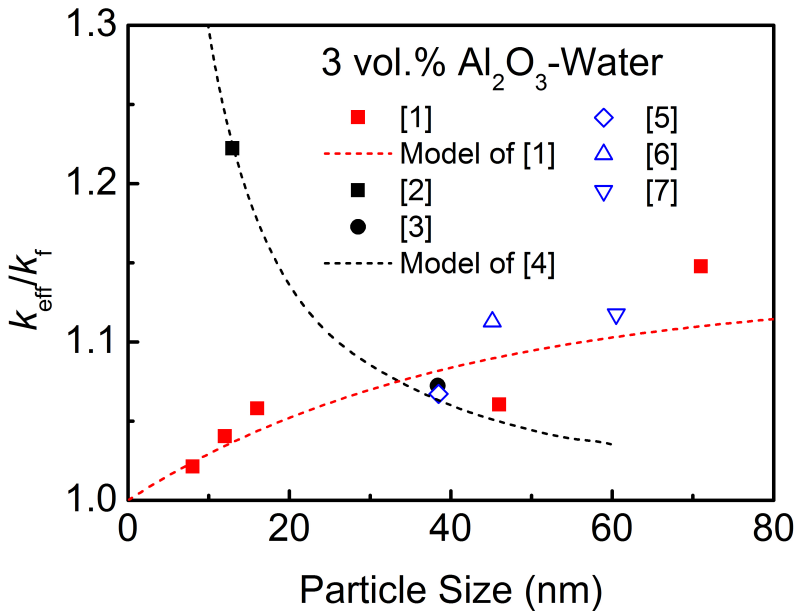


Fig. 2.30 Effect of particle size to the thermal conductivity enhancement of 3 vol.% Al_2O_3 -water nanofluids. Experimental data from previous studies are collected. Prediction using models from [1] and [4] are represented in red and black dash line, respectively. Red and black symbols are data used in each [1] and [4] model prediction. [1] Beck et al., 2009; [2] Masuda et al., 1993; [3] Lee et al., 1999; [4] Jang and Choi, 2007; [5] Das et al., 2003; [6] Oh et al., 2008; [7] Xie et al., 2002.

ticles in fluid can be attached and move together, and the heat transfer due to particles will occur between aggregates not between single particles. This heat transfer mechanism is called clustering or particle aggregation, and is discussed in section 2.5.2. There are conflicting opinions also on particle aggregation.

Fluid temperature and material

Thermal conductivity of liquids depend on temperature as discussed in section 2.4.1, and therefore the thermal conductivity enhancement of nanofluids due to existence of nanoparticles at specific temperature should be compared with the thermal conductiv-

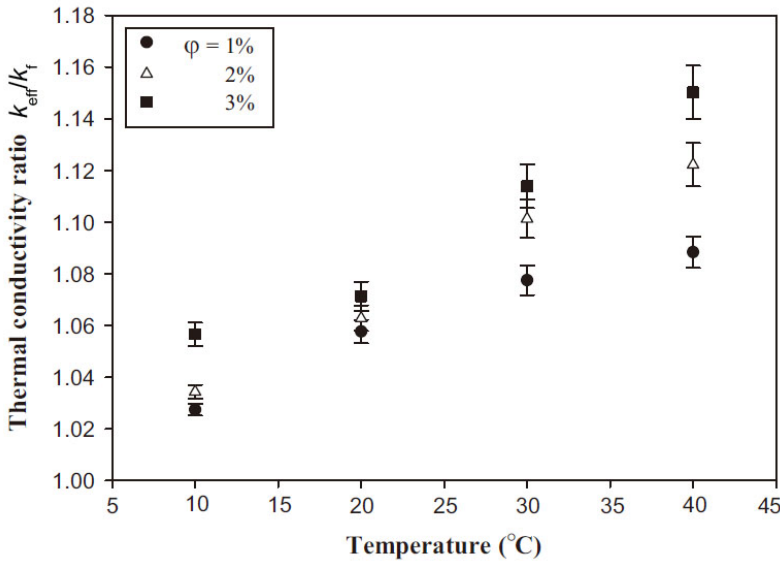


Fig. 2.31 Temperature effect on the thermal conductivity enhancement of 1, 2 and 3 vol.% Fe_3O_4 -water nanofluids from [Abareshi et al. \(2010\)](#). Thermal conductivity ratio here is $\frac{k_{eff}(T)}{k_f(20^\circ\text{C})}$.

ity of the base fluid at the temperature as:

$$\text{Enhancement at temperature } T = \frac{k_{eff}(T)}{k_f(T)}. \quad (2.36)$$

However, as in Fig. 2.31, some of previous studies used $\frac{k_{eff}(T)}{k_f(20-25^\circ\text{C})}$ ratio to show the fluid temperature effect ([Abareshi et al., 2010](#); [Das et al., 2003](#); [Jang and Choi, 2004](#)). Because the enhancement in these studies includes the enhancement coming from the fluid itself, the enhancement should be re-evaluated using Eq. 2.36. For example, thermal conductivity of water increases as temperature increases at 0 – 100 °C; $k_{\text{water}}(100^\circ\text{C}) = 1.13k_{\text{water}}(20^\circ\text{C})$ as in table 2.7.

There are contrary results on the temperature effect to thermal conductivity enhancement of nanofluids. [Beck et al. \(2010\)](#); [Singh et al. \(2009\)](#); [Timofeeva et al.](#)

(2007); Venerus et al. (2006) showed that the increase in thermal conductivity by increase in temperature are mostly from base fluid. Especially, Beck et al. (2010) observed this with 10 nm alumina particles dispersed into water, ethylene glycol and water+ethylene glycol mixture. On the other hand, Chon et al. (2005); Patel et al. (2003) showed the enhancement depending on the fluid temperature using Eq. 2.36. Chon et al. (2005) discussed that the Brownian velocity is the key mechanism to describe the temperature dependence.

***pH* of fluid, additives and sonication power and time**

The effect of *pH* (Gowda et al., 2010), surfactants (Murshed et al., 2012), and sonication power and time (Gowda et al., 2010; Hong et al., 2006, 2005) showed that the thermal conductivity can be increased by controlling these parameters. As discussed previously in sections 2.2 and 2.3, the acidity of the base fluid and additives such as surfactants or dispersants, and sonication power and time all influence the stability of nanofluids; particle dispersion in fluid and their agglomeration phenomena.

Only a few studies considered and observed the overall stability of nanofluids as summarized in section 5.1; the thermal conductivity of nanofluids were higher with better stability (Hwang et al., 2008; Lee et al., 2014; Li et al., 2007, 2008; Philip and Shima, 2012; Wang et al., 2009; Witharana et al., 2013; Yu and Xie, 2012). Others controlled one or two parameters to avoid rapid sedimentation that can be noticed visually or to produce and achieve higher thermal conductivity enhancement without considering its long term usage.

For example, Li et al. (2008) showed the relationship between stability and thermal conductivity enhancement. The optimal fluid *pH* and SDBS fraction to add to obtain sufficient stability were determined by particle size distribution and zeta potential measurements, respectively. Then the measured thermal conductivity enhancement at the

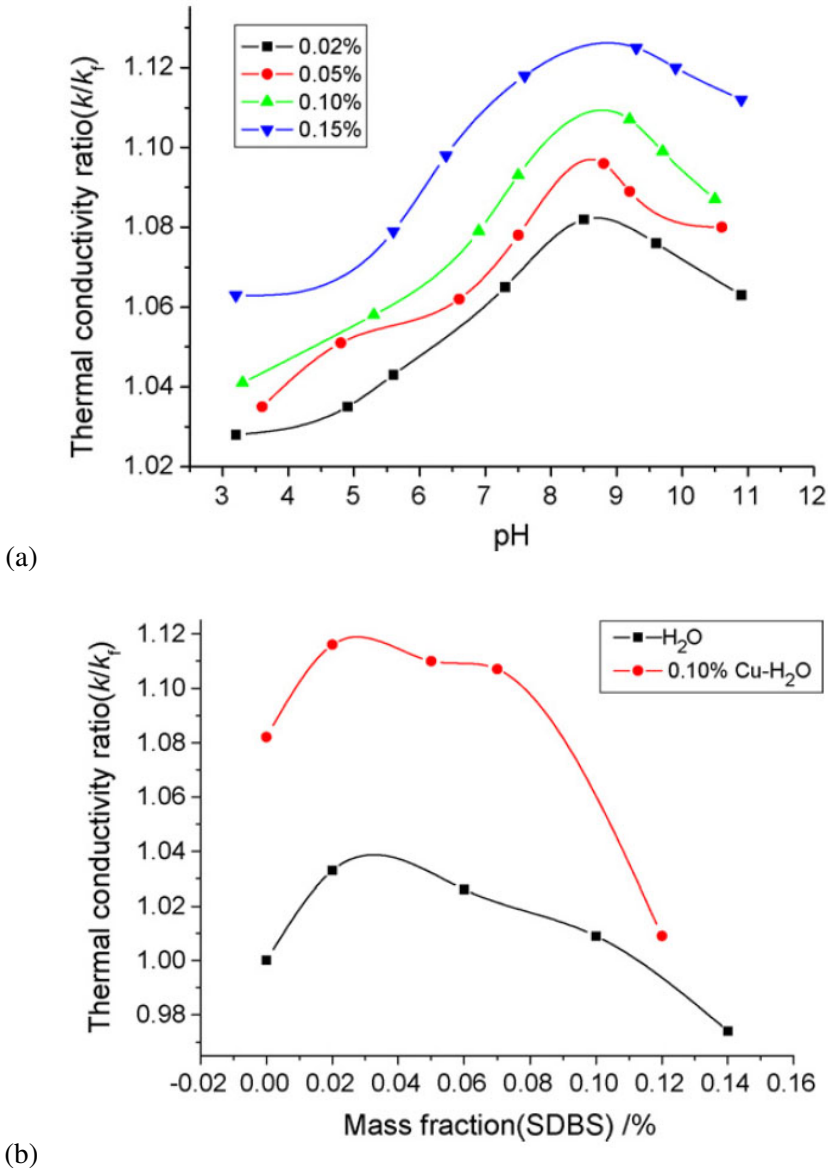


Fig. 2.32 Effect of (a) pH and (b) SDBS concentration on thermal conductivity enhancement of Cu-Water nanofluids from (Li et al., 2008). (a) Mass fraction of Cu is varied from 0.02 wt% to 0.15 wt% and 0.05 wt% SDBS was added in water. (b) Effect of SDBS fraction in water and 0.1 wt% Cu-water fluid is compared.

optimal conditions were higher as in Fig. 2.32.

2.5.2 Mechanisms of Heat Conduction

The proposed heat transfer mechanisms for thermal conductivity enhancement of nanofluids exceeding conventional predictions can be classified into static and dynamic mechanisms. The effect of liquid-layering and particle aggregation are static mechanisms whereas Brownian motion of particles and Brownian-motion-induced convection are dynamic mechanisms (Chandrasekar and Suresh, 2009; Fan and Wang, 2011; Michaelides, 2014). Fig. 2.33 is the sketch of four mechanisms shown by Fan and Wang (2011).

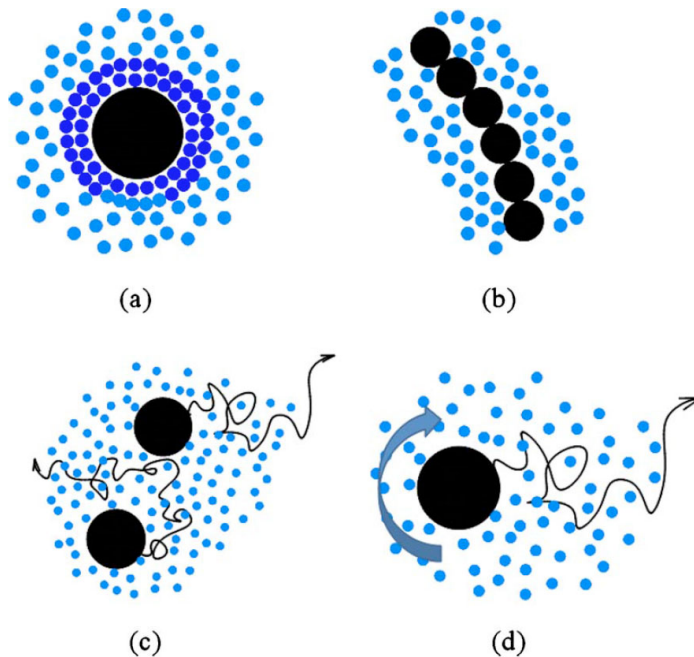


Fig. 2.33 Four mechanisms, (a) liquid-layering, (b) particle aggregation, (c) particle Brownian motion, and (d) Brownian-motion-induced convection to explain the thermal conductivity enhancement of nanofluids from (Fan and Wang, 2011).

Liquid-layering

The effect of liquid-layering was proposed to explain the anomalously increased thermal conductivity of a nanofluid containing carbon nanotube suspensions (Choi et al., 2001). Liquid-layering is the development of an ordered structure close to the solid/liquid interface as in Fig. 2.33(a), and the layer with ordered structure between solid and liquid is called nanolayer. The existence of this layer was thought to be possible after Yu et al. (1999) observed ordered layer of 0.1 nm thickness close to a smooth substrate surface by using synchrotron x-ray reflectivity in thin liquid films of 4.5 – 9 nm.

Choi et al. (2001) claimed the resulting nanolayer is expected to have a higher thermal conductivity than bulk liquid considering the order of magnitude higher thermal conductivity of the solids which have ordered structure when compared with that of liquid. Therefore, the ordered volume fraction with high thermal conductivity will increase with the existence of nanolayer which can act as a thermal bridge across the interface, and this may be the reason for discrepancies between the experimental and theoretical values as shown in Fig. 2.34.

While Leong et al. (2006); Murshed et al. (2006); Xue and Xu (2005); Xue (2003) developed new models to predict thermal conductivity enhancement considering liquid-layering effect and showed their models describe experimental results quite well or better than conventional models, the layer thickness had to be assumed by authors which cannot be measured or predicted precisely. (Kebllinski et al., 2002; Yu and Choi, 2003) did supported the concept but discussed the liquid-layering is not solely responsible for significant enhancement. Therefore, this mechanism is not sufficient to solely explain the thermal conductivity enhancement of nanofluids.

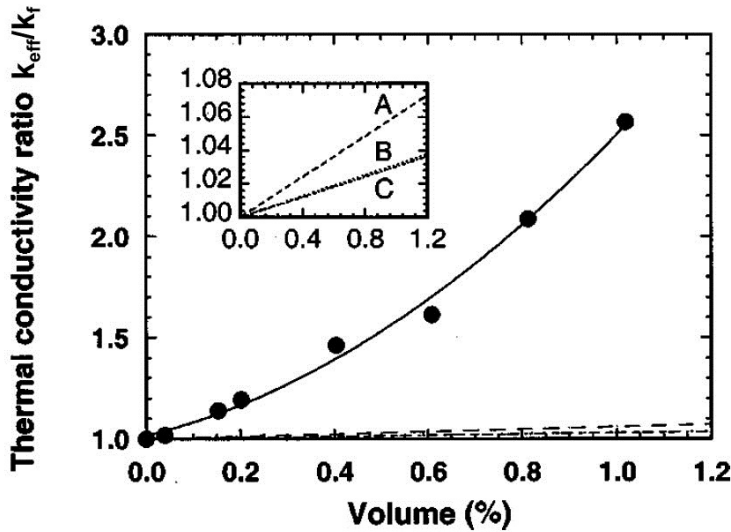


Fig. 2.34 Thermal conductivity enhancement as a function of carbon nanotube volume fraction from (Choi et al., 2001). Solid circles are experimental results and lines are predictions by Hamilton and Crosser (1962) for short dashed A, Bonnecaze and Brady (1990, 1991) for short dotted B, and Maxwell (1873) for dash-dotted C.

Particle aggregation or Clustering

The aggregation of nanoparticles has been proposed as one of the factors of thermal conductivity enhancement of nanofluids, with the suggestion that clusters like in Fig. 2.33(b) can be a path for heat flow and lower the thermal resistance, thus increasing the thermal conductivity (Kebllinski et al., 2002). Nanofluid aggregation in the form of chain structures has been observed as in Fig. 2.35, which is consistent with greater heat transport along the direction of the heat flow. The number of clusters was reported to increase with the volume fraction of nanoparticles (Kebllinski et al., 2002).

However, for clusters to help the heat conduction in nanofluids they should be well dispersed (Prasher et al., 2005) and have a small particle size (Feng et al., 2007), since

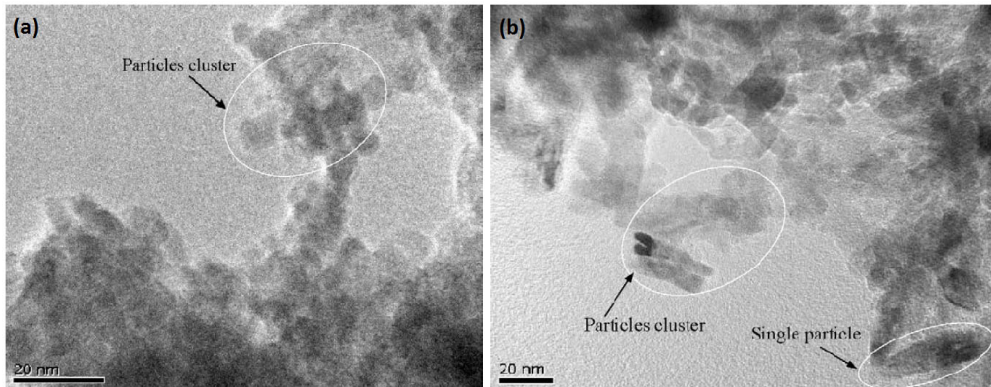


Fig. 2.35 TEM images of (a) spherical 15 nm and (b) cylindrical 10 nm-diameter and 40 nm-long TiO_2 particles in deionized water from (Murshed et al., 2005).

aggregations would make “particle free” liquid regions with reduced heat conduction properties (Chandrasekar and Suresh, 2009; Keblinski et al., 2002). In addition, aggregation of particles make particle to settle down more easily and deteriorate stability. For example, Karthikeyan et al. (2008) showed decreasing thermal conductivity enhancement due to formation of mesh-like structures after 20, 60 and 70 min.

Brownian motion and Brownian-motion-induced convection

The Brownian motion of particles due to the collisions with surrounding liquid molecules as shown in Fig. 2.33(c) has been suggested to increase heat transport among particles and thus increase the fluid thermal conductivity. Using orders-of-magnitude analysis, the contribution of the Brownian motion collisions between nanoparticles and base fluid molecules has been found by simulation to be bigger than collisions between nanoparticles or base fluid molecules (Jang and Choi, 2004, 2007), supporting the effect of Brownian motion (Jang and Choi, 2004; Koo and Kleinstreuer, 2004; Prasher et al., 2005). Fig. 2.36 shows that the new model including this effect has better agree-

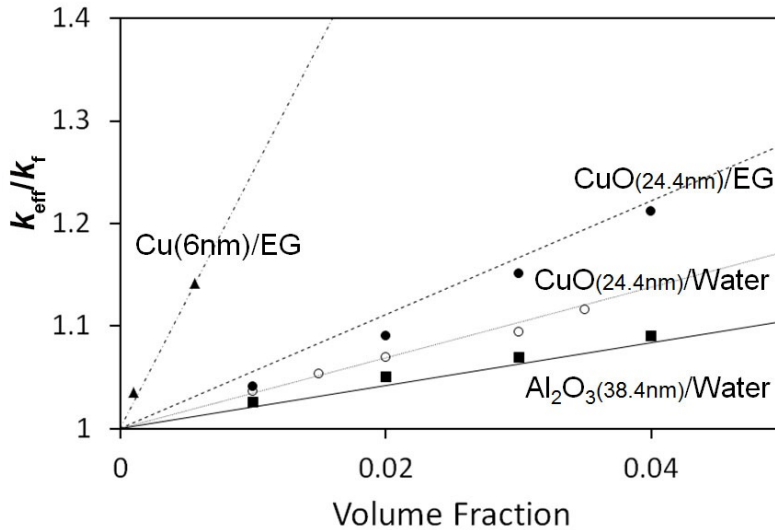


Fig. 2.36 Thermal conductivity enhancement as a function of volume fraction of particles. Symbols are experimental observations and lines are predictions made by new model in (Jang and Choi, 2004). Original figure is redrawn.

ment with experimental thermal conductivity enhancement results, but the model has a critical drawback because it needs empirical assumption.

However, since the ratio of thermal diffusion of particles is orders of magnitude smaller than that of fluid molecules, it has been proven analytically that the effect of Brownian motion is negligible (Beck et al., 2007; Koblinski et al., 2002). The arguments on the effect of Brownian motion are not concluded and theoretical models require fitting parameters (Prasher et al., 2005) which do not help interpretation. Thus, more investigations are needed.

Convection can occur by the random collision of particles and thus enhance the thermal conductivity of nanofluids (Prasher et al., 2005). However, this mechanism will not be considered in this study.

Chapter 3

Experimental

To understand the stability and thermal conductivity of metallic nanofluids, stainless steel 316L nanoparticles (STS) were dispersed into water and ethylene glycol in this study. In addition, aluminum oxide (Al_2O_3) containing nanofluids were also used for comparison since they have been studied extensively in the past.

3.1 Material

Information on particles, base fluids and surfactants that were used is summarized in Table 3.1 and detailed properties are in Table 3.2. Aluminum oxide with two different mean particle sizes were used to observe the size effect. Sodium dodecyl sulphate (SDS), sodium dodecyl benzene sulphonate (SDBS), and hexadecyltrimethylammonium bromide (CTAB) were used to improve the dispersion stability.

Stainless steel 316L nanopowder was manufactured to purity or 99.9% with 70 nm mean diameter. Fig. 3.1 is a transmission electron microscope image of the particles; spherical shaped and measured average particle size is 67 ± 20 nm. The chemical composition of STS particles analysed by using an inductively coupled plasma spectrometer are listed in Table 3.3. Compared with the typical specification of 316L, analysed carbon content was 0.057 wt% which exceeds the maximum specification of 316L stainless steel.

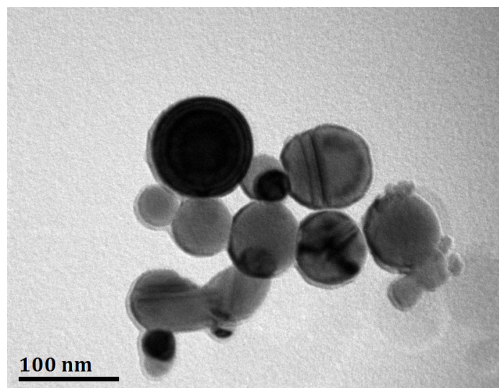


Fig. 3.1 Bright field transmission electron microscope image of stainless steel 316L nanoparticles dispersed in distilled water. Measured average particle size is 67 ± 20 nm.

Table 3.1 Specification of particles, base fluids and surfactants given by manufacturer.

Type	Material	Abbreviation	Specification	Manufacturer
Powder	Stainless steel 316L	STS	mean size 70 nm	RND Korea
	Aluminum Oxide	Al ₂ O ₃	mean size 13 nm, 45 nm	Sigma Aldrich
Fluid	Distilled Water	DW	Water Purification System	Human Corporation
	Deionized Water	DI	Water Purification System	Human Corporation
	Ethylene Glycol	EG	99.5 %	Samchun Chemicals
Surfactant	Sodium dodecyl sulfate	SDS	Anionic surfactant	Samchun Chemicals
	Sodium dodecyl benzene sulphonate	SDBS	Anionic surfactant	Sigma Aldrich
	Hexadecyltrimethyl-ammonium bromide	CTAB	Cationic surfactant	Sigma Aldrich

Table 3.2 Properties of stainless steel, aluminum oxide, water and ethylene glycol at 20 °C. Density ρ [g cm^{-3}], thermal conductivity k [$\text{W m}^{-1} \text{K}^{-1}$], dielectric constant ϵ and refractive index n at specific wavelength λ [nm] in parentheses are from (Lide, 2004) if not noted. [*] Filmetrics [**] calculated using Eq. 2.9.

Material	ρ	k	ϵ	$n(\lambda)$
Stainless steel	7.90	15	2.757 [*]	7.6 (633) [**]
Aluminum Oxide	3.97	35	9.0	1.768 (589.3)
Water	0.9970	0.5984	80.2	1.33211 (632.8)
Ethylene Glycol	1.1135	0.256	41.4	1.4318 (589)

Table 3.3 Composition in wt% of analysed stainless steel 316L particles used in this study compared with stainless steel 316L typical specification from (Bhadeshia and Honeycombe, 2011).

	Cr	Ni	Mo	Mn	Si	C	Fe
Analysed	17.1	11.0	2.0	0.98	0.49	0.057	bal.
Specification	16-18	10-14	2-4	1.5	1.00 max	0.03 max	bal.

3.2 Stability Measurement

To compare the degree of stability and durability of nanoparticle-fluids, five different methods discussed in section 2.3 were used. Sedimentation was observed to examine the durability by comparing the change of color thickness visually over time. A small amount of sample, about 1 ml, was put in a transparent cell, and was stored at rest without motion until sedimentation ended. For transmission electron microscope (JEOL, JEM-2100 and JEM-2100F) observation, a drop of nanoparticle-fluid on a carbon-coated copper grid (Ted Pella, CA) was dried for over 24 h and then the effect of pH or surfactant on the particles was observed. The stability of particles suspended in a fluid was studied by measuring the particle size distribution and zeta potential with Zetasizer (Malvern Instruments, Nano-ZS) within an hour or over time. Absorbance was measured with UV/Vis scanning spectrophotometer (Beckman Coulter, DU 730) over time at rest.

3.3 Nanoparticle-fluid Production

To produce a nanoparticle-fluid with a particular mass fraction, the exact amounts of particles and fluid were placed in the solution-container. Then, agitation was induced by using an ultrasonic bath or ultrasonic processor. For the work presented in chapter 4, solution-containers were immersed in a ultrasonic bath subjected to ultrasonic pulses of 500 W at 40 kHz. Secondly, for the work presented in chapter 5, probe of ultrasonic processor with pulses of 750 W at 20 kHz was immersed in a solution-container to improve the dispersion of particles. Both represent the two-step method, a standard practice in the production of nanofluids (Yu and Xie, 2012). The sonication temperature and time, pH of fluid and surfactant type and concentration were varied in order to characterise the optimum conditions.

NaOH was added to fresh distilled or deionized water to prepare fluids with pH of 8.0, 9.0, 10.0, 11.0 and 12.6 at 20 °C, and pH was measured with a precise pH meter of 0.01 resolution (HANNA Instruments, HI 8424). Since HCl dissolves stainless steel, base fluid with $pH < 7.0$ was abandoned. After sonication, the ζ -potential and absorbance over time were measured. At pH values where stable ζ -potentials and higher absorbance could be recorded, SDS, SDBS and CTAB surfactants were added to enhance the dispersion stability.

3.4 Transient Hot-wire Method

The thermal conductivity of fluids was measured using transient hot-wire method to study the relationship with stability. Principles, apparatus design and corrections on transient hot-wire method are well documented in (Bleazard and Teja, 1995; Carslaw and Jaeger, 1959; Groot et al., 1974; Healy et al., 1976; Kawaguchi et al., 1985; Nagasaka and Nagashima, 1981a,b; Paul et al., 2010). The apparatus used in this study followed the general setup described in literature. Fig. 3.2 shows the transient hot-wire circuit of this study with two fixed resistors R_1 and R_2 , an adjustable resistor R_3 , input voltage V_s , thermal conductivity cell to contain nanofluid with wire having resistance of R_w connected vertically, and a data acquisition system (DAQ). The underlying theories, setup and calibration are introduced in this section.

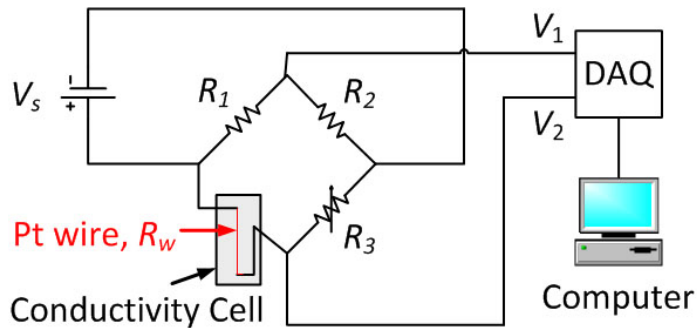


Fig. 3.2 Schematic of experimental setup of transient hot-wire circuit with thermal conductivity cell. V_i and R_i stands for voltages and resistance.

3.4.1 Principle of Measurement

In the transient hot-wire method, the voltage difference $\Delta V = V_1 - V_2$ of a Wheatstone bridge by time is obtained using data logger. This voltage difference is generated by increasing the resistance of a thin metallic wire R_w which is used as both a line heat-source and a temperature sensor, due to increased temperature of the liquid surrounding the wire in the thermal conductivity cell.

The theoretical basis of the method is Fourier's law. The heat diffusion equation in cartesian coordinate with constant thermal conductivity k and without heat generation is:

$$\frac{\partial^2 T}{\partial x^2} + \frac{\partial^2 T}{\partial y^2} + \frac{\partial^2 T}{\partial z^2} = \frac{1}{\alpha} \frac{\partial T}{\partial t}, \text{ where } \alpha = \frac{k}{\rho c_p} \quad (3.1)$$

where T is the temperature gradient, α is the thermal diffusivity, and ρc_p is the volumetric heat capacity. The solution of Eq. 3.1 is as follows from (Carslaw and Jaeger, 1959):

$$T(r, t) = -\frac{q}{4\pi k} E_i\left(-\frac{r^2}{4\alpha t}\right) \quad (3.2)$$

where r is the distance from the wire, t is time, q is the heat flux per unit length and E_i is defined as:

$$E_i(x) = -\int_x^\infty \frac{1}{u} \exp(-u) du = \gamma + \ln x + \frac{x^2}{4} + \dots \quad (3.3)$$

where $\gamma = 0.5772$ is Euler's constant. Substituting Eq. 3.3 to Eq. 3.2, the temperature distribution T for a line heat source is expressed as below by integrating T over the entire length of the line (from $-\infty$ to $+\infty$ in cylindrical coordinates).

$$T(r, t) = T_0 + \frac{q}{4\pi k} \left\{ -\gamma + \ln\left(\frac{4\alpha t}{r^2}\right) + \left[\left(\frac{r^2}{4\alpha t}\right) - \frac{1}{2^2} \left(\frac{r^2}{4\alpha t}\right)^2 + \dots \right] \right\}, \quad (3.4)$$

where T_0 is the initial fluid temperature at $t = 0$.

Assuming that the distance from the wire r is small enough, Eq. 3.4 is simplified into:

$$T(t) = T_0 + \frac{q}{4\pi k} \left[-\gamma + \ln(t) + \ln\left(\frac{4k}{r^2 \rho c_p}\right) \right] \quad (3.5)$$

which is used for approximating the thermal conductivity measured by the transient hot-wire method.

After some delay of measurement time, ΔT versus $\ln t$ becomes a straight line with slope $\frac{q}{4\pi k}$ for a short time before natural convection starts as in Fig. 3.3. With the knowledge of the temperature of the wire T_1 and T_2 at time t_1 and t_2 , the thermal conductivity at temperature T_r can be determined by Eq. 3.5 as:

$$k(T_r) = \left[\frac{q}{4\pi(\Delta T(t_2) - \Delta T(t_1))} \right] \ln\left(\frac{t_2}{t_1}\right), \quad (3.6)$$

where $\Delta T(t_i) = T(t_i) - T_0$ and T_r is the reference temperature of k defined as $T_r = T_0 + \frac{1}{2}(\Delta T(t_1) + \Delta T(t_2))$. Therefore, to calculate the thermal conductivity of a fluid using the above relationship, we need to measure q , t , and $T(t)$ accurately through the apparatus in Fig. 3.2.

The heat flux q , the heat generated by the wire can be calculated using Joule's first law:

$$q = \frac{I_w^2 R_w}{l_w}, \quad (3.7)$$

where $I_w = \frac{V_s}{R_w + R_3}$ is the electric current through the wire, V_s is the stable voltage provided by DC power supply, and l_w is the effective length of the wire in the thermal conductivity cell.

Using the Ohm's law, the resistance of the wire R_w can be calculated from the estimated voltage difference ΔV at time t since other resistances R_1 , R_2 and R_3 are

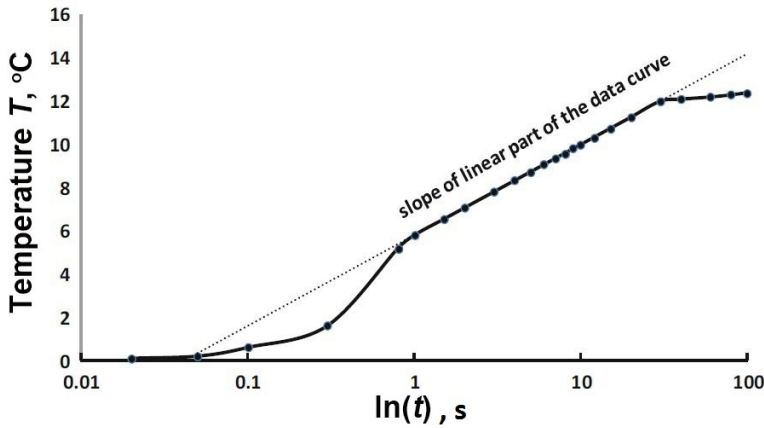


Fig. 3.3 Typical linear part data after some delay from (Michaelides, 2014).

fixed and only R_w increases as the temperature increases as time flows.

$$\Delta V(t) = V_1 - V_2 = \frac{V_s R_1}{R_1 + R_2} - \frac{V_s R_w(t)}{R_w(t) + R_3}, \quad (3.8)$$

and so the resistance of the wire can be calculated as:

$$R_w = R_3 \left\{ \left(1 - \frac{R_2}{R_1 + R_2} + \frac{\Delta V(t)}{V_s} \right)^{-1} - 1 \right\}. \quad (3.9)$$

Then the temperature change of the wire and surrounding fluid during measurement $\Delta T(t)$ is calculated from the known linear relationship between resistance and temperature of the wire:

$$R_w = R_{T_0} [1 + \beta_1 (T(t) - T_0)] = R_{T_0} [1 + \beta_1 \Delta T(t)], \quad (3.10)$$

where β_1 is the temperature coefficient of resistance, $3.90 \times 10^{-3} \text{ K}^{-1}$ for the platinum wire. R_{T_0} is the resistance of the wire at T_0 which is determined by the relationship

between the resistance, diameter and length:

$$R_{T_0} = \rho_{T_0} \frac{l_w}{A_w}, \quad (3.11)$$

where ρ_{T_0} is the electrical resistivity of the material at T_0 , and A_w is the surface area of the wire. For platinum, $\rho_{20^\circ\text{C}} = 105 \times 10^{-9} \Omega\text{m}$ (Lide, 2004).

With the chosen platinum wire, $R(20^\circ\text{C})$ can be calculated by Eq. 3.11, and substitution into Eq. 3.10 makes R_w as a function of $T(t)$. Then using Eq. 3.9 and Eq. 3.10, $T(t)$ becomes a function of $V_s(t)$ as:

$$\Delta T(t) = \frac{1}{\beta_1} \left[\frac{R_3}{R_0} \left\{ \left(1 - \frac{R_2}{R_1 + R_2} + \frac{\Delta V(t)}{V_s} \right)^{-1} - 1 \right\} - 1 \right], \quad (3.12)$$

and can be calculated with collected data of $V_s(t)$. Finally, the thermal conductivity of a fluid can be calculated by substituting Eq. 3.12 into Eq. 3.6.

3.4.2 Setup

The setup of the transient hot-wire method depends on research groups. In this study, R_1 and R_2 were fixed to 10Ω , and V_s was set to 0.55 V to have q of $0.3 - 0.4 \text{ W m}^{-1}$ to be in the range of $0.3 - 0.8 \text{ W m}^{-1}$ from literature (Das et al., 2007; Kawaguchi et al., 1985). R_3 was adjusted to satisfy $\Delta V = 0$ without fluid in the cell, and ΔV was programmed to be recorded for 10 s with a rate of 600 Hz . The platinum wire of $50.8 \mu\text{m}$ in diameter and 60 mm in length was coated with a teflon layer of $< 1 \mu\text{m}$ in thickness and soldered tight to a copper wire and a platinum spring in the thermal conductivity cell of 3 cm in diameter and 10 cm in length. The resistance of the platinum wire used in this study is $R_w = 3.14 \Omega$ at $T_0 = 20^\circ\text{C}$. Agilent E3620A DC power supply and National Instruments cDAQ-9174 and 9205 data acquisition system were used in the apparatus of Fig. 3.2.

In the initial stage of the setup, thicker platinum wires were chosen for better durability. However, the measurements were difficult due to the low resistance of the wire (refer to Eq. 3.11); the voltage difference in this case showed a wide range of fluctuation, and therefore a thinner platinum wire was applied.

Simple and self-programmed LabVIEW code was used to read and store the data accumulated into a computer. Data set, t , V_1 and V_2 , were measured and stored for 10 s and then the temperature of the wire at t was calculated using equations derived above. The temperature increase is not linear for the entire logarithm time interval as shown in Fig. 3.3. It takes time for the circuit to be stabilized in the initial stage, 0.2 ~ 0.3 s in current setup, and the natural convection starts after few seconds. Literatures reported the different onset time of natural convection in the fluid during measurement which may depend on the diameter and the length of the platinum wire or the conductivity cell (Das et al., 2007; Kawaguchi et al., 1985). In current setup, natural convection occurred after 2 ~ 3 s which was detected after several trials and only the linear section data was considered in calculating the thermal conductivity of nanofluids.

3.4.3 Calibration

The calibration which determines the accuracy of the measurement is important, and generally, water, ethylene glycol and toluene which are popular coolants are used as they are easy to compare with data from the literature.

Because the wire was insulated to measure water-based fluids, the effect of the insulation layer along with the effect of finite wire properties and finite outer cell diameter discussed in Bleazard and Teja (1995); Healy et al. (1976); Nagasaka and Nagashima (1981b) were considered. Corrections δT_i following the references were made to the measured temperature rise calculated using Eq. 3.12 and this is distinguished to be ΔT_{id} . Thus, $T(t)$ used in Eq. 3.6 to calculate the thermal conductivity of

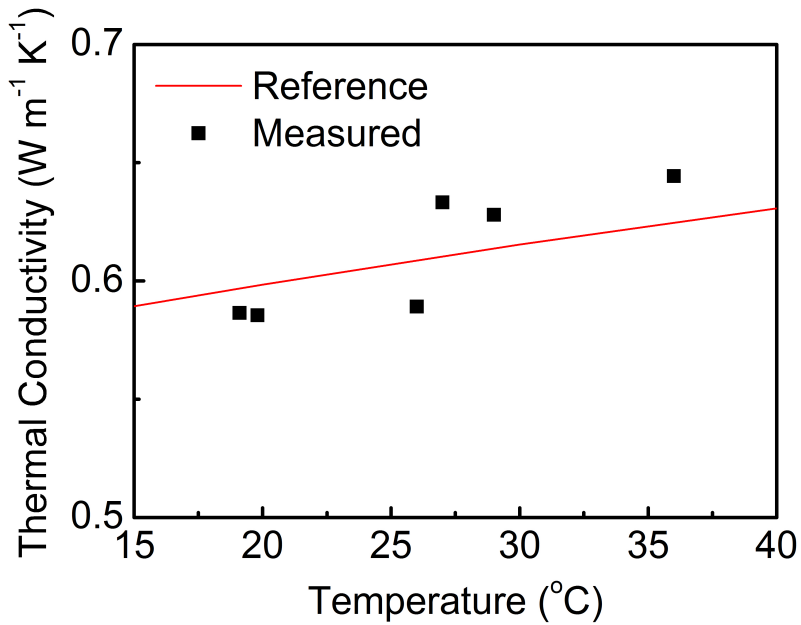


Fig. 3.4 Measured thermal conductivity of water compared with reference from (Lide, 2004).

a fluid is $T(t) = T_0 + \Delta T_{id} + \delta T_i$.

The thermal conductivity of water at 20 – 40°C was measured for the calibration and the estimated accuracy of the present method was $\pm 5\%$, compared with data in Lide (2004), as shown in Fig. 3.4.

Chapter 4

Stability of 0.017 wt% Stainless steel–Water Mixture

4.1 Introduction

Metallic-nanofluid has its advantages in two respects; (1) it has a higher thermal conductivity enhancement than oxide-nanofluids as in Fig. 1.1, and (2) metallic powder/particles are more cost-efficient than nanotubes. Although fluids containing nanotubes show generally better thermal conductivity enhancement, the value can be achieved with some metallic-nanofluids.

Previous studies on metallic-nanofluids focused on the production of nanofluids with good thermal properties. Mostly studied particle and fluid are copper and ethylene glycol, respectively, due to oxidation of metallic particles in water. Xuan and Li (2000) increased the thermal conductivity of water up to 78 % by dispersing 7.5 vol.% of copper using two-step method, and Chopkar et al. (2006) reported almost 130 % enhancement in 2.5 vol.% Al₇₀Cu₃₀–EG nanofluid. Eastman et al. (2001); Hong et al. (2005); Liu et al. (2006); Sinha et al. (2009) observed thermal conductivity enhance-

ment in the range of 20 – 60 % and [Garg et al. \(2008\)](#); [Patel et al. \(2003\)](#); [Yu et al. \(2010\)](#) had $\sim 10\%$ enhancement. These previous studies are summarized in Table 5.1.

Metallic-nanofluids are not studied much, and their thermal conductivity enhancement varies among groups. In addition, rapid thermal conductivity degradation reported by [Karthikeyan et al. \(2008\)](#); [Liu et al. \(2006\)](#); [Philip and Shima \(2012\)](#) lead to the importance of considering dispersion stability, as the relation between stability and thermal conductivity of nanofluids had been verified as discussed in section 2.5.1.

To solve oxidation, storage and safety problems and difficulties in production because of larger particle density related to metallic particles, stainless steel nanoparticles were chosen in this study. Stainless steel nanopowder may be a potential candidate because of the resistance to corrosion or chemical reaction with fluid, and besides it has not been studied previously.

4.2 0.017 wt% Production Parameters

The concentration 0.017 wt% was chosen because ζ -potential and particle size distribution measurements become reliable at this concentration. The particle concentration was reduced from 1 wt%, because higher concentration than 0.017 wt% meant that the sample was not dilute enough for light to scatter as discussed in sections 2.3.3 and 2.3.4.

4.2.1 Light absorption of stainless steel particles

To observe the sedimentation of particles over time, absorbance was measured repeatedly until it becomes zero. Fig. 4.1 shows the UV-Vis spectra of stainless steel particles dispersed in distilled water. Because a small peak is observed at the wavelength of 330 nm in 0.017 wt% and 0.008 wt% stainless steel-water fluids, absorbance at 330 nm was used afterwards to determine the sedimentation.

Fig. 4.2 shows the linear relationship between absorbance measured right after production and particle concentration follows the Beer-Lambert law. Linearity implies that particles are well dispersed. However, as will be shown in chapter 5, stainless steel particles are not completely dispersed by using ultrasonication bath. More powerful method is required for complete and uniform dispersion of 70 nm sized stainless steel particles that is used in this work. Thus, the slope of Fig. 4.2 is not the correct value of $\epsilon b = \frac{A}{c}$.

$A = 0.567$ at the wavelength of 330 nm is the absorbance value coming from the maximum amount of particles that are dispersed after 1 h of sonication, not the absorbance of the entire 0.017 wt% stainless steel particles in water. So, $A = 0.567$ at the wavelength of 330 nm will be used to determine the relative sedimentation of 0.017 wt% stainless steel-water nanoparticle fluids over time in this chapter.

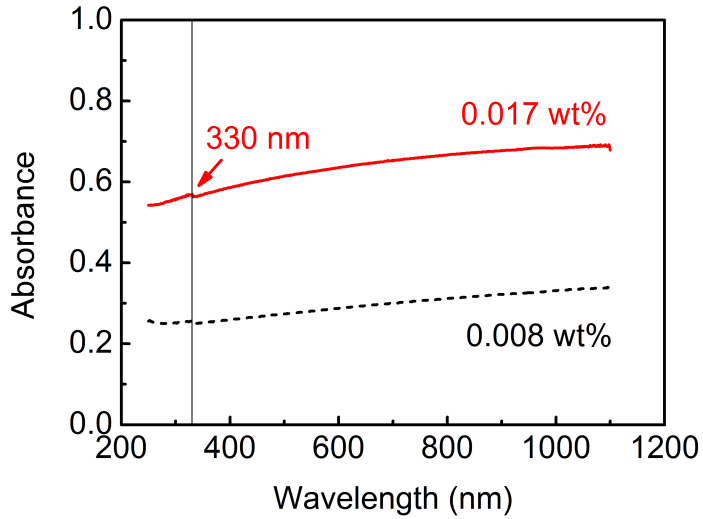


Fig. 4.1 The UV-Vis spectra of stainless steel 316L particles dispersed in distilled water.

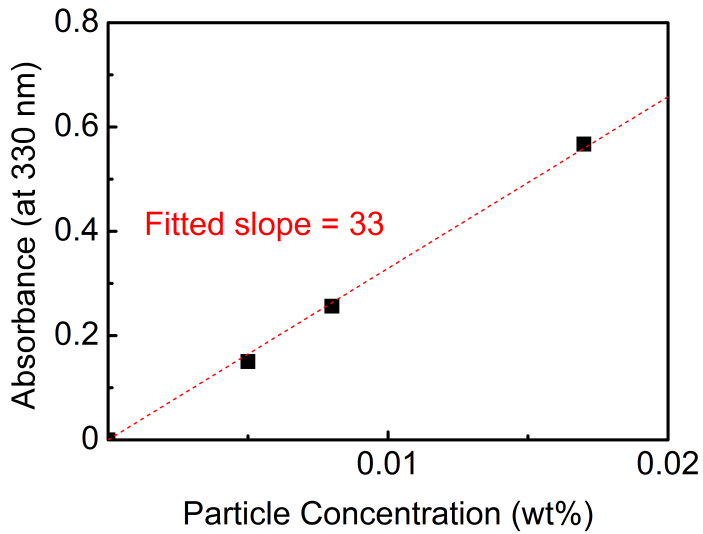


Fig. 4.2 Relationship between particle concentration and absorbance at 330 nm of stainless steel 316L particles dispersed in distilled water using ultrasonication bath.

4.2.2 Temperature Control

The sonication bath temperature had to be controlled because the temperature of water in the sonication bath increased up to 45 °C from 20 °C after an hour of sonication with pulses of 500 W at 40 kHz. Thus, the dynamic viscosity of water decreases from $1.01 \times 10^{-3} \text{ kg m}^{-1} \text{ s}^{-1}$ at 20 °C to $6.31 \times 10^{-4} \text{ kg m}^{-1} \text{ s}^{-1}$ at 45 °C (Bayazitoğlu and Özışık, 1988).

From Stoke's law of Eq. 2.1, the sedimentation velocity is a function of temperature, the primary effect being the change in the viscosity of the water; the sedimentation of particles can be slowed down by increasing the fluid viscosity (Cosgrove, 2010). Therefore, to control the temperature, the water in the bath was refreshed with cold water at a sufficient rate to maintain the target temperature of 23 – 25 °C.

The effect of temperature control is shown by sedimentation observation as in Fig. 4.3. For comparison, sedimentation of alumina (Al_2O_3) particles having mean particle size of 13 nm and 45 nm in water were also tested. The sedimentation of stainless steel-water at ambient temperature is much slower in case of temperature controlled group A, being a few days, than group B when the temperature of the bath was uncontrolled and allowed to rise. However, alumina-water fluids do not show apparent difference between group A and B, presumably because of the lower density and the smaller size of alumina compared with stainless steel particles; the calculated sedimentation rate of stainless steel particles is at least an order of magnitude faster than that of alumina particles.

The dependence of sedimentation rate of stainless steel-water fluids on temperature is shown in Fig. 4.4(a),(b) in terms of particle size distribution and absorbance change over time. When the sonication bath temperature is not controlled, particles aggregate more easily and sedimentation occurs faster, consistent with the results in Fig. 4.3. These results give the importance of considering temperature on the stability,

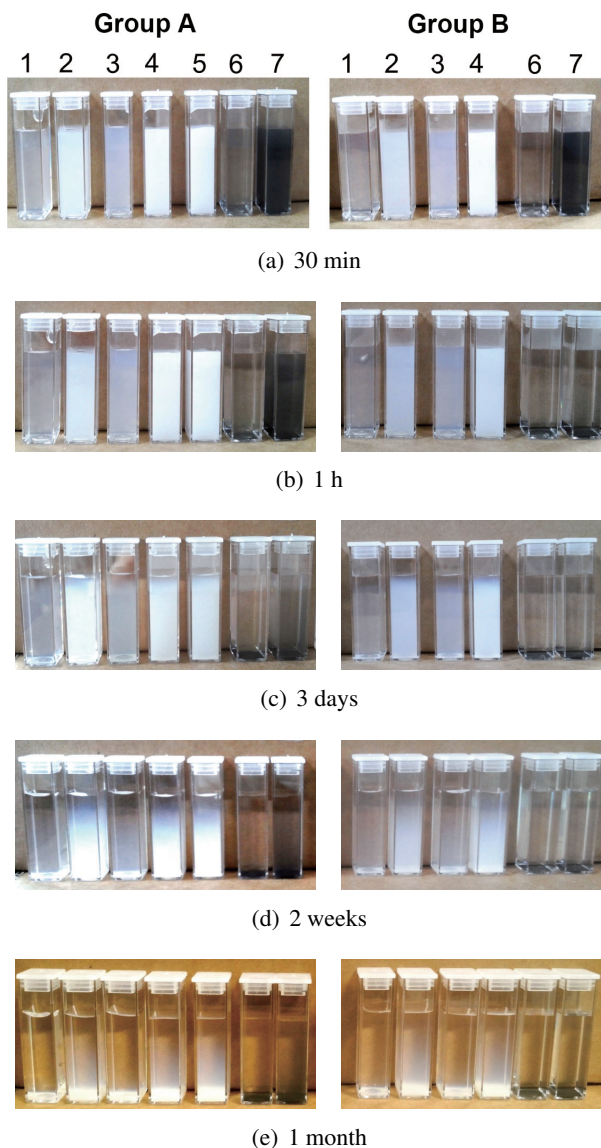


Fig. 4.3 Sedimentation of water-based Al_2O_3 and stainless steel fluids as a function of time after production at rest. Group A is produced with sonication bath temperature maintained in the range of 23-25 °C for 1 h, and Group B is produced without temperature control (in the range of 23-45 °C) for 1 h.

(1) 13 nm alumina, 0.04 wt%; (2) 13 nm alumina, 0.4 wt%; (3) 45 nm alumina, 0.04 wt%; (4) 45 nm alumina, 0.4 wt%; (5) 45 nm alumina, 0.65 wt%; (6) 70 nm steel, 0.005 wt%; (7) 70 nm steel, 0.04 wt%.

particularly in metallic nanoparticle-fluid mixtures.

4.2.3 Process Scale

To assess reproducibility as a function of the size of the experiment, the size of the fluid produced was increased from 15 ml to 50 ml whilst maintaining identical experimental conditions, including the duration of sonication of 1 h. The temperature of the sonication bath was controlled at 23-25 °C, and the fluids were assembled in tubes of identical length (115 mm) but different diameters (15 mm for 15 ml, 28 mm for 50 ml). The concentration of stainless steel particles in all cases was 0.017 wt% in order to facilitate sufficient transparency for distribution and potential measurements.

The resulting size distribution data presented in Fig. 4.5(a) shows that for the same sonication, the particles in the larger volume of fluid are less dispersed, having a greater possibility to aggregate and settle down. The ζ -potential plotted in Fig. 4.5(b) shows that although both are close to the stability of colloidal suspension in terms of $|\zeta| \gtrsim 30\text{mV}$ (Das et al., 2007), the 15 ml sample has higher surface potential, probably stronger repulsion between particles and difficult to aggregate. The size of production was also increased to 1 L with identical conditions, but because the particles remained aggregated severely after 1 h sonication, it was impossible to measure the particle size distribution and ζ -potential due to fast sedimentation.

Results show that the required sonication conditions for sufficient dispersion will also depend on the process scale, which has not been mentioned in most of the previous studies on nanofluids, which can explain one of the reason of the failure in reproducibility. Although 15 ml sample shows better stability here, the size was considered to be too small to test stability and thermal conductivity in this study. Therefore, the experiments afterwards were done in 50 ml scale to find the optimal stability conditions with *pH* control and surfactant addition.

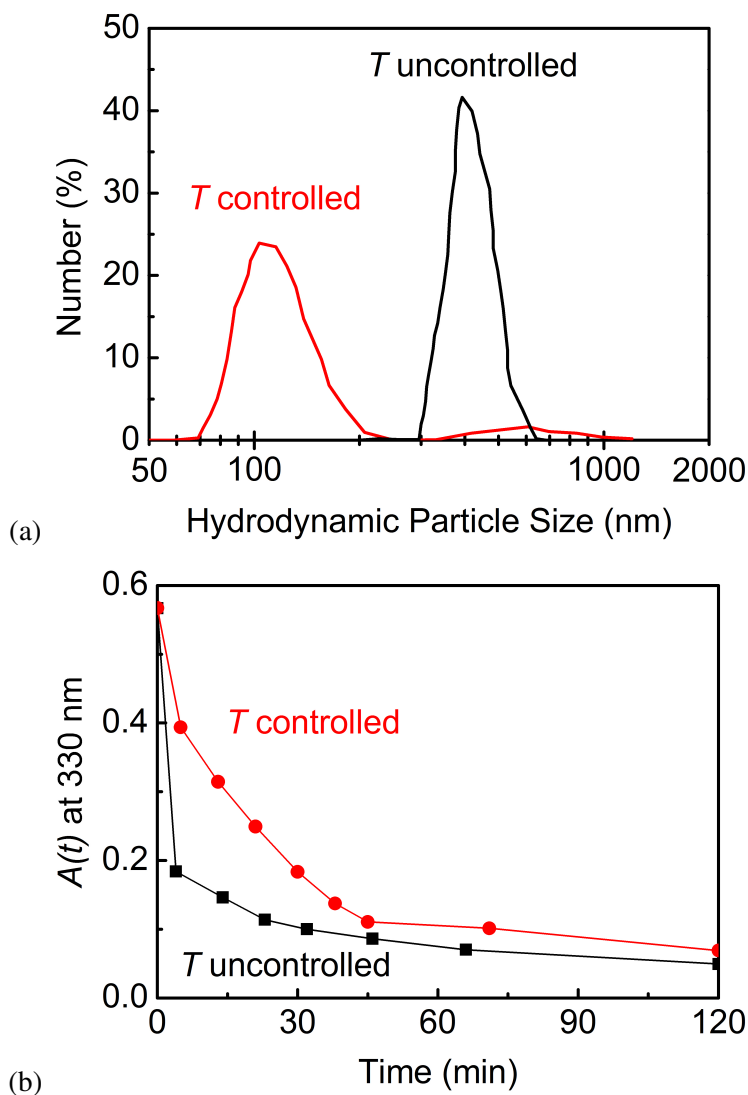


Fig. 4.4 The effect of sonication bath temperature control compared by (a) particle size distribution measured within 10 min after production and (b) absorbance change over time of 0.017 wt% STS - water nanoparticle-fluids. Samples were prepared using 50 ml conical tubes and were sonicated for 1 h.

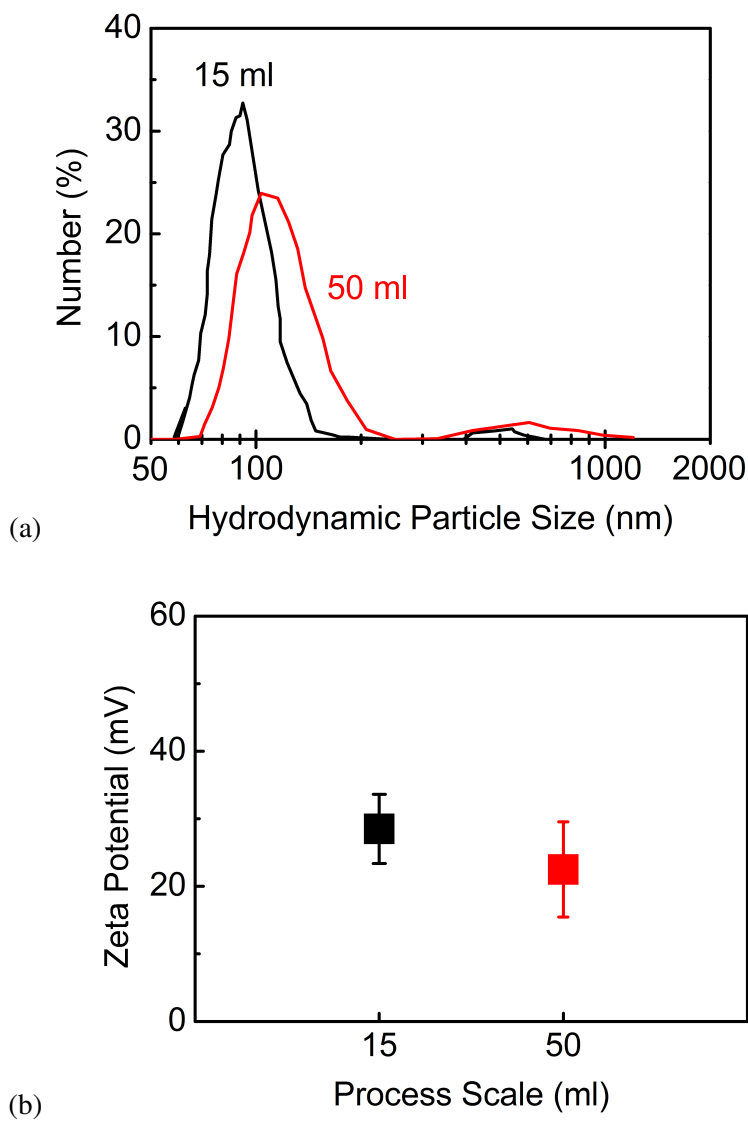


Fig. 4.5 The effect of process scale compared by (a) particle size distribution and (b) ζ -potential of 0.017 wt% STS - water nanoparticle-fluids prepared using 15 ml and 50 ml conical tubes. Measurements done within 10 min after the production.

4.2.4 Sonication Time

The effect of sonication time is shown in Fig. 4.6 in terms of the particle size distribution and zeta potential when the sonication temperature and the process scale were controlled. While ζ -potential does not vary much, the particle size distribution results show that particles are well dispersed when sonication time is increased from 30 min to 60 min and then may aggregate with longer sonication of 90 min. Therefore, the sonication time of 60 min was selected in this study.

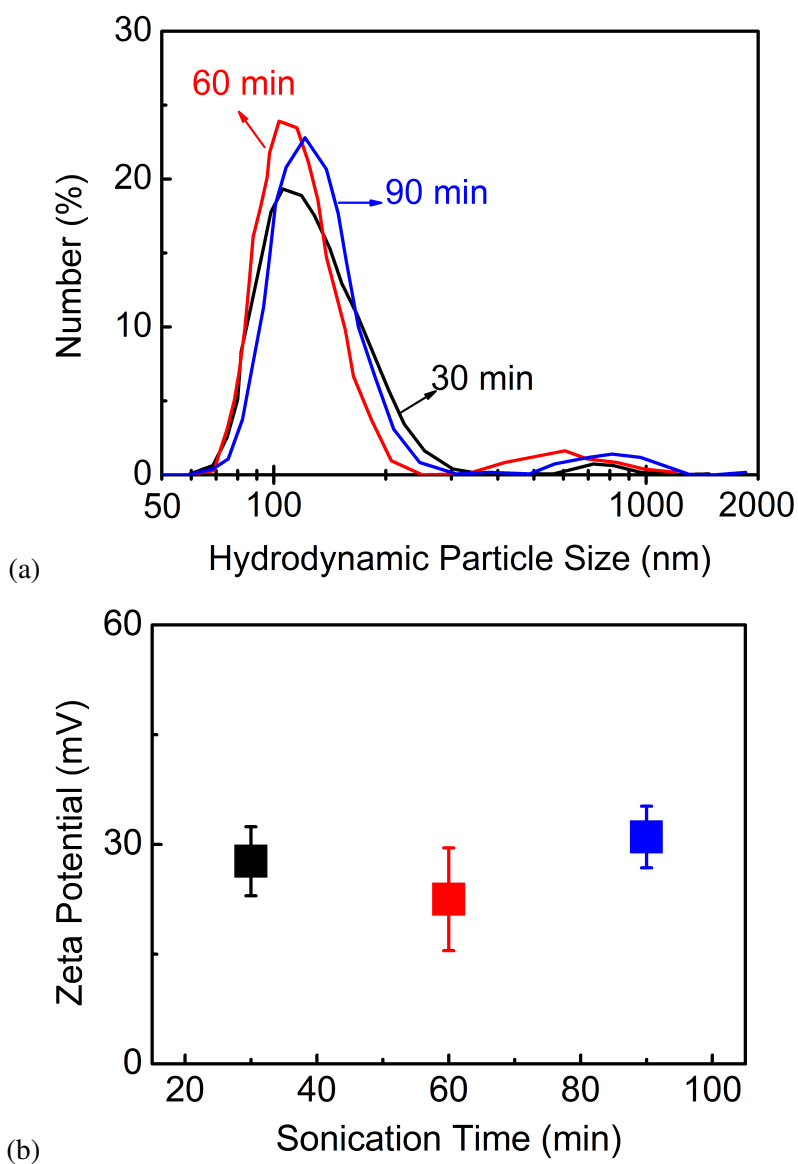


Fig. 4.6 The effect of sonication time shown by (a) particle size distribution and (b) ζ -potential of 0.017 wt% STS - water nanoparticle-fluids. Sonication temperature was controlled and the process scale was 50 ml. Measurements done within 10 min after the production.

4.3 *pH* Effect

The 316L stainless steel contains iron, chromium, nickel, molybdenum, manganese, silicon and carbon as in Table 3.3. While IEP of Fe, Cr and Ni are known to be $pH > 7$ (Parks, 1965), values of pH 3–4 have been quoted for the surface of stainless steels which are covered with oxide layers (Lefèvre et al., 2009); the ζ -potential of the mixture is expected to be in a stable range when the pH of the fluid is far from the IEP of the stainless steel particles (also refer to section 2.3.4).

With reference to the sodium hydroxide experiments, Fig. 4.7(a) shows the ζ -potential change with respect to the pH of 0.017 wt% nanoparticle-fluids. The charged surfaces of particles become unstable when the pH increases from 7 to about 9, and the IEP of 0.017 wt% stainless steel particles in distilled water was found to be pH 7.8. IEP of $pH > 7$ tell the surface of particles used in this study is not oxidized.

Further addition of NaOH increases the number of anions that surround the particles, leading to electrostatic stabilisation at pH 10 and pH 10.9 where ζ -potentials are -49.8 ± 0.6 mV and -59.0 ± 4.2 mV, respectively. At pH 12.6, the excess ions suppress the electrical double layer of the particles, the Debye length decreases, and the repulsive force between particles decreases; the excess OH^- ions disrupted the electrostatic stabilisation.

The corresponding absorbance-time data are shown in Fig. 4.7(b), measured from 20 min to 60 min after the production. All samples have identical concentrations, thus the absorbance decrease is smaller in samples with less sedimentation. The sedimentation was slowest at pH 11, consistent with the ζ -potential results.

These experimental results can be verified by the total interparticle potential calculations based on DLVO theory discussed in section 2.2.3. To be consistent with the zeta potential measurement, the refractive index of stainless steel 316L at the wavelength of 633 nm was selected, and the dielectric constant was calculated. Then the Lifshitz-van

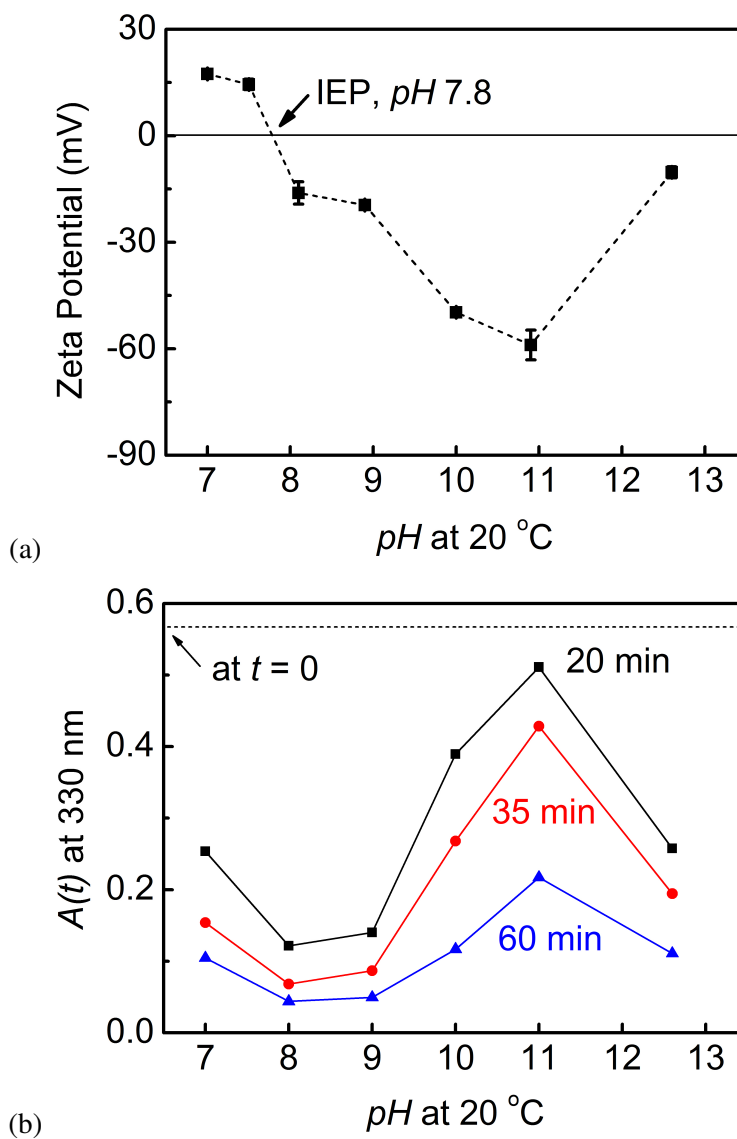


Fig. 4.7 Measurements for 0.017 wt% stainless steel-water nanoparticle-fluids with temperature control and 1 h sonication. (a) ζ -potential as a function of pH varied by adding NaOH and (b) corresponding absorbance results 20 to 60 min after production. Short dash line in (b) is expected absorbance after production.

der Waals constant of stainless steel particles in water A_{SWS} can be calculated using Eq. 2.10:

$$A_{\text{SWS}} = 2.88 \times 10^{-19} \text{ J},$$

which is in the range of $2 \times 10^{-19} - 5 \times 10^{-19} \text{ J}$ known for metals (Israelachvili, 2011). The value of parameters used in the calculation are listed in Table 3.2.

Therefore, the total interparticle potential of stainless steel particles in water can be calculated using the measured ζ -potential as shown in Fig. 4.8. The primary maximum at *pH* 10 and *pH* 11 is over $50 k_{\text{B}}T$, higher than the maximum energy of the Brownian collision (Cosgrove, 2010; Israelachvili, 2011), so the particles will be electrostatically stable. Since the attractive force is independent of *pH* of the fluid, the positive energy barrier formed for *pH* 10 and *pH* 11 is because of the strong repulsive potentials between particles with higher absolute ζ -potentials. Therefore, the dependence of the stability on interparticle forces can be explained by this calculation with ζ -potential measurement.

For the 0.017 wt% STS-water nanoparticle-fluids produced by 1 h temperature controlled sonication in bath, the optimal *pH* found is *pH* 11 which shows good stability without any surfactant addition. In addition, Fig. 4.7 and Fig. 4.8 show that zeta potential and sedimentation by absorbance measurements should be considered together to determine the overall stability of nanoparticle-fluids.

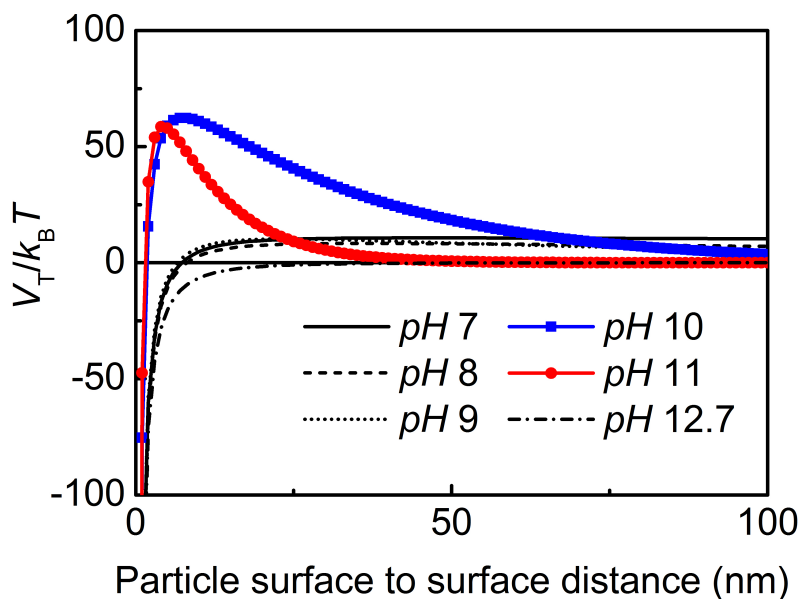


Fig. 4.8 Calculated total interparticle potential of 0.017 wt% stainless steel-water nanoparticle-fluids in Fig. 4.7. $A_{SSS} = 2.88 \times 10^{-19}$ J, measured ζ potential from Fig. 4.7, calculated Debye lengths by Eq. 2.14, $r_p = 35$ nm and $T = 300$ K were used in calculation. The calculated Debye length at pH 10 and pH 11 are 30.8 nm and 9.75 nm, respectively.

4.4 Surfactant Effect

In previous studies, the optimal surfactant concentration has been found only at optimal pH values (Li et al., 2007, 2008; Wang et al., 2009). However, the excess addition of any ions can lower the dispersoid stability. Therefore, the surfactant effect was characterised also for other samples with lower pH in this study because the addition of surfactants at the optimal pH 11 may accelerate aggregation of particles due to high concentration of ions.

First, to establish the type of the surfactant best suited for the stainless steel nanoparticle-water fluid, anionic SDS and SDBS, and cationic CTAB were added to 0.017 wt% STS-water fluids at pH 7. Fig. 4.9(a),(b) show the result of SDBS and CTAB addition, where the mass fraction of SDBS and CTAB relative to stainless steel particles was varied as 0.5, 1.0 and 1.5. In case of SDS, the addition to fluid greatly increased the sedimentation rate, and it was impossible to measure the potential.

The addition of anionic SDBS changed the sign of ζ -potential; the particle surface is thus surrounded by adsorbed anions. Both SDBS and CTAB addition increased $|\zeta|$ – the anionic or cationic “heads” of the surfactant molecules are adsorbed to the particle surface and confer steric stability. Results show that the decrease in particle concentration is slowest when SDBS and CTAB to particle mass ratio is 0.5 and 1.0 (SDBS 0.5 and CTAB 1.0), respectively.

However, CTAB was not tested more for several reasons: sedimentation was slower when SDBS was added; it is preferable to add as little surfactant as possible to investigate the heat transfer mechanism between metallic nanoparticles, so adding SDBS with mass ratio of 0.5 is better; cationic surfactants is known not to work well in high pH solutions; it is easier to use surfactants that do not change the sign of the previously formed ion boundary, thus anionic type is preferable in NaOH added fluids; and because of the chemical reaction between bromine and stainless steel particles which

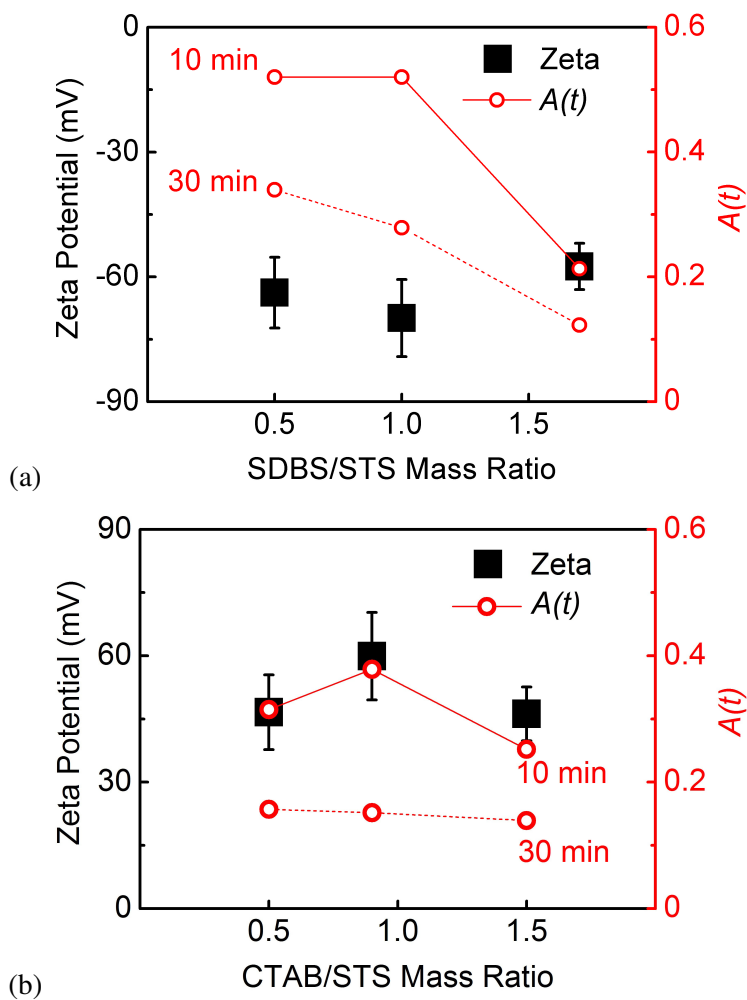


Fig. 4.9 Effect of (a) anionic SDBS and (b) cationic CTAB surfactants on 0.017 wt% stainless steel-water nanoparticle-fluids.

is discussed in section 4.5.2. Therefore, SDBS was selected on the basis of steric stabilisation.

4.4.1 SDBS Concentration

The effect of SDBS addition at various pH is shown in Fig. 4.10 by ζ -potential change. The addition of SDBS was very effective in distilled water (pH 7) but not significant at NaOH added samples, especially at pH 10 - pH 11 where the electrostatic stabilisation was previously formed. ζ -potential decreases at some pH when SDBS is added more to the fluid; SDBS 0.5 is sufficient to form steric stabilisation and there will be excessive ions in SDBS 1.0 and SDBS 1.7 fluids. At pH 7, the anionic heads adsorbed to the particle surfaces easily and formed steric stabilisation since no other salts or NaOH had been added before.

The results in Fig. 4.11 also shows that SDBS 0.5 is the optimal condition. The absorbance range after 60 min is highest at SDBS 0.5 samples compared with SDBS 0.1 and SDBS 1.7 samples. As the concentration of SDBS increases, decrease in $A(t)$ increases, which implies an *increase* in sedimentation rate. This is because excessive surfactants increase both the ions adsorbed on the particle surface and the remaining counter ions. The latter will enter into the inner adsorbed layer, leading to a decrease in the ζ -potential of the particle, and hence to a decreased interparticle repulsion. Therefore from the ζ -potential and absorbance measurements, the optimal SDBS mass fraction relative to stainless steel nanoparticles is 0.5 for pH controlled 0.017 wt% stainless steel-water mixture.

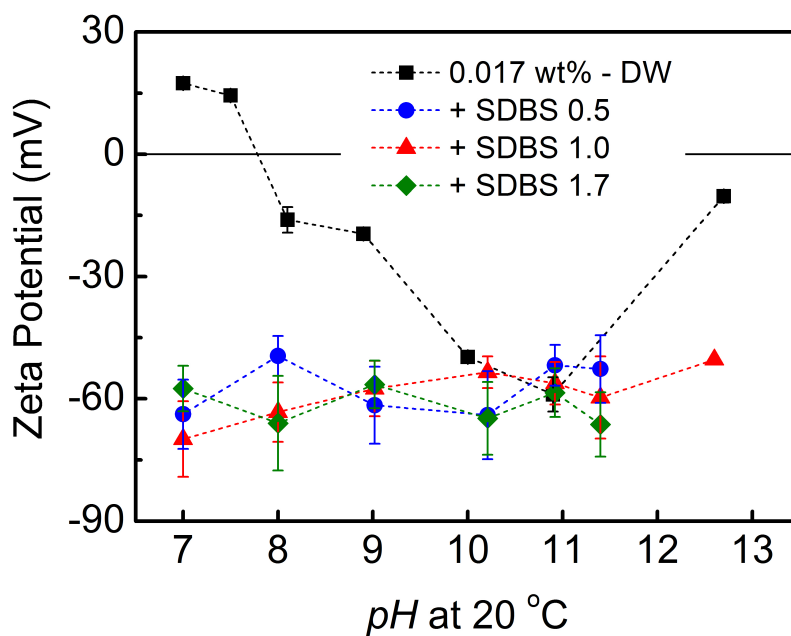


Fig. 4.10 Effect of SDBS on the ζ potential of 0.017 wt% stainless steel-water nanoparticle-fluids with temperature controlled 1 h sonication. The mass ratios of added SDBS to stainless steel particles were 0.5, 1.0 and 1.7.

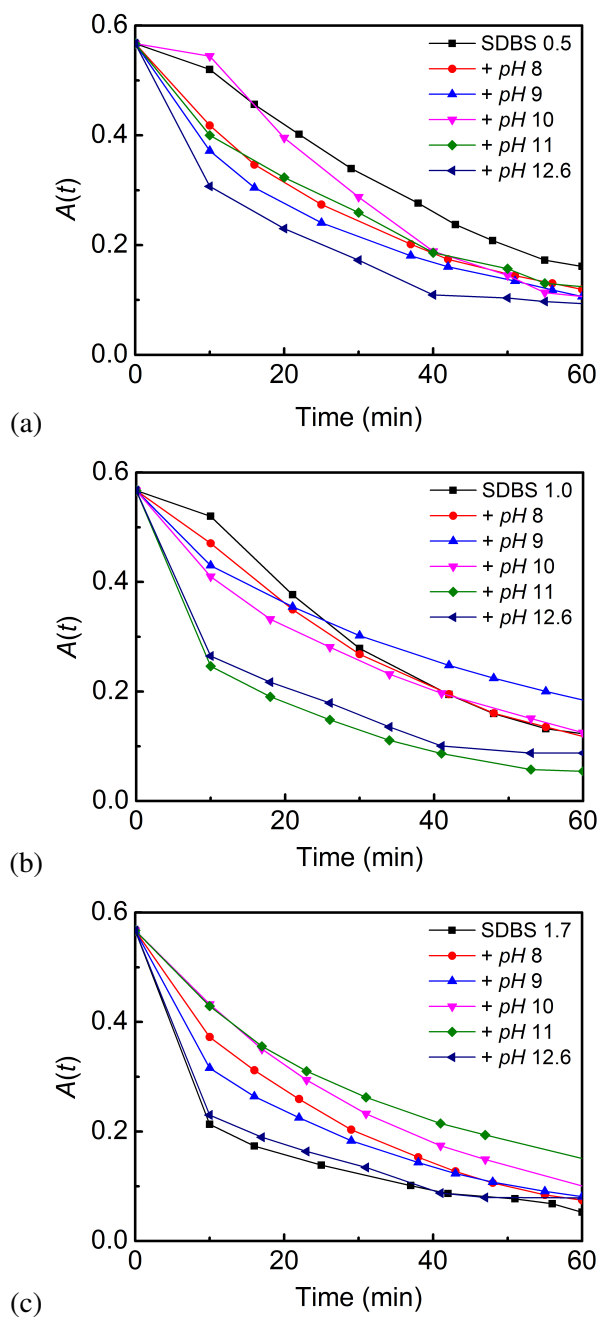


Fig. 4.11 Effect of SDBS concentration on sedimentation of fluids in Fig. 4.10 during 1 h.

4.5 Optimal Stability Conditions

Before concluding that *pH* 11 and SDBS 0.5 are optimal conditions found to increase dispersion stability for 0.017 wt% STS - water fluids, long term and chemical stability should be tested too. Stability of *pH* 10 and *pH* 10+SDBS 0.5 fluids were observed in addition to *pH* 11 and SDBS 0.5 fluids because sedimentation after 30 min was slower in these four samples as shown in Fig. 4.12; A(30 min) is high in the order of *pH* 11, SDBS 0.5, *pH* 10, and *pH* 10+SDBS 0.5.

4.5.1 Long term stability

The ζ -potential and long term stability of the 0.017 wt% nanoparticle-fluids are compared in Fig. 4.13 and Fig. 4.14 for the optimal conditions found in previous sections; *pH* 11, SDBS 0.5, *pH* 10, and *pH* 10+SDBS 0.5. The $|\zeta|$ of the SDBS 0.5 fluids are slightly higher than *pH* 10 and *pH* 11 fluids, but the sedimentation is slowest at *pH* 11 fluid until 150 min as shown in Fig. 4.14(a). Fig. 4.14(a) shows particles settle down rapidly for 3 h and only less than 20 % of particles remain dispersed in the fluid. After 3 h, sedimentation rate is relatively slower and the overall long term stability was 10 days for *pH* 11, 3 days for *pH* 10 and DW, and less than 1 day for other fluids.

Above results show the electrostatic stabilisation is more effective in conferring greater stability than steric stabilisation for the 0.017 wt% stainless steel-distilled water nanoparticle-fluids. It can be concluded that *pH* 11 is the optimal stability condition found for 0.017 wt% stainless steel-water nanoparticle-fluids having slowest sedimentation rate.

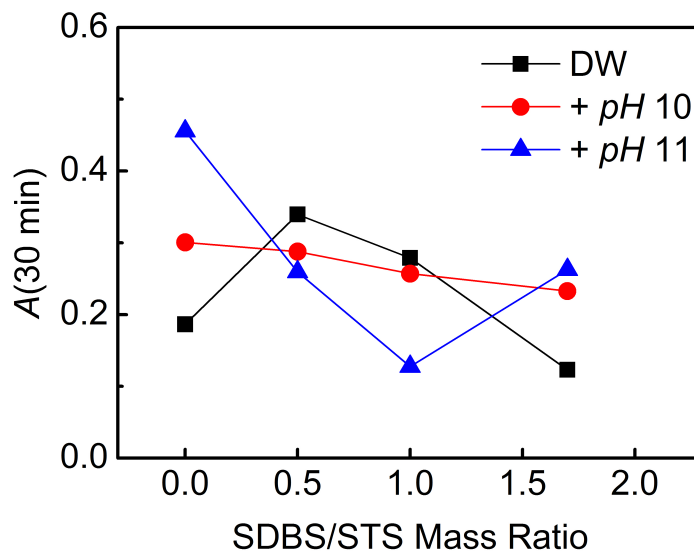


Fig. 4.12 Effect of SDBS concentration on stability of DW ($pH 7$), $pH 10$ and $pH 11$ fluids. $A(30 \text{ min})$ is absorbance measured 30 min after production.

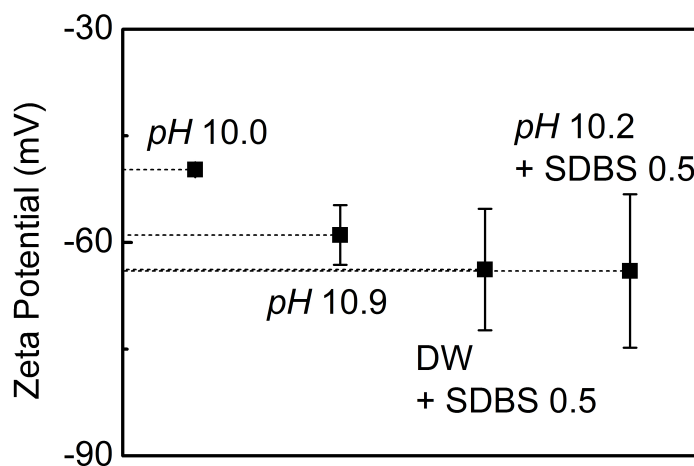


Fig. 4.13 The ζ -potential of selected 0.017 wt% stainless steel-water nanoparticle-fluids.

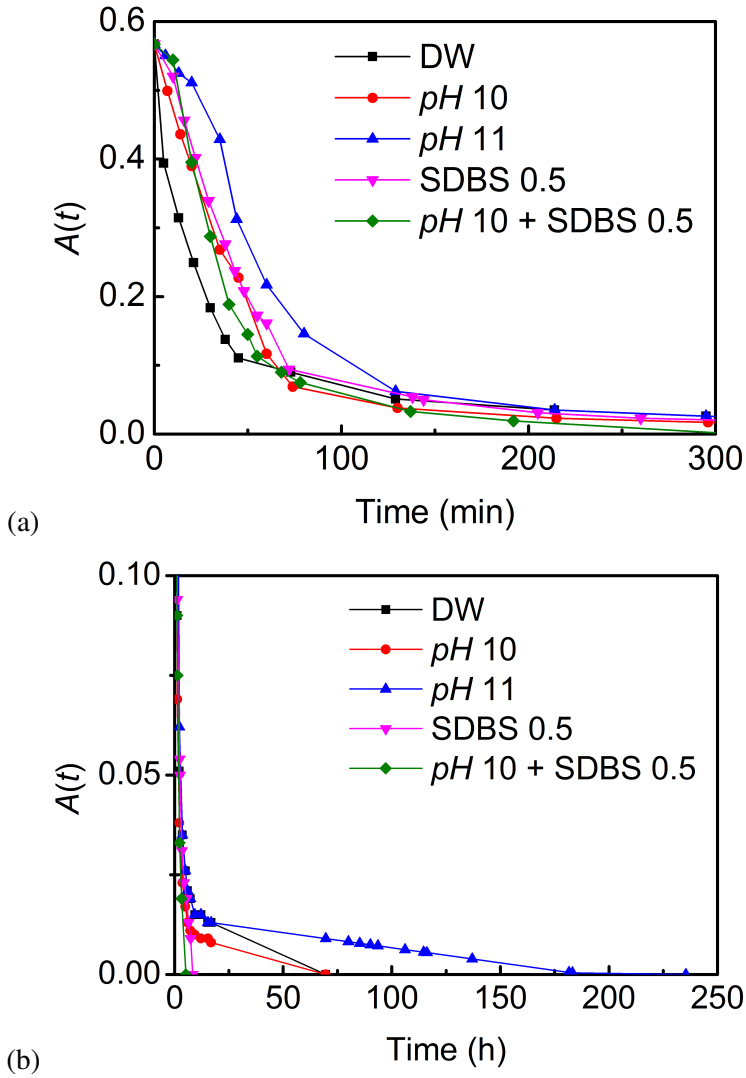
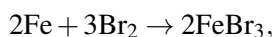


Fig. 4.14 (a) The short term and (b) long term stability of selected 0.017 wt% stainless steel-water nanoparticle-fluids.

4.5.2 Chemical stability

Before concluding that NaOH or SDBS addition help stainless steel particles dispersion, there is a need to identify that no chemical reaction exist between additives and particles. After storing fluids at stay for 5 days after production, the particle morphology was observed by TEM. Fig. 4.15(a),(b),(c) show there is no apparent particle shape change compared with Fig. 3.1, so using NaOH or SDBS is thought not to cause any chemical reaction. However, although it is difficult to conclude by Fig. 4.15(d), it seems that the shape of stainless steel particles changed by the addition of CTAB.

The molecular formula of CTAB is $C_{19}H_{42}BrN$, and in aqueous solution it ionize to Br^- and CTA^+ ions. Iron and bromine can react with the chemical equation of:



to form ferric bromide (iron(III) bromide). Samples with NaOH, SDBS and CTAB were stored at stay for 3 months to verify the chemical reaction that may happen. After 3 months, there were no difference in NaOH and SDBS added samples, but formation of transparent crystalloids was observed in CTAB added sample.

Fig. 4.16 shows the crystalloid is bromide. Its composition is analyzed by energy-dispersive X-ray spectroscopy (EDS) analysis using FE-TEM(JEM-2100F,JEOL). Because TEM sample was made from the mixture of stainless steel particles, CTAB and water, non-spherical shaped particles found in the sample is something else, not stainless steel particles which was not observed in other samples. From EDS result, the amount of Mn, Ni and Mo was negligible < 0.1 wt%, and majority was 24.72 ± 6.18 wt% Fe and 75.28 ± 6.18 wt% Br. Therefore, surfactants containing bromide should be abandoned when using iron containing nanoparticles.

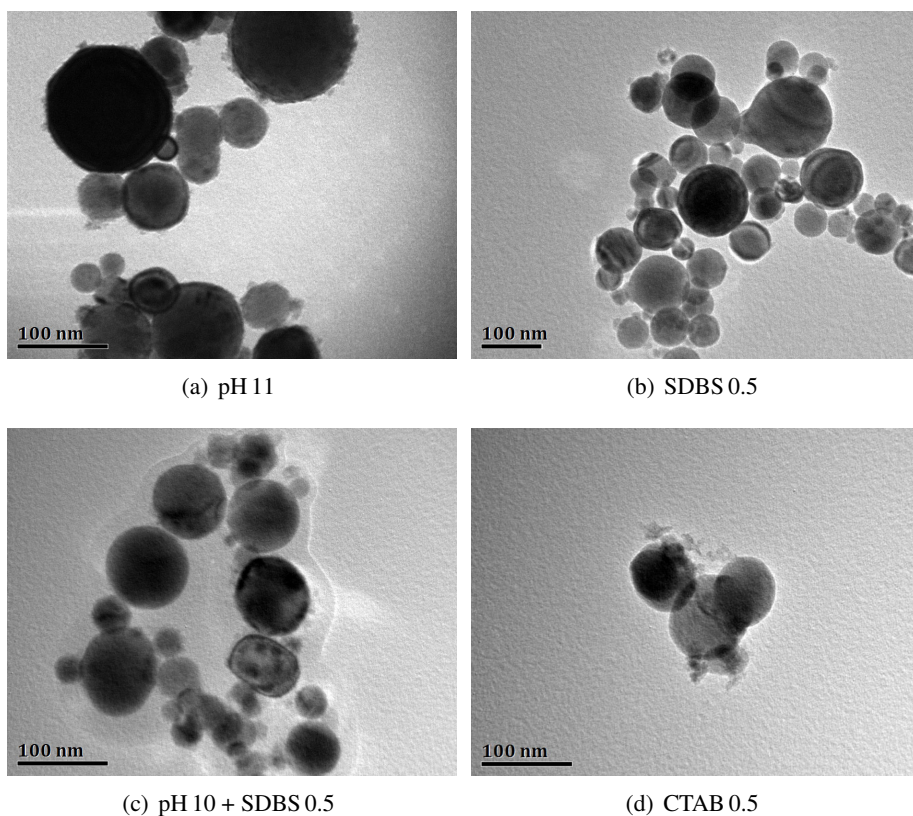


Fig. 4.15 TEM images of stainless steel 316L nanoparticles dispersed in NaOH or surfactant added distilled water. To observe the effect of NaOH or surfactant on particle shape, nanoparticle-fluids were stored at room temperature for 5 days and then sonicated for 30 min before making the TEM sample.

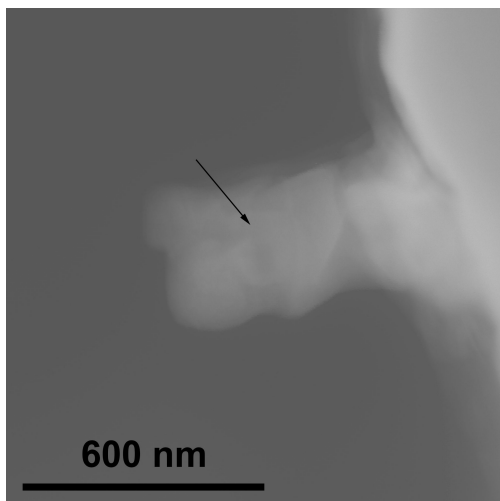


Fig. 4.16 Formation of bromide (marked by arrow) verified by energy-dispersive X-ray spectroscopy analysis using TEM from 3 months stored CTAB added stainless steel-water sample.

4.5.3 Thermal conductivity at optimal conditions

Fig. 4.17 shows the thermal conductivity enhancement k_{nf}/k_f of the samples in Fig. 4.13 (pH 11, SDBS 0.5, pH 10, pH and 10+SDBS 0.5) compared with DW sample at 24–26 °C. To measure the thermal conductivity using the conductivity cell in Fig. 3.2, 250 ml of sample is required. Because the process scale was fixed to 50 ml in stability investigations of this chapter, several identical fluids were prepared at once and mixed before the thermal conductivity measurement for dispersion consistency.

Fig. 4.17 shows that the measured thermal conductivity enhancement is higher when the overall stability is better; measured k_{nf}/k_f at 10 min after production is highest at pH 11 sample, the most stable fluid among studied. Large deviations and k_{nf}/k_f ranging under 1.0 having smaller k_{nf} than water, is probably because of rapid sedimentation during measurements. Although the time of the measurement is very short, particles will continuously settle down as shown in Fig. 4.14.

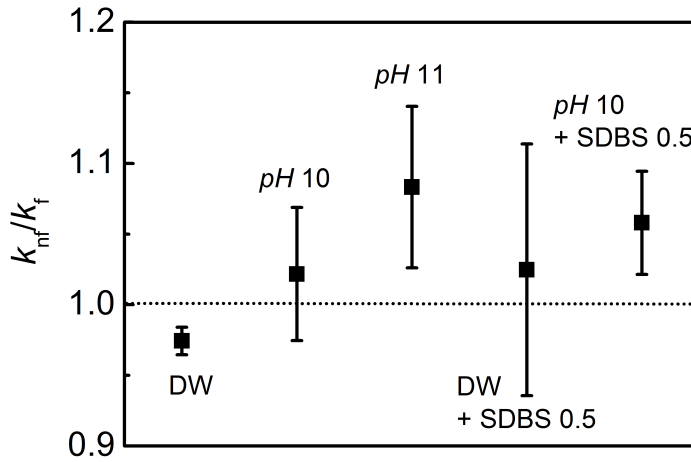


Fig. 4.17 The thermal conductivity enhancement k_{nf}/k_f of selected 0.017 wt% stainless steel-water nanoparticle-fluids. Measurement was done within 10 min after production.

Fig. 4.18 presents the thermal conductivity enhancement as a function of particle concentration for stainless steel particles dispersed in base fluids of pH 11. It shows that the thermal conductivity enhancement increases as particle concentration increases. Thermal conductivity enhancement of 8.3% with very small amount of stainless steel particles of 0.0021 vol% (0.017 wt%) is significant, far exceeding the Maxwell's prediction (Maxwell, 1873). This is comparable to the 23.8% enhancement with 0.1 vol.% copper particles in water reported by Liu et al. (2006).

However, the decrease of thermal conductivity enhancement was too fast, converging to 1.0 in 30 min. Although 30 min is longer than 10 min reported for copper-water fluids (Liu et al., 2006), there is a need to slow down the sedimentation to make use of excellent initial heat transfer property of stainless steel-water fluids. In addition, Fig. 4.18 shows non-linear relationship between enhancement and particle volume fraction; enhancement at 0.024 wt% is similar to 0.017 wt%, and the linear fit of two

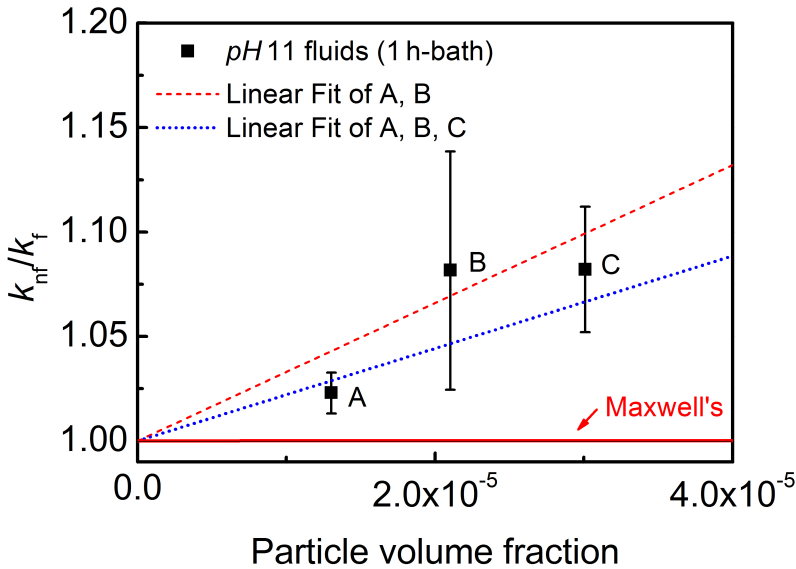


Fig. 4.18 The thermal conductivity enhancement k_{nf}/k_f of *pH* 11 stainless steel-water fluids as a function of particle volume fraction. Thermal conductivity measurement was done within 10 min after production. Maxwell's prediction was done using Eq. 1.1 with $k_{STS} = 15 \text{ W m}^{-1} \text{ K}^{-1}$ and $k_{\text{water}} = 0.5984 \text{ W m}^{-1} \text{ K}^{-1}$ at 20°C from Table 3.2.

points and three points have some gap. This non-linearity at higher concentrations was also observed in some previous studies that produced nanofluids at several concentrations with optimal stability condition found in certain concentration (Li et al., 2008; Murshed et al., 2005) (refer to Fig. 5.1).

4.6 Conclusion

The stability (resistance to sedimentation) of stainless steel nanoparticles and water mixtures has been characterised, including the tendency of the particles to avoid agglomeration. The parameters studied include size distribution, ζ -potential and absorbance change of the nanoparticles in distilled water with *pH* control and surfactant additions. It is clear that both ζ -potential and absorbance (sedimentation) measurements are important in measuring the stability of nanoparticle-fluids.

Dispersion via ultrasonic vibration was used to induce the separation of agglomerated particles; however, it was found that stainless steel-water mixtures require a constant low temperature in the sonication bath. Otherwise, the viscosity of the water is reduced when the temperature increases, causing rapid sedimentation during the sonication treatment. In addition, it is shown that increasing the sonication time does not always increase the stability of mixtures.

Sodium hydroxide additions were used to control the *pH* of the fluid; the isoelectric point was found to be at *pH* 7.8 for 0.017 wt% stainless steel-water mixture. The experiments revealed that *pH* 11 led to optimal condition, where the magnitude of the ζ -potential was much larger than the value of 25 mV considered as a threshold in maintaining particle separation.

The stability at *pH* 11 counter to expectations, decreased when the surfactant sodium dodecyl benzene sulphonate (SDBS) was added whereas the stability of distilled water fluid (*pH* 7) was found to increase when the SDBS concentration was kept to about half that of the stainless steel powder. Although, the most stable condition was at *pH* 11 (*pH* 10.9 – *pH* 11.1) without any SDBS in this work. However, one of optimal conditions may have higher stability when more powerful dispersion methods are used effectively.

The long term stability was 10 days at *pH* 11, 3 days at *pH* 10 and distilled water

without any addition and less than 5 hours for others. Particles settled down rapidly for 1 h after the production and the remaining dispersed particles were less than half of the initial concentration. This initial rapid sedimentation problem should be solved in the future. In addition, the reaction between particles and surfactants or *pH* controlled fluids should be considered carefully for the long term usage of fluids. No chemical reaction between NaOH and SDBS with stainless steel particles and formation of iron-bromide in CTAB added fluid were verified.

The thermal conductivity of 0.017 wt% stainless steel nanoparticle-water fluids was higher at optimal condition, *pH* 11, showing a strong relationship between the fluid stability and heat transfer property. Thermal conductivity was increased 8.3 % at *pH* 11 fluid with 0.0021 vol.% of stainless steel particles.

Chapter 5

Stainless steel–Nanofluids: Stability to Thermal conductivity

5.1 Introduction

In chapter 4, the optimal stability condition for 0.017 wt% STS-DW fluid was studied, and the measured thermal conductivity enhancement at lower and higher concentration showed non-linear relationship as in Fig. 4.18.

Although the optimal pH , surfactant and its concentration, and dispersion methods have been studied for some nanofluids at specific concentrations (Ghadimi and Metselaar, 2013; Habibzadeh et al., 2010; Haghghi et al., 2013; Hwang et al., 2007; Lee et al., 2014; Li et al., 2008; Meibodi et al., 2010; Nasiri et al., 2011, 2012; Philip and Shima, 2012; Saterlie et al., 2011; Wang et al., 2009), the stability at various concentrations has not been studied, which is required to characterise the thermal conductivity enhancement with respect to the particle concentration. In addition, there are only four previous studies on metallic-nanofluids among these; Li et al. (2008); Saterlie et al. (2011); Wang et al. (2009) studied copper-water nanofluids with surfactants, and

Lee et al. (2014) studied silver-water nanofluids.

Studies on thermal conductivity of metallic-nanofluids are listed in Table 5.1, and the number of studies is much less than oxides or nanotubes containing fluids. Table 5.1 shows that enhancement varies among groups, and mostly studied particle and fluid are copper and EG, respectively.

As shown in Fig. 5.1, the thermal conductivity enhancement is not linear with particle fraction; enhancement decreases at certain higher concentrations (Li et al., 2008; Murshed et al., 2005; Sundar et al., 2013). The decrease in the enhancement slope appear around 1 vol.% for Fe_3O_4 and TiO_2 , 0.05 vol.% for Cu, and 0.002 vol.% for STS containing water-based fluids, and the possible reasons can be as follows: probably because the optimal stability conditions found for lower concentrations were used for fluids at higher concentrations, or there are critical concentration for each nanoparticle and fluid mixture that the thermal conductivity enhancement due to addition of particles is maximized.

Therefore, there is a need to verify will the stability condition found at specific concentration work for other concentrations, and if not, how to measure or determine ‘complete particle dispersion’ at various concentrations. Then, the linearity of particle volume fraction and thermal conductivity enhancement should be investigated under ‘complete particle dispersion’ state. This will be shown in this chapter, with the stainless steel particles dispersed in water and ethylene glycol.

Table 5.1 Previous studies on metallic-nanofluids. Ref. is reference, ϕ is particle volume percent in the unit of vol.%, En. is thermal conductivity enhancement $\frac{k_{nf}-k_f}{k_f} \times 100\%$, and PM is the production method used where 1 and 2 indicate one-step and two-step, respectively.

Ref.	Particle	Fluid	ϕ	En.	PM
Xuan and Li (2000)	Cu(100)	Water	7.5	78	2
Eastman et al. (2001)	Cu(< 10)	EG +thioglycolid acid	0.3	40	1
Patel et al. (2003)	Cu(< 10)	EG	0.55	15	
	Au(3 – 4)	Toluene	0.011	7	1
	Au(10 – 20)	Water	0.00026	4.6	1
Hong et al. (2005)	Ag(60 – 80)	Water	0.001	3.2	1
	Fe(< 10)	EG	0.55	18	2
	Liu et al. (2006)	Cu(50 – 100)	Water	0.1	23.8
Chopkar et al. (2006)	Al ₇₀ Cu ₃₀ (20 – 40)	EG	2.5	130	2
Putnam et al. (2006)	C ₆₀ -C ₇₀	Toluene	0.36	0.008	2
	Au(2)	Toluene	0.25	0.014	
	Au(4)	Ethanol	0.06	0.013	1
Chopkar et al. (2008)	Al ₂ Cu(30)	EG	2.0	85	2
	Al ₂ Cu(30)	Water		98	
	Ag ₂ Al(30)	EG		95	
	Ag ₂ Al(30)	Water		105	
Garg et al. (2008)	Cu(200)	EG	2.0	12	2
Sinha et al. (2009)	Cu(10 – 20)	EG	1.0	60	2
	Fe(7 – 10)	EG		27	
Yu et al. (2010)	Cu(5 – 10)	EG	0.3	8-10	2

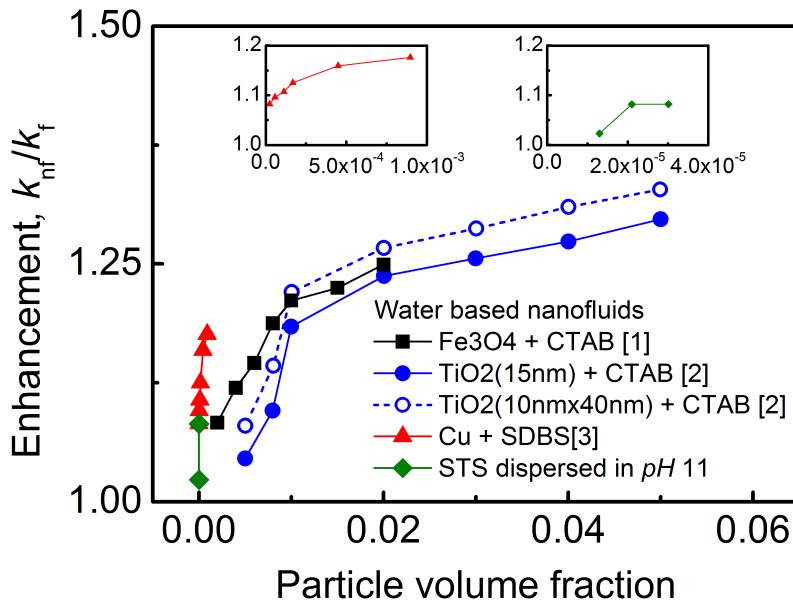


Fig. 5.1 Thermal conductivity enhancement versus particle volume fraction of some water-based nanofluids with surfactants added to increase stability. Green diamond represents stainless steel dispersed in pH 11 water, data from Fig. 4.18. The particle mass fraction of [3] is converted into volume fraction using Eq. 5.2 with $\rho_{\text{water}} = 998.5 \text{ kg m}^{-3}$ (Sundar et al., 2013) and $\rho_{\text{Cu}} = 8940 \text{ kg m}^{-3}$ (Callister, 2007). [1] Sundar et al., 2013, [2] Murshed et al., 2005, [3] Li et al., 2008.

5.2 Determining Complete Dispersion

5.2.1 Nanofluid production

In previous chapter, the production parameters at 0.017 wt% were 1 h temperature controlled sonication using ultrasonication bath with the production scale of 50 ml. However, there were difficulties when measuring thermal conductivity because at least 250 ml was required in the use of thermal conductivity cell. In addition, higher sonication power was necessary for having good particle dispersion to find the molar absorptivity of the particle (this will be discussed in this section). Therefore, ultrasonic processor was used in this chapter, which has higher sonication power and increased production scale up to 1 litre. The production scale was fixed to 300 ml, and the temperature was controlled not to exceed 30 °C by placing the solution-container in a bath with cold water which was replaced regularly.

The particle concentration can be noted as either in mass fraction (w) or volume fraction (ϕ), and both will be used; generally, mass fraction for stability and volume fraction for thermal conductivity are used. The particle mass fraction can be converted into volume fraction using the relationship of (Sundar et al., 2013):

$$\phi_p = \frac{\frac{m_p}{\rho_p}}{\frac{m_p}{\rho_p} + \frac{m_f}{\rho_f}}, \quad (5.1)$$

where m is the mass of the particle or fluid and the particle mass fraction is defined as $w_p = \frac{m_p}{m_p + m_f}$. Then, the particle volume fraction is,

$$\phi_p = \left(1 + \frac{1 - w_p}{w_p} \times \frac{\rho_p}{\rho_f} \right)^{-1}. \quad (5.2)$$

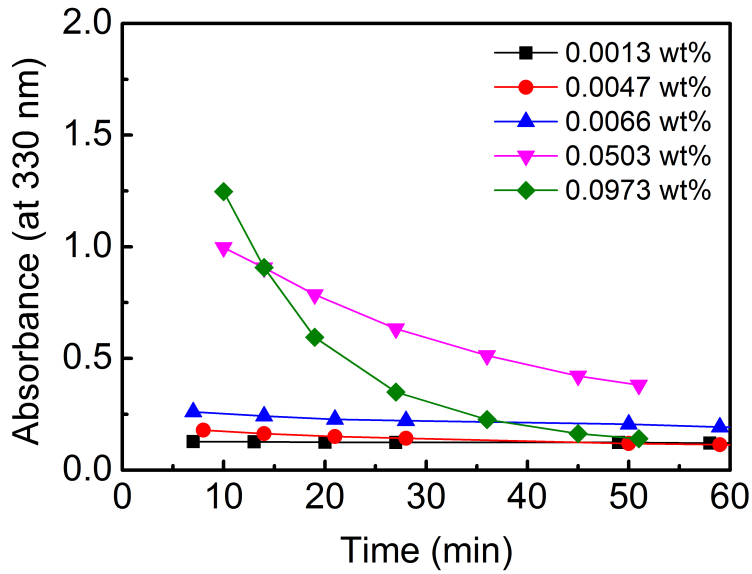
5.2.2 Molar absorptivity of STS particles

By Beer-Lambert law, absorbance is linear to the particle concentration; $A = \epsilon bc$. With the knowledge of molar absorptivity ϵ , it is possible to predict the absorbance at certain concentration. Because the molar absorptivity of stainless steel particles was not found in the literature, this value was measured first.

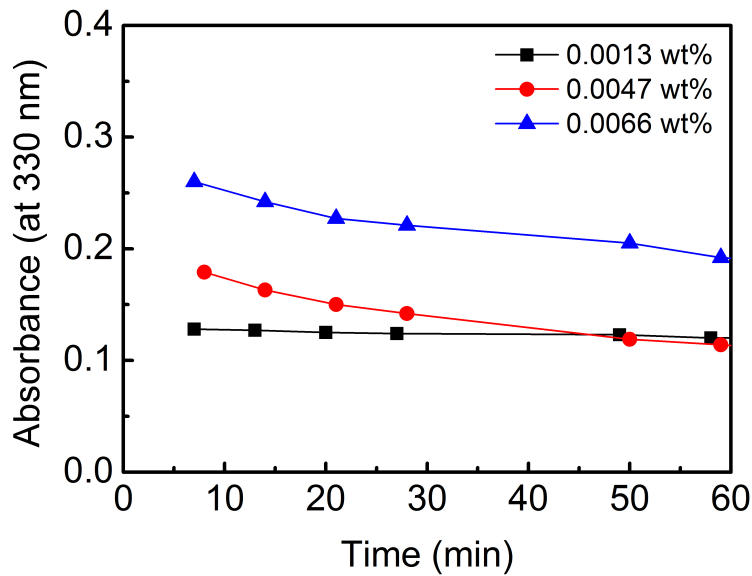
The molar absorptivity of 70 nm sized stainless steel particles can be determined experimentally if the selected samples are well dispersed, without sedimentation during the absorbance measurement. Therefore, the particle molar absorptivity was found at the very dilute particle concentration range, at where the absorbance over time of samples were almost constant over minutes. As in Fig. 5.2(a), when the particle concentration is lower than 0.01 wt%, the decrease of absorbance over time was very small only with 1 h temperature controlled sonication in bath. In Fig. 5.2(b), 0.0013 wt% fluid is very stable, almost no absorbance decrease during 1 h.

Using the measured absorbance of samples in Fig. 5.2(b), the slope of absorbance versus particle concentration was fitted to a line passing through the origin. However, Fig. 5.3(a) shows the fitted two slopes are different; one was fitted using three samples of Fig. 5.2(b), and the other was fitted only with 0.0013 wt% sample. This is because the values used for fitting in case of 0.0047 wt% and 0.0066 wt% samples are the absorbance at $t = 7$ min, after some particles settled down as shown in Fig. 5.3(b). In the 0.0013 wt% sample, the observed decrease in absorbance during 1 h was 0.008, which is negligible.

Although the best stability of 0.017 wt% stainless steel - distilled water at pH 11 well agrees the with the linear fit of three samples, it seems that the slope obtained only by 0.0013 wt% sample is correct. This implies that the particles cannot be dispersed completely using ultrasonication bath. Thus, ultrasonic processor was then used to test the increase in absorbance and dispersion stability.

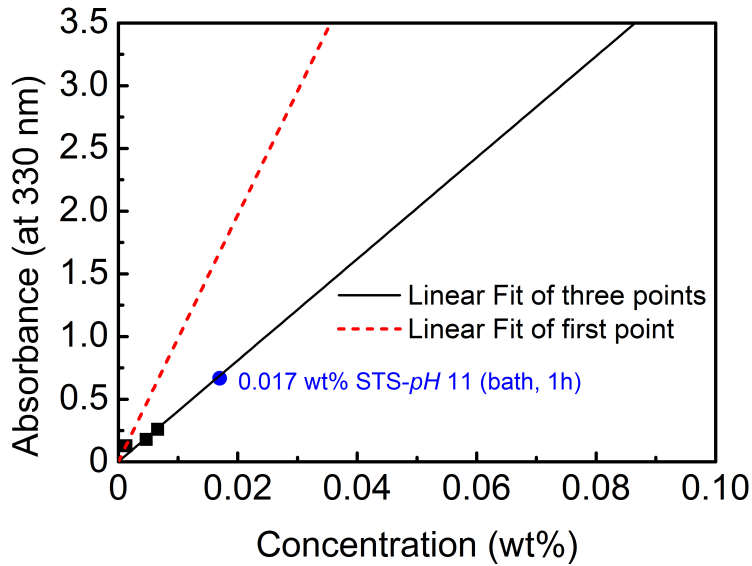


(a)

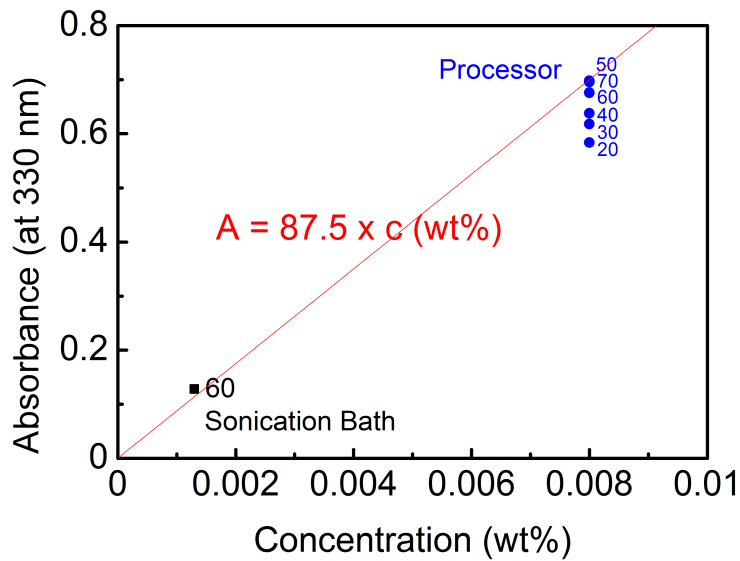


(b)

Fig. 5.2 Absorbance over time for stainless steel - water nanofluids at several concentrations. Sample production done using ultrasonication bath for 1 h, temperature controlled. No addition of surfactants and NaOH.



(a)



(b)

Fig. 5.3 Absorbance versus concentration of (a) 70 nm stainless steel particles dispersed in water with identical samples of Fig. 5.2, and (b) 0.008 wt% samples produced using ultrasonic processor.

Fig. 5.3(b) shows the measured absorbance of 0.008 wt% STS-water fluid produced by ultrasonic processor increase up to the line fitted with 0.0013 wt% when sonication time was increased to 50 min. The uniform dispersion of particles was enhanced as the sonication time increased from 20 min to 50 min, and then particles started to settle down (decrease in absorbance) with longer sonication time than 50 min. This is the reason of using agitation with higher sonication power and finding optimal sonication time for each sample.

In conclusion, the absorbance of 0.013 wt%-water produced with 1 h ultrasonication bath and 0.008 wt%-water produced with 50 min ultrasonic disrupter are the absorbance that can be measured with complete dispersion of particles at each concentration. The molar absorptivity was calculated by fitting these two points passing through the origin. The measured molar absorptivity of 70 nm-sized spherical stainless steel 316L particles at 330 nm is $87.5 \text{ cm}^{-1} \text{ wt}\%^{-1}$. If $A = 87.5 \times c$ ($b = 1 \text{ cm}$ and c in wt%) is measured for a fluid with a particle concentration c , the sample can be considered to be in complete dispersion condition. Also, because molar absorptivity is a material property, this should also work well in ethylene glycol-based fluids, too.

5.2.3 Complete dispersion condition at various concentrations

To verify the experimental molar absorptivity and the applicability of using molar absorptivity to determine the complete particle dispersion at various concentrations, stainless steel particles were dispersed in water and ethylene glycol at various concentrations. Using ultrasonic processor for dispersion of particles, the sonication time was increased by 10-20 minute intervals until the measured absorbance right after the production at each concentration was within $\pm 1 \%$ of the prediction.

Fig. 5.4 shows that the molar absorptivity of $87.5 \text{ cm}^{-1} \text{ wt}\%^{-1}$ agrees well with particle concentration up to 0.04 wt% and also when stainless steel particles are dis-

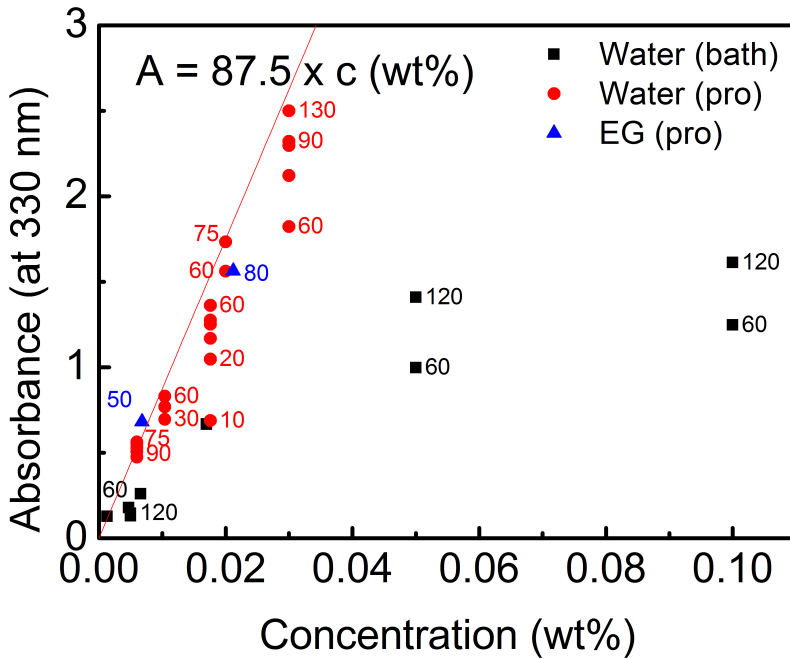


Fig. 5.4 Absorbance versus concentration of samples with various concentration. Sonication time in the unit of minute is indicated in the figure. 'bath' and 'pro' mean samples produced using ultrasonication bath and processor, respectively.

persed in ethylene glycol, too. Because the maximum absorbance allowed by the equipment is 3.0, concentrations that are expected to have absorbance over 3.0 when dispersed completely were not tested in this study.

Above results show that dispersion of particles were not enough when using sonication bath, and the sonication time required to get complete dispersion increased as the concentration increased. Therefore, optimal stability condition at certain concentration is not sufficient to obtain dispersion stability at other concentrations, especially at higher concentrations.

5.3 Thermal conductivity enhancement

5.3.1 Thermal conductivity enhancement under complete dispersion of particles

It is interesting that the nonlinear relationship between absorbance and particle concentration in water-based samples produced using sonication bath of Fig. 5.4 is similar to the relationship between thermal conductivity enhancement and particle volume fraction of these samples which was shown in Fig. 4.18. This is the result that can explain the disagreement in thermal conductivity enhancement of nanofluids between groups. Although identical particles and base fluid are used, the heat transfer property will depend on their dispersion stability that will vary between groups due to different production parameters.

Under complete dispersion of particles, thermal conductivity enhancement was observed, and the result is in Fig. 5.5. The particle mass fraction was converted into volume fraction using Eq. 5.2, and the sonication time of each sample was controlled to have complete particle dispersion. Under the complete dispersion, the enhancement due to stainless steel particles was higher at water-based fluids than EG-based, and both showed linear relationship with particle volume fraction.

Thermal conductivity enhancement by stainless steel particles is significant, far exceeding the Maxwell's prediction (Maxwell, 1873) and also comparable with other metallic-particles; thermal conductivity enhancement was 4.6 % with 0.00026 vol.% gold in water (Patel et al., 2003), 23.8 % with 0.1 vol.% copper in water (Liu et al., 2006), and 18 % with 0.55 vol.% iron in ethylene glycol (Hong et al., 2005). Considering the bulk thermal conductivity of gold, copper and iron are 317, 400, and 80 $\text{W m}^{-1} \text{K}^{-1}$ (Lide, 2004), the enhancement by stainless steel particles can be explained by obtaining sufficient stability.

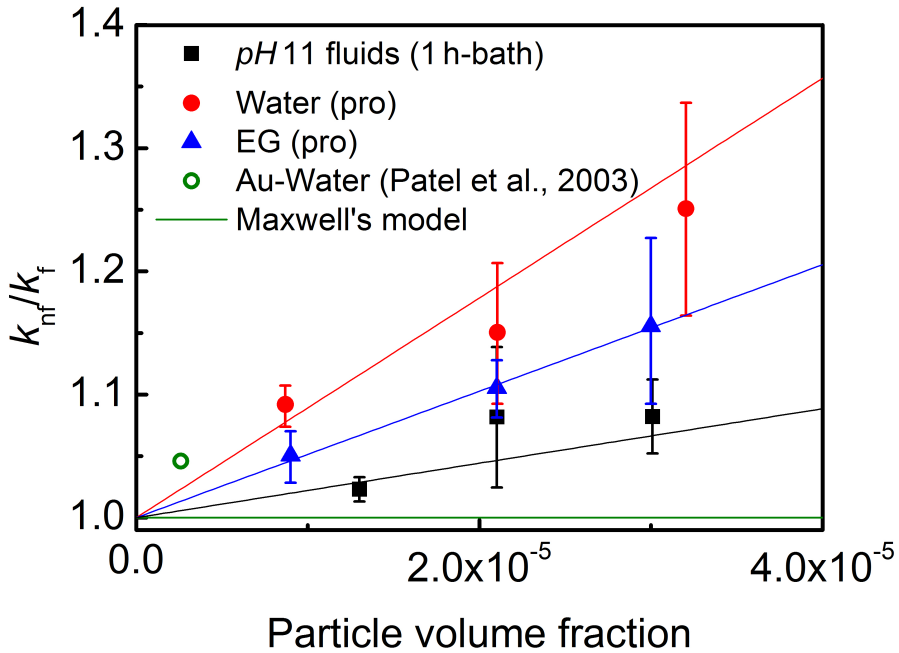


Fig. 5.5 Thermal conductivity enhancement as a function of particle volume fraction of stainless steel-nanofluids compared with Maxwell's model (refer to Fig. 4.18) and Au-water nanofluid (Patel et al., 2003). Measurement was done 10 min after production, and the red, blue and black lines are fitted lines.

5.3.2 Possibility of overestimate by using transient hot-wire method

In some previous studies, the possibility of overestimate when using transient hot-wire method to measure the thermal conductivity of nanofluids was raised, as transient hot-wire method was originally designed for thermal conductivity measurement of gases and liquids. For example, Ghosh (2010); Ghosh et al. (2011) conducted molecular dynamics and stochastic simulations and showed that there exists pulse-like heat pickup that causes increase in heat conduction of nanofluids when using transient hot-wire method, due to the collision between nanoparticles and the heat source. They concluded that the elastic and other physical properties of nanoparticles also influence the

thermal properties of nanofluids.

While the simulated result was shown to match well with measured thermal conductivity enhancement, the existence of pulse-like heat pickup was not experimentally verified. The simulation was done by modelling the collision between 4 nm copper particles and copper heat source to predict the thermal conductivity enhancement of copper particles dispersed in pure water. However, the heat source should be insulated when measuring the thermal conductivity of water-based fluids because water is an electrically conducting fluid, and therefore the simulation model has limitations in describing the transient hot-wire measurement.

If the result of Ghosh *et al.*, additional heat conduction by particle and heat source collisions exist, then the distance from the heat source to particles may also influence the heat conduction of nanofluids. Thicker fluid film between heat source and particles can disturb the movement of particles and the heat conduction.

To observe this effect, thermal conductivity of Al₂O₃-ethylene glycol fluid was measured at various fluid thicknesses. Ethylene glycol was chosen to exclude the error coming from electrical conduction, and 13 nm alumina was selected to increase the particle dispersion and avoid particle aggregations. The fluid thickness is the distance from the heat source to particles, so the radius of the thermal conductivity cell. As in Fig. 5.6, removable glass tubes with radii of 8 mm, 17 mm and 27 mm were placed in a 120 mm thick glass cell. For consistency, the same sample fluid was used to measure the thermal conductivity at each fluid thickness.

Fig. 5.7 shows that there is no fluid thickness effect. The thermal conductivity of ethylene glycol was within $\pm 5\%$ compared with the reference value (Lide, 2004) at all tested fluid thicknesses and was increased when nanoparticles were added. This result also shows that using too thin a cell in the transient hot-wire method can cause overestimation in measurements, because the measured thermal conductivity was higher at

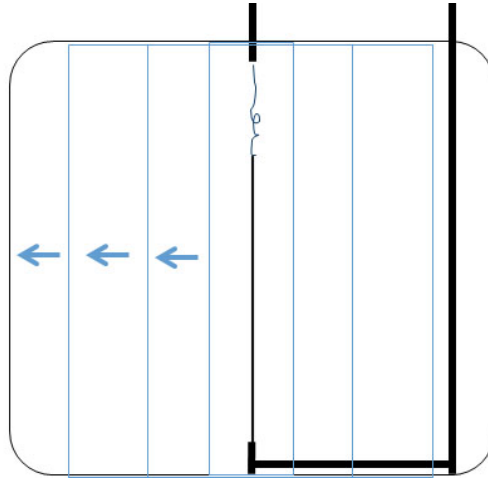


Fig. 5.6 Sketch of thermal conductivity cell with removable tubes to control fluid thickness.

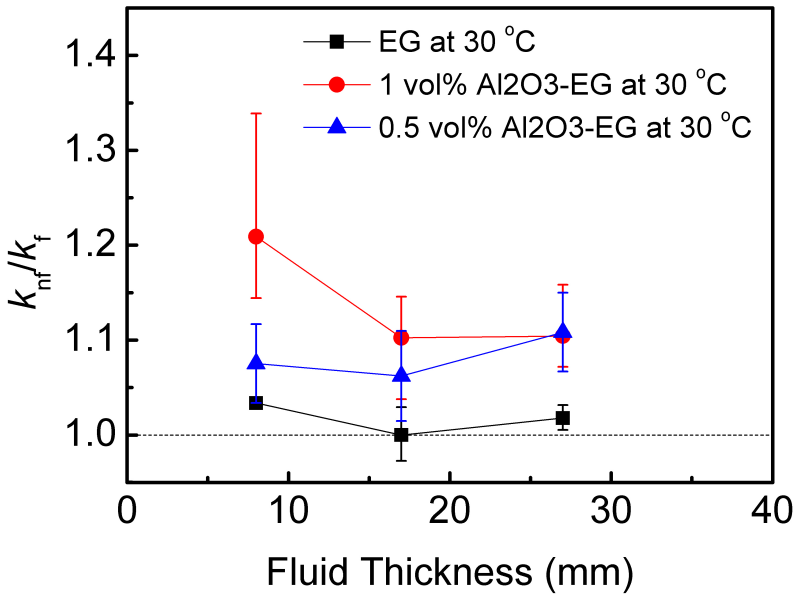


Fig. 5.7 Measured thermal conductivity enhancement of ethylene glycol with and without 13 nm Al₂O₃ particles at 30 °C at various fluid thickness.

8 mm thickness even without any nanoparticles.

The effect of particle volume fraction cannot be discussed in case of Al_2O_3 -EG fluids used in Fig. 5.7 as the complete particle dispersion was not tested for these fluids. In conclusion, the possibility of additional heat conduction coming from collision between particles and heat source when using transient hot-wire method was not found in this study.

5.4 Conclusion

The molar absorptivity of 70 nm-sized spherical stainless steel 316L particles at 330 nm is measured to be $87.5 \text{ cm}^{-1} \text{ wt}\%^{-1}$. Complete dispersion of particles can be determined by using this value, and it is verified that the stability condition at one concentration does not work for wide range of concentrations. For example, sonication time required for complete dispersion increased as particle concentration increased.

Linear relationship of volume fraction and thermal conductivity enhancement was observed when fluid is sufficiently stable. Stability is important, and without considering stability, the enhancement achieved will not be that efficient.

The possibility of overestimate using transient hot-wire method was tested and was not found in this study.

Chapter 6

Conclusions

Based on the theoretical and experimental studies that have been done to reveal the mechanism behind the enhanced heat transport property of nanofluids, it was concluded that the parameters known to influence the conductivity are volume fraction, material size and shape of nanoparticles, the material and acidity of the base fluid, temperature of nanofluids, sonication power and time, and additives such as surfactants. Researchers tried to achieve good thermal conductivity enhancement by controlling these parameters, but the results varied among groups and some samples were not reproducible. In addition, although metallic-nanofluids showed higher thermal conductivity enhancement than oxide-nanofluids, only few previous studies were done.

Therefore, thorough study on stability and thermal conductivity of stainless steel-nanofluids to represent metallic-nanofluids was done in this work. First, the stability criteria at 0.017 wt% stainless steel-water fluids were found and *pH*, 11 and SDBS 0.5 fluids using 1 h temperature controlled sonication by bath showed better stability with lower sedimentation rate. However, when this stability condition was applied to other concentrations, thermal conductivity enhancement was not linear to particle volume fraction.

There was a need to determine the complete dispersion at certain concentration, which was not discussed before. In this study, this problem was solved using Beer-Lambert law, and the molar absorptivity of stainless steel particles were first measured. The molar absorptivity of 70 nm-sized spherical stainless steel 316L particles at 330 nm is found to be $87.5 \text{ cm}^{-1} \text{ wt}\%^{-1}$, and complete dispersion of particles was determined using this value. It was verified that the stability condition at one concentration does not work for wide range of concentrations; sonication time required for complete dispersion increased as particle concentration increased.

Linear relationship of volume fraction and thermal conductivity enhancement was observed when fluid is sufficiently stable. Thermal conductivity enhancement of stainless steel-water nanofluids was approximately 10 %, 15 % and 20 % at the volume of 0.001 vol.%, 0.002 vol.% and 0.003 vol.%, respectively. This is comparable to the 23.8 % enhancement with 0.1 vol.% copper particles in water reported by [Liu et al. \(2006\)](#) and 4.6 % enhancement with 0.00026 vol.% gold particles in water reported by [Patel et al. \(2003\)](#). Stability is important, and without considering stability, the enhancement achieved will not be that efficient.

Thermal conductivity enhancement related strongly to the stability of nanofluid suspensions. Known effect parameters can be categorized into three groups; to be studied, conventional and stability. Thermal conductivity of particle and fluid, particle volume fraction are parameters considered in conventional theories. Sonication power and time, *pH*, and additives are related to dispersion stability of nanofluids that will eventually influence thermal conductivity of nanofluids. Particle size and fluid temperature need more study.

References

- Abareshi, M., Goharshadi, E. K., Mojtaba Zebarjad, S., Khandan Fadafan, H., and Youssefi, A. (2010). Fabrication, characterization and measurement of thermal conductivity of Fe₃O₄ nanofluids. *Journal of Magnetism and Magnetic Materials*, 322:3895–3901.
- Assael, M., Metaxa, I., Kakosimos, K., and Constantinou, D. (2006). Thermal Conductivity of Nanofluids - Experimental and Theoretical. *International Journal of Thermophysics*, 27:999–1017.
- Bayazıtöđlu, Y. and Özışık, M. N. (1988). *Elements of heat transfer*. McGraw-Hill.
- Beck, M., Yuan, Y., Warriar, P., and Teja, A. (2010). The thermal conductivity of alumina nanofluids in water, ethylene glycol, and ethylene glycol + water mixtures. *Journal of Nanoparticle Research*, 12(4):1469–1477.
- Beck, M. P., Sun, T., and Teja, A. S. (2007). The thermal conductivity of alumina nanoparticles dispersed in ethylene glycol. *Fluid Phase Equilibria*, 260:275–278.
- Beck, M. P., Yuan, Y., Warriar, P., and Teja, A. S. (2009). The effect of particle size on the thermal conductivity of alumina nanofluids. *Journal of Nanoparticle Research*, 11:1129–1136.
- Bergström, L. (1997). Hamaker constants of inorganic materials. *Advances in Colloid and Interface Science*, 70:125–169.
- Bhadeshia, H. and Honeycombe, R. (2011). *Steels: Microstructure and Properties: Microstructure and Properties*. Butterworth-Heinemann.
- Birkhoff, R., Painter, L., and Jr, J. H. (1978). Optical and dielectric functions of liquid glycerol from gas photoionization measurements. *The Journal of Chemical Physics*, 69:4185.
- Bleazard, J. G. and Teja, A. S. (1995). Thermal conductivity of electrically conducting liquids by the transient hot-wire method. *Journal of Chemical and Engineering Data*, 40:732–737.

- Bonnecaze, R. and Brady, J. (1990). A method for determining the effective conductivity of dispersions of particles. *Proceedings of the Royal Society of London. Series A: Mathematical and Physical Sciences*, 430:285–313.
- Bonnecaze, R. and Brady, J. (1991). The effective conductivity of random suspensions of spherical particles. *Proceedings of the Royal Society of London. Series A: Mathematical and Physical Sciences*, 432:445–465.
- Bruggeman, D. (1935). Calculation of various physics constants in heterogenous substances i dielectricity constants and conductivity of mixed bodies from isotropic substances. *Annalen der Physik*, 24:636–664.
- Callister, W. D. (2007). *Materials Science and Engineering: An Introduction*. John Wiley & Sons, Hoboken, New Jersey.
- Carslaw, H. S. and Jaeger, J. C. (1959). *Conduction of heat in solids*. Oxford University Press, New York, USA.
- Chandrasekar, M. and Suresh, S. (2009). A review on the mechanisms of heat transport in nanofluids. *Heat Transfer Engineering*, 30:1136–1150.
- Chen, H., Ding, Y., and Lapkin, A. (2009). Rheological behaviour of nanofluids containing tube/rod-like nanoparticles. *Powder Technology*, 194:132–141.
- Cheng, S. and Vachon, R. (1969). The prediction of the thermal conductivity of two and three phase solid heterogeneous mixtures. *International Journal of Heat and Mass Transfer*, 12:249–264.
- Chitra, S. and Sendhilnathan, S. (2014). Investigation on Thermal Studies of Nanofluids Related to Their Applications. *Heat Transfer-Asian Research*.
- Choi, S. and Eastman, J. (1995). *Enhancing thermal conductivity of fluids with nanoparticles*.
- Choi, S., Zhang, Z., Yu, W., Lockwood, F., and Grulke, E. (2001). Anomalous thermal conductivity enhancement in nanotube suspensions. *Applied Physics Letters*, 79:2252–2254.
- Chon, C., Kihm, K., Lee, S., and Choi, S. (2005). Empirical correlation finding the role of temperature and particle size for nanofluid (al₂o₃) thermal conductivity enhancement. *Applied Physics Letters*, 87:1–3.
- Chopkar, M., Das, P. K., and Manna, I. (2006). Synthesis and characterization of nanofluid for advanced heat transfer applications. *Scripta Materialia*, 55:549–552.
- Chopkar, M., Sudarshan, S., Das, P., and Manna, I. (2008). Effect of particle size on thermal conductivity of nanofluid. *Metallurgical and Materials Transactions A: Physical Metallurgy and Materials Science*, 39:1535–1542.

- Cosgrove, T. (2010). *Colloid science: principles, methods and applications*. Wiley-Blackwell.
- Das, S., Choi, S., Yu, W., and Pradeep, T. (2007). *Nanofluids: Science and Technology*. John Wiley & Sons, Inc., Hoboken, New Jersey, USA.
- Das, S., Putra, N., Thiesen, P., and Roetzel, W. (2003). Temperature Dependence of Thermal Conductivity Enhancement for Nanofluids. *Journal of Heat Transfer*, 125:567–574.
- Davis, R. (1986). The effective thermal conductivity of a composite material with spherical inclusions. *International Journal of Thermophysics*, 7:609–620.
- Derjaguin, B. and Landau, L. (1941). The theory of stability of highly charged lyophobic sols and coalescence of highly charged particles in electrolyte solutions. *Zh. Eksp. Teor. Fiz*, 11:802–821.
- Duangthongsuk, W. and Wongwises, S. (2009). Measurement of temperature-dependent thermal conductivity and viscosity of TiO₂-water nanofluids. *Experimental Thermal and Fluid Science*, 33:706–714.
- Eastman, J., Choi, S., Li, S., Thompson, L., and Lee, S. (1996). Enhanced thermal conductivity through the development of nanofluids. *MRS Proceedings*, 457.
- Eastman, J., Choi, S., Li, S., Yu, W., and Thompson, L. (2001). Anomalously increased effective thermal conductivities of ethylene glycol-based nanofluids containing copper nanoparticles. *Applied Physics Letters*, 78:718.
- El-Kashef, H. (2000). The necessary requirements imposed on polar dielectric laser dye solvents. *Physica B: Condensed Matter*, 279:295–301.
- Fan, J. and Wang, L. (2011). Review of heat conduction in nanofluids. *Journal of Heat Transfer*, 133:1–14.
- Fedele, L., Colla, L., Bobbo, S., Barison, S., and Agresti, F. (2011). Experimental stability analysis of different water-based nanofluids. *Nanoscale Research Letters*, 6:300.
- Feng, Y., Yu, B., Xu, P., and Zou, M. (2007). The effective thermal conductivity of nanofluids based on the nanolayer and the aggregation of nanoparticles. *Journal of Physics D: Applied Physics*, 40:3164–3171.
- Filmetrics. Refractive Index Database, accessed at 2013-12-09, <http://www.filmetrics.com/refractive-index-database>.
- Fourier, J. (1822). *Theorie analytique de la chaleur, par M. Fourier*. Chez Firmin Didot, père et fils.

- Garg, J., Poudel, B., Chiesa, M., Gordon, J. B., Ma, J. J., Wang, J. B., Ren, Z. F., Kang, Y. T., Ohtani, H., Nanda, J., McKinley, G. H., and Chen, G. (2008). Enhanced thermal conductivity and viscosity of copper nanoparticles in ethylene glycol nanofluid. *Journal of Applied Physics*, 103:074301.
- Ghadimi, A. and Metselaar, I. H. (2013). The influence of surfactant and ultrasonic processing on improvement of stability, thermal conductivity and viscosity of titania nanofluid. *Experimental Thermal and Fluid Science*, 51:1–9.
- Ghosh, M. (2010). *A Model of Thermal Conductivity of Nanofluids and its Experimental Validation*. PhD thesis, Indian Institute of Technology, Kharagpur.
- Ghosh, M., Ghosh, S., and Pabi, S. (2013). Effects of Particle Shape and Fluid Temperature on Heat-Transfer Characteristics of Nanofluids. *Journal of Materials Engineering and Performance*, 22:1525–1529.
- Ghosh, M. M., Roy, S., Pabi, S. K., and Ghosh, S. (2011). A molecular dynamics-stochastic model for thermal conductivity of nanofluids and its experimental validation. *Journal of nanoscience and nanotechnology*, 11:2196–2207.
- Gowda, R., Sun, H., Wang, P., Charmchi, M., Gao, F., Gu, Z., and Budhlall, B. (2010). Effects of Particle Surface Charge, Species, Concentration, and Dispersion Method on the Thermal Conductivity of Nanofluids. *Advances in Mechanical Engineering*, 2010:1–10.
- Groot, J. J. D., Kestin, J., and Sookiazian, H. (1974). Instrument to measure the thermal conductivity of gases. *Physica*, 75:454–482.
- Habibzadeh, S., Kazemi-Beydokhti, A., Khodadadi, A. A., Mortazavi, Y., Omanovic, S., and Shariat-Niassar, M. (2010). Stability and thermal conductivity of nanofluids of tin dioxide synthesized via microwave-induced combustion route. *Chemical Engineering Journal*, 156:471–478.
- Haghighi, E. B., Nikkam, N., Saleemi, M., Behi, M., Mirmohammadi, S. a., Poth, H., Khodabandeh, R., Toprak, M. S., Muhammed, M., and Palm, B. (2013). Shelf stability of nanofluids and its effect on thermal conductivity and viscosity. *Measurement Science and Technology*, 24:105301.
- Hamaker, H. (1937). The London–van der Waals attraction between spherical particles. *Physica*, 4:1058–1072.
- Hamilton, R. and Crosser, O. (1962). Thermal conductivity of heterogeneous two-component systems. *Industrial & Engineering chemistry fundamentals*, 1:187–191.
- Haynes, W., Lide, D., and Bruno, T. (2012). *CRC Handbook of Chemistry and Physics 2012-2013*. CRC press.

- Healy, J. J., Groot, J. J. D., and Kestin, J. (1976). The theory of the transient hot-wire method for measuring thermal conductivity. *Physica B+C*, 82:392–408.
- Hippel, A. V. (1954). *Dielectric Materials and Applications. Papers by 22 Contributors*. New York.
- Ho, C., Powell, R., and Liley, P. (1972). Thermal Conductivity of the Elements. *Journal of Physical and Chemical Reference Data*, 1:279.
- Hong, K., Hong, T., and Yang, H. (2006). Thermal conductivity of Fe nanofluids depending on the cluster size of nanoparticles. *Applied Physics Letters*, 88:031901.
- Hong, T., Yang, H., and Choi, C. (2005). Study of the enhanced thermal conductivity of fe nanofluids. *Journal of Applied Physics*, 97:1–4.
- Horrocks, J. and McLaughlin, E. (1963). Temperature dependence of the thermal conductivity of liquids. *Transactions of the Faraday Society*, 59:1709–1716.
- Hwang, Y., Lee, J., Jeong, Y., Cheong, S., Ahn, Y., and Kim, S. (2008). Production and dispersion stability of nanoparticles in nanofluids. *Powder Technology*, 186:145–153.
- Hwang, Y., Lee, J., Lee, C., Jung, Y., Cheong, S., Lee, C., Ku, B., and Jang, S. (2007). Stability and thermal conductivity characteristics of nanofluids. *Thermochimica Acta*, 455:70–74.
- Incropera, F. (2011). *Fundamentals of heat and mass transfer*. John Wiley & Sons.
- Instruments, M. (2011). Zeta potential: An introduction in 30 minutes. *Zetasizer Nano Serles Technical Note. MRK654-01*.
- Israelachvili, J. (2011). *Intermolecular and surface forces: revised third edition*. Academic press.
- Jang, S. P. and Choi, S. U. S. (2004). Role of Brownian motion in the enhanced thermal conductivity of nanofluids. *Applied Physics Letters*, 84:4316.
- Jang, S. P. and Choi, S. U. S. (2007). Effects of Various Parameters on Nanofluid Thermal Conductivity. *Journal of Heat Transfer*, 129:617.
- Jeffrey, D. J. (1973). Conduction through a random suspension of spheres. *Proceedings of the Royal Society of London. A. Mathematical and Physical Sciences*, 335:355–367.
- Jiang, L., Gao, L., and Sun, J. (2003). Production of aqueous colloidal dispersions of carbon nanotubes. *Journal of Colloid and Interface Science*, 260:89–94.

- Karthikeyan, N., Philip, J., and Raj, B. (2008). Effect of clustering on the thermal conductivity of nanofluids. *Materials Chemistry and Physics*, 109:50–55.
- Kaviany, M. (2008). *Heat transfer physics*. Cambridge University Press.
- Kawaguchi, N., Nagasaka, Y., and Nagashima, A. (1985). Fully automated apparatus to measure the thermal conductivity of liquids by the transient hot-wire method. *Review of Scientific Instruments*, 56:1788–1794.
- Kebllinski, P., Phillpot, S., Choi, S., and Eastman, J. (2002). Mechanisms of heat flow in suspensions of nano-sized particles (nanofluids). *International Journal of Heat and Mass Transfer*, 45:855–863.
- Kleinstreuer, C. and Feng, Y. (2011). Experimental and theoretical studies of nanofluid thermal conductivity enhancement: A review. *Nanoscale Research Letters*, 6:1–13.
- Knopoff, L. and Shapiro, J. (1970). Pseudo-Grüneisen parameter for liquids. *Physical Review B*, 1:1–3.
- Koo, J. and Kleinstreuer, C. (2004). A new thermal conductivity model for nanofluids. *Journal of Nanoparticle Research*, 6:577–588.
- Krupp, H., Schnabel, W., and Walter, G. (1972). The Lifshitz-Van der Waals constant: Computation of the Lifshitz-Van der Waals constant on the basis of optical data. *Journal of Colloid and Interface Science*, 39:421–423.
- Kumar, G., Prasad, G., and Pohl, R. (1993). Experimental determinations of the Lorenz number. *Journal of materials science*, 28:4261–4272.
- Kuroki, T., Kagawa, N., Endo, H., Tsuruno, S., and Magee, J. W. (2001). Specific Heat Capacity at Constant Volume for Water, Methanol, and Their Mixtures at Temperatures from 300 K to 400 K and Pressures to 20 MPa. *Journal of Chemical & Engineering Data*, 46:1101–1106.
- Lee, J., Han, K., and Koo, J. (2014). A novel method to evaluate dispersion stability of nanofluids. *International Journal of Heat and Mass Transfer*, 70:421–429.
- Lee, S., Choi, S., Li, S., and Eastman, J. (1999). Measuring thermal conductivity of fluids containing oxide nanoparticles. *Journal of Heat Transfer*, 121:280–289.
- Lefèvre, G., Cerović, L., Milonjić, S., Fédoroff, M., Finne, J., and Jaubertie, A. (2009). Determination of isoelectric points of metals and metallic alloys by adhesion of latex particles. *Journal of colloid and interface science*, 337:449–55.
- Leong, K., Yang, C., and Murshed, S. (2006). A model for the thermal conductivity of nanofluids – the effect of interfacial layer. *Journal of Nanoparticle Research*, 8:245–254.

- Li, X., Zhu, D., and Wang, X. (2007). Evaluation on dispersion behavior of the aqueous copper nano-suspensions. *Journal of Colloid and Interface Science*, 310:456–63.
- Li, X. F., Zhu, D. S., Wang, X. J., Wang, N., Gao, J. W., and Li, H. (2008). Thermal conductivity enhancement dependent *pH* and chemical surfactant for Cu-H₂O nanofluids. *Thermochimica Acta*, 469:98–103.
- Lide, D. (2004). *CRC Handbook of Chemistry and Physics*. CRC press, 84 edition.
- Liu, M., Ching-Cheng Lin, M., Huang, I., and Wang, C. (2005). Enhancement of thermal conductivity with carbon nanotube for nanofluids. *International Communications in Heat and Mass Transfer*, 32:1202–1210.
- Liu, M., Lin, M., Tsai, C., and Wang, C. (2006). Enhancement of thermal conductivity with Cu for nanofluids using chemical reduction method. *International Journal of Heat and Mass Transfer*, 49:3028–3033.
- Liu, Z. and Li, Y. (2012). A new frontier of nanofluid research ? Application of nanofluids in heat pipes. *International Journal of Heat and Mass Transfer*, 55:6786–6797.
- Lu, S. and Lin, H. (1996). Effective conductivity of composites containing aligned spheroidal inclusions of finite conductivity. *Journal of Applied physics*, 79:6761.
- Masuda, H., Ebata, A., Teramae, K., and Hishinuma, N. (1993). Alteration of Thermal Conductivity and Viscosity of Liquid by Dispersing Ultra-Fine Particles. Dispersion of Al₂O₃, SiO₂ and TiO₂ Ultra-Fine Particles. *Netsu Bussei*, 7:227–233.
- Maxwell, J. (1873). *A treatise on electricity and magnetism*, volume 1. Clarendon Press.
- Meibodi, M. E., Vafaie-Sefti, M., Rashidi, A. M., Amrollahi, A., Tabasi, M., and Kalal, H. S. (2010). The role of different parameters on the stability and thermal conductivity of carbon nanotube/water nanofluids. *International Communications in Heat and Mass Transfer*, 37:319–323.
- Michaelides, E. (2014). *Nanofluidics*. Springer International Publishing, Switzerland.
- Milling, A. (1999). *Surface characterization methods: principles, techniques, and applications*, volume 87. CRC Press.
- Mintsa, H., Roy, G., Nguyen, C., and Doucet, D. (2009). New temperature dependent thermal conductivity data for water-based nanofluids. *International Journal of Thermal Sciences*, 48:363–371.
- Murshed, S., Leong, K., and Yang, C. (2005). Enhanced thermal conductivity of tio₂-water based nanofluids. *International Journal of Thermal Sciences*, 44:367–373.

- Murshed, S., Leong, K., and Yang, C. (2008a). Investigations of thermal conductivity and viscosity of nanofluids. *International Journal of Thermal Sciences*, 47:560–568.
- Murshed, S., Leong, K., and Yang, C. (2009). A combined model for the effective thermal conductivity of nanofluids. *Applied Thermal Engineering*, 29:2477–2483.
- Murshed, S., Tan, S., and Nguyen, N. (2008b). Temperature dependence of interfacial properties and viscosity of nanofluids for droplet-based microfluidics. *Journal of Physics D: Applied Physics*, 41:085502.
- Murshed, S. M. S., de Castro, C. a. N., and Lourenço, M. J. V. (2012). Effect of Surfactant and Nanoparticle Clustering on Thermal Conductivity of Aqueous Nanofluids. *Journal of Nanofluids*, 1:175–179.
- Murshed, S. M. S., Leong, K. C., and Yang, C. (2006). a Model for Predicting the Effective Thermal Conductivity of Nanoparticle-Fluid Suspensions. *International Journal of Nanoscience*, 05:23–33.
- Nagasaka, Y. and Nagashima, A. (1981a). Absolute measurement of the thermal conductivity of electrically conducting liquids by the transient hot-wire method. *Journal of Physics E: Scientific Instruments*, 14:1435.
- Nagasaka, Y. and Nagashima, A. (1981b). Simultaneous measurement of the thermal conductivity and the thermal diffusivity of liquids by the transient hot-wire method. *Review of Scientific Instruments*, 52:229.
- Nasiri, A., Shariaty-Niasar, M., Rashidi, A., Amrollahi, A., and Khodafarin, R. (2011). Effect of dispersion method on thermal conductivity and stability of nanofluid. *Experimental Thermal and Fluid Science*, 35:717–723.
- Nasiri, a., Shariaty-Niasar, M., Rashidi, A., and Khodafarin, R. (2012). Effect of CNT structures on thermal conductivity and stability of nanofluid. *International Journal of Heat and Mass Transfer*, 55:1529–1535.
- Oh, D.-W., Jain, A., Eaton, J. K., Goodson, K. E., and Lee, J. S. (2008). Thermal conductivity measurement and sedimentation detection of aluminum oxide nanofluids by using the 3ω method. *International Journal of Heat and Fluid Flow*, 29:1456–1461.
- Ojha, U., Das, S., and Chakraborty, S. (2010). Stability, pH and viscosity relationships in Zinc oxide based nanofluids subject to heating and cooling cycles. *Journal of Materials Science and Engineering*, 4:24–29.
- Özering, S., Kakaç, S., and Yazıcıoğlu, A. (2010). Enhanced thermal conductivity of nanofluids: A state-of-the-art review. *Microfluidics and Nanofluidics*, 8:145–170.

- Pang, C., Jung, J., and Kang, Y. (2014). Aggregation based model for heat conduction mechanism in nanofluids. *International Journal of Heat and Mass Transfer*, 72:392–399.
- Parks, G. (1965). The Isoelectric Points of Solid Oxides, Solid Hydroxides, and Aqueous Hydroxo Complex Systems. *Chemical Reviews*, 65:177–198.
- Parks, G. and Bruyn, P. (1962). THE ZERO POINT OF CHARGE OF OXIDES. *The Journal of Physical Chemistry*, 66:967–973.
- Patel, H. E., Das, S. K., Sundararajan, T., Sreekumaran Nair, a., George, B., and Pradeep, T. (2003). Thermal conductivities of naked and monolayer protected metal nanoparticle based nanofluids: Manifestation of anomalous enhancement and chemical effects. *Applied Physics Letters*, 83:2931.
- Paul, G., Chopkar, M., Manna, I., and Das, P. (2010). Techniques for measuring the thermal conductivity of nanofluids: A review. *Renewable and Sustainable Energy Reviews*, 14:1913–1924.
- Philip, J. and Shima, P. (2012). Thermal properties of nanofluids. *Advances in Colloid and Interface Science*, 183-184:30–45.
- Powell, R. and Blanpied, W. (1954). Thermal conductivity of metals and alloys at low temperatures: a review of the literature. Technical report, DTIC Document.
- Powell, R., Roseveare, W., and Eyring, H. (1941). Diffusion, thermal conductivity, and viscous flow of liquids. *Industrial and Engineering Chemistry*, 33:430–435.
- Prasher, R., Bhattacharya, P., and Phelan, P. (2005). Thermal Conductivity of Nanoscale Colloidal Solutions (Nanofluids). *Physical Review Letters*, 94:025901.
- Pugh, R. and Bergström, L. (1994). *Surface and colloid chemistry in advanced ceramics processing*, volume 51. CRC Press.
- Putnam, S. a., Cahill, D. G., Braun, P. V., Ge, Z., and Shimmin, R. G. (2006). Thermal conductivity of nanoparticle suspensions. *Journal of Applied Physics*, 99:084308.
- Rosenberg, H. M. (1955). The Thermal Conductivity of Metals at Low Temperatures. *Philosophical Transactions of the Royal Society of London. Series A, Mathematical and Physical Sciences*, 247:441–497.
- Russel, W., Saville, D., and Schowalter, W. (1992). *Colloidal dispersions*. Cambridge University Press.
- Saidur, R., Leong, K., and Mohammad, H. (2011). A review on applications and challenges of nanofluids. *Renewable and Sustainable Energy Reviews*, 15:1646–1668.

- Saleh, R., Putra, N., Wibowo, R., Septiadi, W., and Prakoso, S. (2014). Titanium dioxide nanofluids for heat transfer applications. *Experimental Thermal and Fluid Science*, 52:19–29.
- Saterlie, M., Sahin, H., Kavlicoglu, B., Liu, Y., and Graeve, O. (2011). Particle size effects in the thermal conductivity enhancement of copper-based nanofluids. *Nanoscale Research Letters*, 6:217.
- Schenkel, J. and Kitchener, J. (1960). A test of the Derjaguin-Verwey-Overbeek theory with a colloidal suspension. *Transactions of the Faraday Society*, 56:161–173.
- Singh, D., Timofeeva, E., Yu, W., Routbort, J., France, D., Smith, D., and Lopez-Cepero, J. M. (2009). An investigation of silicon carbide-water nanofluid for heat transfer applications. *Journal of Applied Physics*, 105:064306.
- Sinha, K., Kavlicoglu, B., Liu, Y., Gordaninejad, F., and Graeve, O. A. (2009). A comparative study of thermal behavior of iron and copper nanofluids. *Journal of Applied Physics*, 106:064307.
- Sundar, L., Singh, M., and Sousa, A. (2013). Thermal conductivity of ethylene glycol and water mixture based Fe₃O₄ nanofluid. *International Communications in Heat and Mass Transfer*, 49:17–24.
- Swinehart, D. (1962). The beer-lambert law. *Journal of Chemical Education*, 39:333.
- Tam, W. and Zardecki, A. (1982). Multiple scattering corrections to the beer-lambert law. 1: Open detector. *Applied Optics*, 21:2405–2412.
- TFCalc. Based on optical database from the sopra s.a. from tfcalc by software spectra. <http://www.sspectra.com/>, <http://www.sspectra.com/sopra.html>.
- Timofeeva, E., Gavrilov, A., McCloskey, J., Tolmachev, Y., Sprunt, S., Lopatina, L., and Selinger, J. (2007). Thermal conductivity and particle agglomeration in alumina nanofluids: Experiment and theory. *Physical Review E*, 76(6):061203.
- Timofeeva, E., Moravek, M., and Singh, D. (2011). Improving the heat transfer efficiency of synthetic oil with silica nanoparticles. *Journal of Colloid and Interface Science*, 364:71–9.
- Tritt, T. (2004). *Thermal conductivity: theory, properties, and applications*. Springer US.
- Venerus, D., Kabadi, M., Lee, S., and Perez-Luna, V. (2006). Study of thermal transport in nanoparticle suspensions using forced rayleigh scattering. *Journal of Applied Physics*, 100:094310.

- Verwey, E. and Overbeek, J. (1948). *Theory of the stability of lyophobic colloids : the interaction of sol particles having an electric double layer*. Amsterdam [etc.] : Elsevier.
- Visser, J. (1972). On Hamaker constants: A comparison between Hamaker constants and Lifshitz-van der Waals constants. *Advances in Colloid and Interface Science*, 3:331–363.
- Viswanath, D. and Rao, M. (1970). Thermal conductivity of liquids and its temperature dependence. *Journal of Physics D: Applied Physics*, 3:1444.
- Wang, X., Li, H., Li, X., Wang, Z., and Lin, F. (2011). Stability of TiO₂ and Al₂O₃ Nanofluids. *Chinese Physics Letters*, 28:086601.
- Wang, X., Zhu, D., and Yang, S. (2009). Investigation of pH and SDBS on enhancement of thermal conductivity in nanofluids. *Chemical Physics Letters*, 470:107–111.
- Weber, M. (2010). *Handbook of optical materials*. CRC press.
- Wen, D., Lin, G., Vafaei, S., and Zhang, K. (2009). Review of nanofluids for heat transfer applications. *Particuology*, 7:141–150.
- Wiesner, M., Lowry, G., Alvarez, P., Dionysiou, D., and Biswas, P. (2006). Assessing the risks of manufactured nanomaterials. *Environmental science & technology*, 40:4336–4345.
- Williams, R., Yarbrough, D., Masey, J., Holder, T., and Graves, R. (1981). Experimental determination of the phonon and electron components of the thermal conductivity of bcc iron. *Journal of Applied Physics*, 52:5167.
- Witharana, S., Palabiyik, I., Musina, Z., and Ding, Y. (2013). Stability of glycol nanofluids – The theory and experiment. *Powder Technology*, 239:72–77.
- Wong, K. and De Leon, O. (2010). Applications of nanofluids: Current and future. *Advances in Mechanical Engineering*, 2010:1–12.
- Xie, H., Lee, H., Youn, W., and Choi, M. (2003). Nanofluids containing multiwalled carbon nanotubes and their enhanced thermal conductivities. *Journal of Applied Physics*, 94:4967.
- Xie, H., Wang, J., Xi, T., Liu, Y., and Ai, F. (2002). Dependence of the thermal conductivity of nanoparticle-fluid mixture on the base fluid. *Journal of Materials Science Letters*, 21:1469–1471.
- Xuan, Y. and Li, Q. (2000). Heat transfer enhancement of nanofluids. *International Journal of Heat and Fluid Flow*, 21:58–64.

- Xue, Q. and Xu, W.-M. (2005). A model of thermal conductivity of nanofluids with interfacial shells. *Materials Chemistry and Physics*, 90:298–301.
- Xue, Q.-z. (2003). Model for effective thermal conductivity of nanofluids. *Physics Letters A*, 307:313–317.
- Yang, L., Du, K., Ding, Y., Cheng, B., and Li, Y. (2012). Viscosity-prediction models of ammonia water nanofluids based on various dispersion types. *Powder Technology*, 215-216:210–218.
- Yu, C. J., Richter, a., Datta, a., Durbin, M., and Dutta, P. (1999). Observation of Molecular Layering in Thin Liquid Films Using X-Ray Reflectivity. *Physical Review Letters*, 82:2326–2329.
- Yu, W. and Choi, S. (2003). The role of interfacial layers in the enhanced thermal conductivity of nanofluids : A renovated Maxwell model. *Journal of Nanoparticle Research*, 5:167–171.
- Yu, W. and Xie, H. (2012). A Review on Nanofluids: Preparation, Stability Mechanisms, and Applications. *Journal of Nanomaterials*, 2012:1–48.
- Yu, W., Xie, H., Chen, L., and Li, Y. (2010). Investigation on the thermal transport properties of ethylene glycol-based nanofluids containing copper nanoparticles. *Powder Technology*, 197:218–221.
- Zhu, H., Zhang, C., Liu, S., Tang, Y., and Yin, Y. (2006). Effects of nanoparticle clustering and alignment on thermal conductivities of Fe₃O₄ aqueous nanofluids. *Applied Physics Letters*, 89:023123.

Acknowledgements

I am extremely grateful to my supervisors, Professor Dong-Woo Suh and Professor H. K. D. H. Bhadeshia for their constant guidance, support and great friendship. I learned how to understand the world through science from them, and will remember this throughout my life. I also want to thank to Professor In Gee Kim, Professor Hae-Geon Lee, and Professor Yoon-Uk Heo for their kind advice and support, and Professor Jae Sang Lee, Professor Youn-Bae Kang and Dr. Sung Ryong Ryoo for discussions and advice in writing this thesis. I have to acknowledge Graduate Institute of Ferrous Technology and POSCO for their financial support.

I would like to express my thanks to all of the past and current members of Graduate Institute of Ferrous Technology. Especially thanks to Computational Metallurgy Laboratory for every moments and memories that we share.

Finally I would like to take this opportunity to express my deepest gratitude to my family and my family-in-law for their support and encouragement. Thank you and thank you to my mother, father and brother for their love and everything. Also thanks to mother-, father- and sisters-in-law. Last and but not least, thank you my love, my husband.

I will remember all I have learned and share this throughout my life, and will try to contribute to the advancement of science and technology.

Curriculum Vitae

Name: Song, You Young (송 유 영)

Contact: spirited@postech.ac.kr

Education

B.S. 2002~2008, Department of Computer Science and Engineering & Department of Mathematics, Pohang University of Science and Technology, Republic of Korea

M.S. 2008~2010, Graduate Institute of Ferrous Technology, Pohang University of Science and Technology, Republic of Korea

Ph.D. 2010~2015, Graduate Institute of Ferrous Technology, Pohang University of Science and Technology, Republic of Korea

Publication

Seo, S. W., Song, Y. Y., Rahman, G., Kim, I. G., Weinert, M., and Freeman, A. J.: A Convergence Test of the Full-potential Linearized Augmented Plane Wave (FLAPW) Method: Ferromagnetic Bulk BCC Fe, *Journal of Magnetism* 14 (2009): 137-143.

Kim, I. G., Rahman, G., Jang, J. H., Song, Y. Y., Seo, S. W., Bhadeshia, H. K. D. H., Freeman, A. J., and Olson G. B.: A Systematic Study on Iron Carbides from First-Principles, *Materials Science Forum* 654 (2010): 47-50.

Heo, Y. U., Song, Y. Y., Park, S. J., Bhadeshia, H. K. D. H. and Suh, D. W.: Influence of silicon in low density Fe-C-Mn-Al Steel, *Metallurgical and Materials Transactions A* 43 (2012): 1731-1735.

Duong V. T., Song, Y. Y., Park, K. S., Bhadeshia, H. K. D. H., and Suh, D. W.: Austenite in Transformation-Induced Plasticity Steel Subjected to Multiple Isothermal Heat Treatments, *Metallurgical and Materials Transactions A* 45 (2014): 4201-4209.

Song, Y. Y., Bhadeshia, H. K. D. H., and Suh, D. W.: Stability of stainless-steel nanoparticle and water mixtures, *Powder Technology* (in press), 2015.

Song, Y. Y., Bhadeshia, H. K. D. H., and Suh, D. W.: Stainless steel-nanofluids: Stability to Thermal conductivity. *To be submitted*, 2015.